SMART NANOCOMPOSITES

Volume 8, Issue 1, 2017

TABLE OF CONTENTS

Synthesis of $NaBaPO_4:Eu^{2+}$ Luminescent Phosphors with Enhanced Dispersion 1
Vadim V. Bakhmetyev, Vitalii V. Malygin, Mariia V. Keskinova, Maxim M. Sychov, and Sergey V. Mjakin

Thermodynamic Modeling of the Behavior of Higher Fullerenes C_{84} when Heated in an Inert Atmosphere: Computer Experiment 7
Nick M. Barbin, Vasiliy P. Dan, Dmitriy I. Terentiev, and Sergey G. Alekseev

The Use of Porous Gallium Phosphide as Substrates for Supercapacitors 15
Anton O. Belorus, Boris D. Klimenkov, Veniamin L. Koshevoi, Nikolai S. Pshchelko, and Vyacheslav A. Moshnikov

New Empirical Approach for the Covalent Bonding Class of (System of) Atoms in Simulation Obtaining Thin Films Process Technology 19
V. A. Tupik, V. I. Margolin, and Chu Trong Su

Growth and Properties of Al_2O_3 Nanolayers on III–V Semiconductors 25
Yu. K. Ezhovskii

SAXS and WAXS Investigations and Thermal Analysis of Structural Transformation of Polyorganosiloxane and of the Systems of Polyorganosiloxane – Silicate and Polyorganosiloxane – Oxide within the Temperature Range from 20° to 600°C 33
Irina B. Glebova and Valery L. Ugolkov

Calculation of an Experimental Pseudocapacitor Self-Discharge Rate with the Use of Cyclic Voltammograms 43
Alexandra G. Ivanova, Oleg A. Zagrebelnyy, Maria S. Masalovich, Irina Yu. Kruchinina, and Olga A. Shilova

Hydrophobic and Superhydrophobic Coatings Based on Fluorosiloxane Block Copolymers 51
Yu. V. Khoroshavina, Yu. V. Frantsuzova, I. N. Tsvetkova, O. A. Shilova, and G. A. Nikolaev

Impurity Centers U-Minus TIN in Chalcogenide Semiconductors A4b6 and A5b6 57
M. Yu. Kozhokar

Mechanical Properties of Polyacrylic Acid - Polyvinyl Alcohol Hydrogels at Compression and Extension 63
I. S. Kuryndin, I. Yu. Dmitriev, N. V. Bobrova, Z. F. Zoolshoev, and G. K. Elyashevich

Solubility, Thermal Analysis, and Association in Water Solutions of the Adducts of Fullerene C_{60} with Lysine, L-Threonine, L-Hydroxiproline **67**
Dmitry G. Letenko, Konstantin N. Semenov, Nikolay A. Charykov, Viktor A. Keskinov, Natalya A. Kulenova, Nikolay M. Saf'yannikov, Natalya N. Duryagina, Polina V. Garamova, Vyacheslav V. Klepikov, Andrey A. Zolotarev, and Alexey S. Ivanov

Thermal Desorption of Inert Gases in Metal-Oxide Nanomaterials **73**
Evgeniya V. Maraeva, Anton A. Bobkov, Vyacheslav A. Moshnikov, and Igor A. Averin

Data Inconsistency on Transport Phenomena in $A_2^V B_3^{VI}$ Materials with the Hole Conductivity **79**
Sergey A. Nemov, Ali A. Allahkhah, and Arseny A. Rulimov

Sol-Gel Synthesis and Characterization of Tungsten Oxide Nanolayers for Electrochromic Devices **85**
Vera S. Zemko, Elena V. Kolobkova, Evgenia V. Sokhovich, and Sergey V. Mjakin

Charge Carriers and Conductivity Mechanism in VO_2 Films **91**
E. A. Tutov, H. I. Al-Khafaji, and V. P. Zlomanov

The Computer Simulation of Mixers Signals **101**
Yu. A. Nikitin and V. A. Yurova

SHORT COMMUNICATIONS **107**

Investigations of Ion Velocity Distribution Function for Novel Plasma Nanotechnologies **109**
Alexander Mustafaev, Artiom Grabovskiy, Anastasiya Strakhova, and Vladimir Soukhomlinov

Probe Plasma Diagnostics with No Velocity Space Symmetry **115**
Alexander Mustafaev, Artiom Grabovskiy, Anastasiya Strakhova, and Vladimir Soukhomlinov

Discussion of Data Inconsistencies on Transport Phenomena in Crystals of p-$Sb_2Te_{3-x}Se_x$ **121**
Sergey A. Nemov, Ali A. Allakhah, and Arseny A. Rulimov

Phase Analysis of Internal Oxidation Zone of Electrical Steel **123**
Sergey N. Saltykov, Natalia V. Tarasova, Daria A. Mironova, Nikolay S. Saltykov, Tatyana A. Trunova, and Nikolay A. Rogozhnikov

nova
science publishers
New York

Smart Nanocomposites

This Journal presents new studies in the fast growing area of smart materials, in particular, composite nanostructured materials. It focuses on the physics and physical chemistry of surfaces, interfaces, thin films and coatings, nanoparticles and other nanostructures, as well as on their new and smart applications. Original approaches in fabrication and applications of nanostructured materials will get special attention. Nanostructured ceramics, alloys, various nanocarbon forms (nanotubes, fullerenes, graphene) and their composites used in sensors (including single molecule sensing) and actuators, artificial metabolism, drug delivery, selective membranes, fuel cells, energy storage, and photovoltaics are just a few examples of new classes of materials and applications that are within the scope of the Journal. It features the results of interdisciplinary research from universities, national labs, and privately owned companies.

The Journal is peer-reviewed with the highest standards and quality of publications. The purpose of this Journal is to bring the most up-to-date advances in nanotechnology together, and to give research groups the opportunity to compare their results with other groups' data. To achieve this, the Journal focuses mostly on practical applications of nanodevices, and on proof of the concept publications. Areas of interest include (but not are limited to): sensors, smart membranes, smart coatings for corrosion protection, aspects of significance to nanorobots: power supplies, nanorobot manipulating devices, and microchips for artificial intelligence. The Journal also deals with safety issues: safety of nanotechnology to the environment, controlling the nanodevices, and other aspects.

Smart Nanocomposites
is published in two issues per year by

Nova Science Publishers, Inc.
400 Oser Avenue, Suite 1600
Hauppauge, New York 11788-3619, U.S.A.
E-mail: nova.main@novapublishers.com
Web: www.novapublishers.com

ISSN: 1949-4823

Subscription Rate per Volume
Print: $245 Electronic: $245 Combined Print + Electronic: $367

Additional color graphics might be available in the e-version of this journal.

Smart Nanocomposites
Volume 8, Number 1
ISSN: 1949-4823

SYNTHESIS OF $NaBaPO_4:Eu^{2+}$ LUMINESCENT PHOSPHORS WITH ENHANCED DISPERSION

Vadim V. Bakhmetyev*, Vitalii V. Malygin, Mariia V. Keskinova, Maxim M. Sychov, and Sergey V. Mjakin
Department of Material Science, Saint Petersburg State Institute of Technology (Technical University), Saint Petersburg, Russia

ABSTRACT

$NaBaPO_4:Eu^{2+}$ luminescent phospors with enhanced dispesity are obtained by sol-gel precipitation followed by high temperature annealing in molten NaCl. The suggested approach involving annealing in molten NaCl provides $NaBaPO_4:Eu^{2+}$ phosphors with nanocrystalline structure, 3.8-fold reduced average particle size and 11-fold increased content of finely dispersed (less than 1 μm) fraction compared with a similar material synthesized without NaCl addition.

Keywords: luminescent phosphors, sol-gel, mixed phosphate, Eu^{2+}

INTRODUCTION

$NaBaPO_4:Eu^{2+}$ phosphors are known to provide an efficient blue luminescence upon stimulation with either UV or X-ray irradiation. Therefore, they can be used as components of white light diodes and in medicine to activate specific drugs for photodynamic therapy of cancer. The considered applications require finely dispersed phosphors. One of the approaches to obtaining finely dispersed materials is based on sol-gel precipitation from solutions [1, 2] affording an adjustable particle size distribution. However, thus prepared phosphors require a subsequent high temperature processing that results in sintering of small particles into large agglomerates.

This study is aimed at the development of a process for obtaining finely dispersed $NaBaPO_4:Eu^{2+}$ phosphors using a sol-gel precipitation followed by a high temperature annealing in a molten salt according to the approach earlier suggested in [3] for $Y_2O_3:Eu^{3+}$ based phosphors.

* Corresponding Author E-mail: vadim_bakhmetyev@mail.ru

MATERIALS AND METHODS

The synthesis involved $BaCl_2$ and $EuCl_3$ as initial reagents and $Na_3PO_4 \cdot 12H_2O$ as the precipitation agent. The precipitation from an aqueous solution followed by evaporation yields a solid mixture of $NaBaPO_4:Eu^{3+}$ and NaCl subsequently annealed in air at 600°C and milled. Then Eu^{3+} was reduced to Eu^{2+} by annealing in $5\%H_2 + 95\%N_2$ gas mixture at 1050°C followed by washing with hot bidistilled water to remove NaCl. Then the phosphor was separated from the solution by centrifugation and dried under vacuum.

For comparison, a similar phosphor sample was synthesized via a process developed in our previous studies [4] using $Ba(NO_3)_2$ and $Eu(NO_3)_3$ initial reagents and involving sol-gel precipitation and product separation by filtering followed by annealing in air and reducing atmosphere without NaCl addition.

XRD characterization of the synthesized phosphors was carried out using a RINT 2200 X-ray diffractometer. All the synthesized samples were studied by measuring their photoluminescence and photo-excitation spectra. Photoluminescence (PL) was stimulated using a xenon lamp and monochromator. PL spectra were measured in the region 350…600 nm upon stimulation with the wavelength 345 nm. The excitation spectra were stimulated by radiation in the region 250…400 nm and detected at 460 nm. SEM characterization of the powders was performed using a Keyence VE-8800 electron microscope.

RESULTS AND DISCUSSION

SEM data for $NaBaPO_4:Eu^{2+}$ phosphors synthesized with and without annealing in molten NaCl (Figure 1) and the corresponding particle size distributions (Figure 2) indicate that the addition of NaCl as a fluxing agent significantly improves the phosphor dispersion providing a 3.8-fold decrease in the mean equivalent diameter of the phosphor particles to 2.56 μm and an 11-fold increase in the finely dispersed (less than 1 μm) phase content to 44.5% compared with 9.8 μm and 4.0% respectively for the samples annealed in the absence of NaCl.

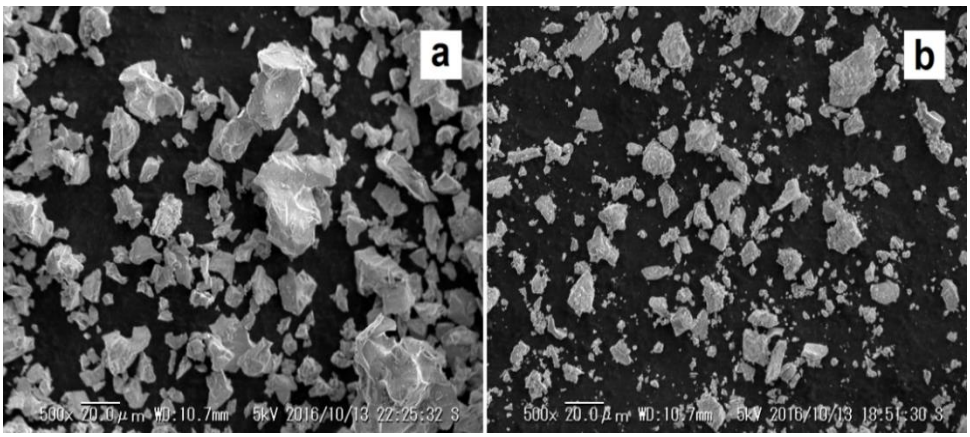

Figure 1. SEM images of $NaBaPO_4:Eu^{2+}$, phosphors synthesized without (a) and with (b) annealing in molten NaCl.

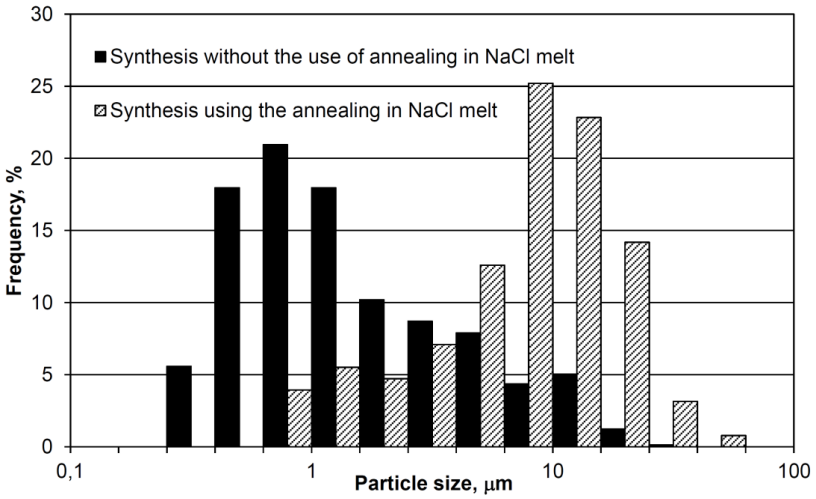

Figure 2. Particle size distributions for $NaBaPO_4:Eu^{2+}$, phosphors synthesized without (a) and with (b) annealing in molten NaCl.

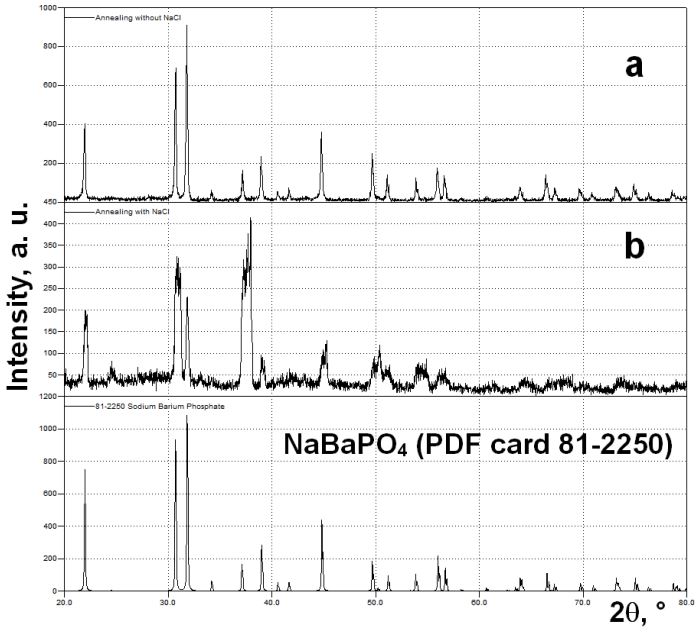

Figure 3. XRD profiles of $NaBaPO_4:Eu^{2+}$ phosphors annealed the absence (a) and in the presence (b) of NaCl melt compared with $NaBaPO_4$ monoclinic phase.

XRD profiles of the synthesized phosphors (Figure 3) correspond to $NaBaPO_4$ monoclinic phase (PDF card 81-2250) free of any admixture phases. However, narrow peaks relating to the phosphor annealed without NaCl indicate its coarsely crystalline structure while the sample prepared in the presence of NaCl features with broad peaks suggesting a nanocrystalline structure. The crystallite size calculated according to the Scherrer equation for the phosphors annealed in the absence and in the presence of NaCl melt is 72.4 nm and 30.2 nm respectively.

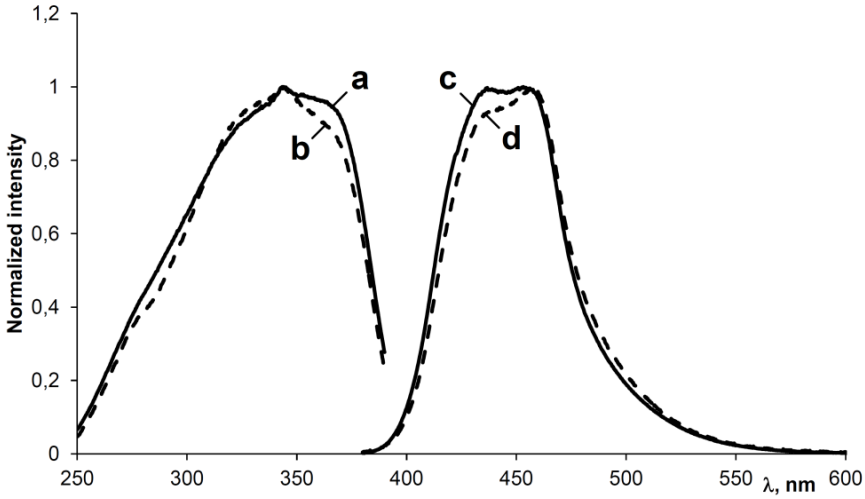

Figure 4. Excitation (a, b) and photoluminescence (c, d) spectra of $NaBaPO_4:Eu^{2+}$ phosphors annealed the absence (a, c) and in the presence (b, d) of NaCl melt.

The excitation and luminescence spectra of the synthesized phosphors are shown in Figure 4. The observed peaks in the excitation spectra are located at the wavelength 344 nm close to the emission band of UV LEDs. The presence of «blue» (430…460 nm) bands in the luminescence spectra affords the use of these phosphors as both «blue» component in white LEDs and as activators for photodynamic therapy drugs in combination with commercial photosensitizers.

PL spectra feature with two prominent peaks relating to the most intensive luminescence bands corresponding to Eu^{2+} ions in $NaBaPO_4$ lattice with coordination numbers 10 and 12, respectively [4, 5]. The short-wave band intensity for the sample annealed in molten NaCl is somehow lower compared with another phosphor. This difference can be explained in terms of the model suggested in our earlier studies to describe luminescence centers in $NaBaPO_4:Eu^{2+}$ phosphors [4]. The synthesis in molten NaCl leads to the decrease of the phosphor particle size that consequently leads to the increase of their surface and content of the surface Eu^{2+} ions. According to this model, Eu^{2+} ions on the surface accept energy from luminescence centers represented by Eu^{2+} ions located in sites with the coordination number 10. This results in a relative decrease of the short-wave band intensity in the PL spectrum in agreement with the observed data confirming the considered model.

CONCLUSION

Thus the performed studies resulted in the development of a process affording the synthesis of $NaBaPO_4:Eu^{2+}$ phosphors with enhanced dispersion. The suggested approach provides a 3.8-fold decrease of the average size of the phosphor particles and 11-fold increase in the content of finely dispersed (less than 1 μm) phase. The observed effect of the phosphor dispersion upon its excitation and photoluminescence spectra is found to be in accordance with the model of luminescence centers composition in $NaBaPO_4:Eu^{2+}$, phosphors suggested in our earlier studies.

ACKNOWLEDGMENTS

The reported study was funded by RFBR according to the research project No. 16-33-00998 мол_а.

REFERENCES

[1] Moshnikov V. A., Gracheva I. E., An'chkov M. G., (2011). Investigation of Sol–Gel Derived Nanomaterials with a Hierarchical Structure. *Glass Physics and Chemistry* 37 (5), 485-495.

[2] Gareev K. G., Gracheva I. E., Moshnikov V. A., (2013). The Sol-Gel Method and Study of Fe_2O_3–NiO–Co_3O_4–SiO_2 Magnetic Nanocomposites. *Glass Physics and Chemistry* 39 (5), 548-554.

[3] Mamonova D. V., Kolesnikov I. E., Golyeva E. V., Mikhailov M. D., Pulkin S. A., Smirnov V. M., (2015). Synthesis and study of $Y_2O_3:Eu^{3+}$ nanoparticles. *Nanotechnologies in Russia* 10 (9), 701-705.

[4] Malygin V. V., Lebedev L. A., Bakhmetyev V. V., Keskinova M. V., Sychov M. M., Mjakin S. V., Nakanishi Y., (2016). Synthesis and study of luminescent materials on the basis of mixed phosphates. *Advances in Intelligent Systems and Computing* 519, 47-54.

[5] Suyin Zhang, Yanlin Huang, Yosuke Nakai, Taiju Tsuboi, Hyo Jin Seo, (2011). The Luminescence Characterization and Thermal Stability of Eu^{2+} Ions-Doped $NaBaPO_4$ Phosphor. *J. Am. Ceram. Soc.* 94 (9), 2987-2992.

Smart Nanocomposites
Volume 8, Number 1
ISSN: 1949-4823

THERMODYNAMIC MODELING OF THE BEHAVIOR OF HIGHER FULLERENES C_{84} WHEN HEATED IN AN INERT ATMOSPHERE: COMPUTER EXPERIMENT

Nick M. Barbin[1,2], Vasiliy P. Dan[1,*], Dmitriy I. Terentiev[1], and Sergey G. Alekseev[1]

[1]The Ural Institute of State Fire Service of Emercom of Russia, Ekaterinburg, Russia
[2]The Ural Agrarian State University, Ekaterinburg, Russia

ABSTRACT

Thermodynamic simulation of the behavior of the higher fullerene C_{84} by heating in inert gas – argon. Was conducted equilibrium constants of the reactions occurring in the system C_{84}-Ar. Was defined plots of compositions of gas and condensed phases on temperature in the considered system. Were constructed graphs of the dependence of the equilibrium constants of the reactions with increasing temperature also were constructed.

Keywords: fullerene, thermodynamic modeling, the equilibrium constants, carbon nanomaterials, heating

INTRODUCTION

The study of carbon fullerene structures is a subject of scientific interest. First, it can be explained as a new molecular form of carbon that is able to encompass the atoms and even molecules [1]. Second, the presence of a unique properties suggests a potential use in creating new materials [2].

The article and stability of higher fullerenes, and discloses the relationship between the characteristics of the structure of higher fullerenes with the possibility of their obtaining was studied [3].

However, to achieve practical applications of these molecular systems it is necessary to study their thermal properties.

This paper studied the behavior of the higher fullerenes C_{84} [4, 5] when heated in argon at atmospheric pressure [6, 7].

* Corresponding Author E-mail: danvp_92@mail.ru, tel: 8 (343) 3608108.

Unlike the most popular representatives of fullerenes – C_{60} and C_{70}, higher fullerenes (C_{72} – C_{86}) obey the rule of isolated pentagons [8, 9]. Fullerene is the third C_{84} fullerene after C_{60} and C_{70} fullerenes, most commonly and in large numbers present in the fullerene soot. However, unlike the above two fullerenes, which according to the rule of isolated pentagons have only one isomer fullerene C_{84} can have twenty-four isomer [10].

The research was conducted using thermodynamic modeling.

THE METHOD OF CALCULATION

Thermodynamic modeling consists of the thermodynamic analysis of the equilibrium state of the system as a whole (a complete thermodynamic analysis) [11, 12]. One of the most developed and effective programs which realise such thermodynamic calculations, is the program complex TERRA, which represents a stage of further development of the software package ASTRA [13].

Thermodynamic modeling was successfully applied to the study of the behavior of radioactive graphite by heating in different environments, and also in physics and material science.

Calculations of the composition of the phases and characteristics of equilibrium are carried out using the reference database on properties of individual substances [15, 16].

RESULTS AND DISCUSSION

Computer experiment allows to determine the phase distribution of carbon in the system C_{84}-Ar on the whole considered temperature interval.

Based on the composition of the gas phase temperature in the system C_{84}-Ar is presented in Figure 1.

When the temperature in the system C_{84}-Ar to 2473 K, the vapor concentration C, C_2, C_3, C_4, C_5 increase.

Vapour concentration C and C_2 increase over the entire temperature range, and upon reaching to 4273 K reach values $9{,}459 \cdot 10^{-4}$ mole fraction and $6{,}043 \cdot 10^{-4}$ mole fraction.

Vapor concentration C_3 and C_4 increases until the system temperature to 4073 K and reach values $1{,}827 \cdot 10^{-3}$ mole fraction and $2{,}990 \cdot 10^{-5}$ mole fraction.

In the temperature interval from 4073 K to 4273 K the vapor concentration C_3 and C_4 are reduced to values of $1{,}584 \cdot 10^{-3}$ mole fraction and $2{,}349 \cdot 10^{-5}$ mole fraction.

A pair of C_5 concentration increases until the system temperature 3973 K and achieves value $9{,}788 \cdot 10^{-5}$ mole fraction. In the temperature interval from 3973 K to 4273 K focus a pair of C_5 decreases to a value $4{,}569 \cdot 10^{-5}$ mole fraction.

When the system temperature 3773 K the composition of the gas phase is replenished with ions C^+, C^{2-}, C^{2+}. At a temperature 4273 K their concentrations are $6{,}482 \cdot 10^{-9}$ mole fraction $6{,}263 \cdot 10^{-9}$ mole fraction and $2{,}088 \cdot 10^{-9}$ mole fraction respectively.

The dependence of the composition of the condensed phase the temperature in the system is presented in Figure 2.

In the interval of temperatures from 473 K to 3973 K condensed the concentration of C decreases to 0,012 mole fraction to $7{,}024 \cdot 10^{-3}$ mole fraction.

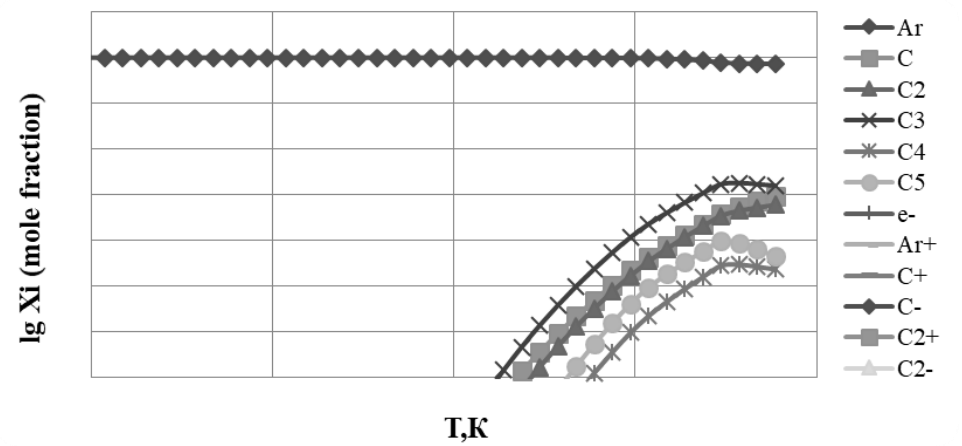

Figure 1. The dependence of the composition of the gas phase temperature in the system C_{84}-Ar at a pressure of 10^5 Pascal.

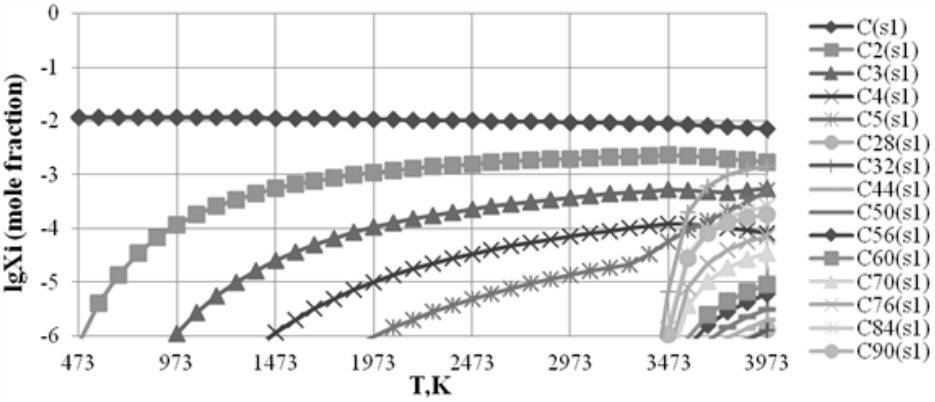

Figure 2. The dependence of the composition of the condensed phase temperature in the system of C_{84}-Ar at a pressure of 10^5 Pascal.

In the temperature range from 473 K to 3473 K the concentration of the condensed C_2 and C_3 increases; they reach values $2{,}286 \cdot 10^{-3}$ mole fraction and $5{,}232 \cdot 10^{-4}$ mole fraction.

In the temperature interval from 3973 K to 3473 K the concentration of condensed C_2 decreases to a value of $1{,}750 \cdot 10^{-3}$ mole fraction.

The concentration of the condensed C_3 in the temperature range from 3473 K to 3773 K reduced to $4{,}590 \cdot 10^{-4}$ mole fraction. In the temperature interval from to 3973 K to 3773 K the concentration of the condensed C_3 is increased to $5{,}599 \cdot 10^{-4}$ mole fraction.

In the temperature range from 973 K to 3573 K increases the concentration of condensed C_4 to the value $1{,}206 \cdot 10^{-4}$ mole fraction. In the temperature interval from 3973 K to 3573 K the concentration of the condensed C_4 decreases linearly to $8{,}298 \cdot 10^{-5}$ mole fraction.

In the interval of temperatures from 1373 K to 3273 K increases the concentration of condensed C_5 to $2{,}165 \cdot 10^{-5}$ mole fraction. In the temperature interval from 3273 K 3973 K condensed C_5 concentration increases linearly and reaches a value of $5{,}025 \cdot 10^{-4}$ mole fraction.

In the temperature interval from 3373 K to 3573 K linearly increase the concentration of condensed C_{94}, C_{84}, C_{90}, C_{70} and C_{76}, reaching values of $2{,}007 \cdot 10^{-4}$ mole fraction,

$3{,}148 \cdot 10^{-5}$ mole fraction, $2{,}755 \cdot 10^{-5}$ mole fraction, $7{,}817 \cdot 10^{-6}$ mole fraction, $3{,}705 \cdot 10^{-6}$ mole fraction. In the interval of temperatures from 3973 K to 3573 K concentration above condensed components of the system increase and reach values $1{,}417 \cdot 10^{-3}$ mole fraction $2{,}571 \cdot 10^{-4}$ mole fraction, $1{,}792 \cdot 10^{-4}$ mole fraction, $7{,}258 \cdot 10^{-5}$ mole fraction $3{,}457 \cdot 10^{-5}$ mole fraction

In the temperature interval from 3973K to 3473 K the concentration of the condensed C_{60}, C_{56}, C_{50}, C_{44}, C_{28} and C_{32} increase and reach values $9{,}213 \cdot 10^{-6}$ mole fraction $6{,}038 \cdot 10^{-6}$ mole fraction $3{,}185 \cdot 10^{-6}$ mole fraction, $2{,}036 \cdot 10^{-6}$ mole fraction, $1{,}354 \cdot 10^{-6}$ mole fraction, $1{,}256 \cdot 10^{-6}$ mole fraction.

Description of the reactions were carried out on the basis of the graphs (Figure 1-2), highlighting temperature intervals of a reaction.

In the considered system where flow physico-chemical processes, which can be divided into 4 groups (Table 1).

Table 1. Reactions occurring in the system C_{84}-Ar

№	The name of the group	Reaction	Temperature range of reaction, K
1	2	3	4
1	Reactions malinali of occurring in the condensed phase:	$2C_{(s)} = C_{2(s)}$	773 - 3373
		$3C_{(s)} = C_{3(s)}$	1273 - 3373
		$4C_{(s)} = C_{4(s)}$	1973 - 3373
		$3C_{(s)} = C_3$	2673 - 3473
		$76C_{3(s)} = 3C_{76(s)}$	3373 - 3773
		$35C_{2(s)} = C_{70(s)}$	3373 - 3873
		$42C_{2(s)} = C_{84(s)}$	3373 - 3673
		$45C_{2(s)} = C_{90(s)}$	3373 - 3673
2	The reaction of thermal dissociation occurring in the condensed phase:	$3C_{94(s)} = 94C_{3(s)}$	3673 - 3973
3	The reaction of evaporation militaria:	$5C_{3(s)} = 3C_5$	3373 - 3773
4	Reaction evaporation with thermal dissociation:	$5C_{84(s)} = 84C_5$	3573 - 3773
		$C_{94(s)} = 94C$	3573 - 4273
		$C_{94(s)} = 47C_2$	3373 - 4273

According to these equations and using found in model calculations of concentration (in molar fractions) of components of the condensed and gas phases was calculated from the appropriate equilibrium constants. The most important reactions are presented by analytical equations:

$$LnK_i = A_i + B_i(1/T) \quad (1)$$

Coefficients (A) and (b) of equation (1) calculated by the least squares method and are given in Table 2.

Table 2. Coefficients (A) and (b) of equation (1)

№	Reaction	ΔT, °K	A	B	R^2
1	$2C_{(к)} = C_{2(к)}$	773-2973	-4946,900	-6,762	0,999
2	$3C_{(к)} = C_{3(к)}$	1273-2973	-10288,000	-8,982	0,999
3	$4C_{(к)} = C_{4(к)}$	1973-2473	-15955,000	-11,116	1,000
4	$3C_{94(к)} = 94C_{3(к)}$	973-1573	-825189,000	383,900	1,000
5	$3C_{(к)} = C_3$	1373-3273	-99920,000	20,516	1,000
6	$5C_{3(к)} = 3C_5$	1973-3273	-10903,000	-4,551	0,999
7	$76C_{3(к)} = 3C_{76(к)}$	773-1373	688281,000	-355,970	1,000
8	$35C_{2(к)} = C_{70(к)}$	873-1273	156721,000	-144,470	1,000
9	$42C_{2(к)} = C_{84(к)}$	1473-2073	152313,000	-138,160	0,999
10	$45C_{2(к)} = C_{90(к)}$	873-1273	201479,000	-172,240	1,000
11	$5C_{84(к)} = 84C_5$	1773-2373	$-1 \cdot 10^6$	339,110	1,000
12	$C_{94(к)} = 94C$	2973-3873	$-7 \cdot 10^6$	1815,600	1,000
13	$C_{94(к)} = 47C_2$	2473-3973	$-4 \cdot 10^6$	981,050	0,999
R – the value of the approximation					

The dependence of the values of the equilibrium constants of the reactions discussed above from 1/T is represented in Figure 3-5. For convenience, they were divided into three temperature ranges: the first from 3973 K to 773 K; the second - from 873 K to 3273 K; the third is from 773 to 3273 K (number of reactions shown in Table 2).

Position of straights in Figure 3-5 shows the magnitude and the character of the dependence of the equilibrium constants of the reactions on temperature. They present an analytical equation (1). It (A) is a factor affecting the position (offset) of straight regarding to the x-axis. The more this ratio (and therefore, more and lnK), the higher on the figure is a straight and reaction is shifted stronger towards formation of the reaction products.

The coefficient (b) indicates the angle between the straight constants of the reaction and the x-axis. The more this ratio, the stronger the reaction proceeds with increasing temperature.

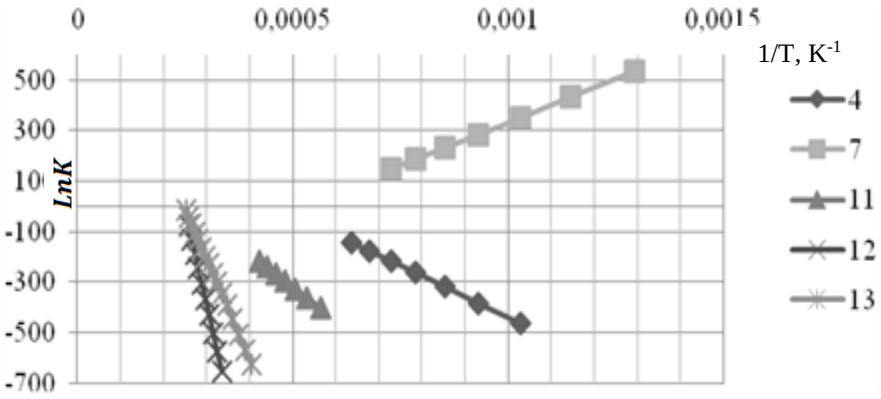

Figure 3. The dependence of the equilibrium constant reactions of 1/T in temperature interval from 773 K to 3973 K.

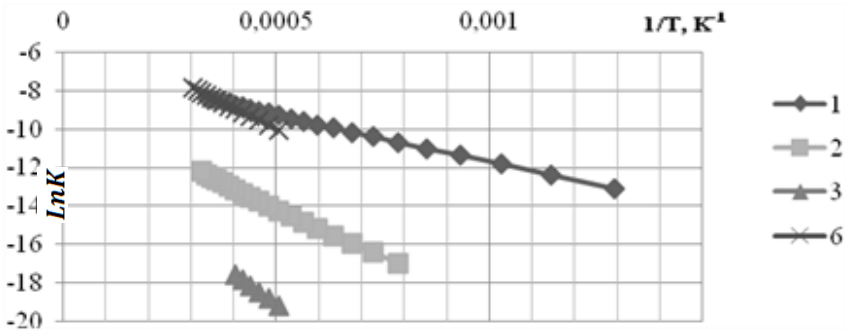

Figure 4. The dependence of the values of equilibrium constants reactions of 1/T in the temperature range from 873 K To 3273 K.

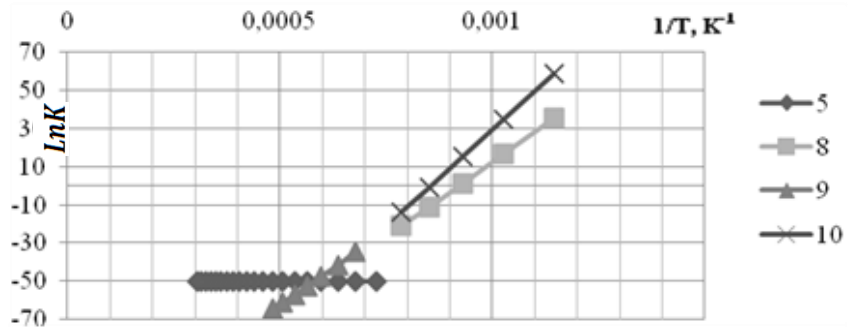

Figure 5. The dependence of the values of equilibrium constants reactions of 1/T in temperature interval from 773 K To 3273 K.

CONCLUSION

The higher fullerene C_{84} is the third representative of fullerene stability, which significantly expands the range of its practical application in various fields of industry. In this work, the processes and temperature ranges of the reactions defined were. Plots of compositions of phases temperature in the system were conducted equilibrium constants of reactions were calculated and plots of constant values of the reactions the temperature in the system were conducted too. The analysis of the data obtained indicates that when reaching a temperature of 800-2500 K in an inert environment results to a process of thermal dissociation and evaporation with thermal dissociation, which leads to an increase in the number of components in the gas and condensed phases.

REFERENCES

[1] Peters, G. A new fullerene synthesis. G. Peters, M. Jansen. *Angew. Chem. Int. Ed*. – 1992. – V. 31. – P. 223-224.

[2] Hirsch, A. *The chemistry of the Fullerenes*. A. Hirsch. - Stuttgart; New York: Thieme, 1994. – 215 p.

[3] Amsharov, K. Synthesis of a higher fullerene precursor—An ‘unrolled’ C84 fullerene. K. Amsharov, M. Jansen. *Chem. Commun.* – 2009. – P. 2691-2693.

[4] Beavers, C. M. Tb3N@C84: An improbable, egg-shaped endohedral fullerene that violates the isolated pentagon rule. C. M. Beavers, T. Zuo, J. C. Duchamp, K. Harich, H. C. Dorn, M. M. Olmstead, A. L. Balch. *J. Am. Chem. Soc*. – 2006. – V. 128. – P. 11352-11353.

[5] Zuo, T. New egg-shaped fullerenes: Non-isolated pentagon structures of Tm3N@CS(51365)-C84 and Gd3N@CS(51365)-C84. T. Zuo, K. Walker, M. M. Olmstead, F. Melin, B. C. Holloway, L. Echegoyen, H. C. Dorn, M. N. Chaur, C. J. Chancellor, C. M. Beavers, A. L. Balch, A. J. Athans. *Chem. Commun*. – 2008. – P. 1067-1069.

[6] Moiseev G. K., Vatolin N. Evaluation of the thermodynamic properties of a number of condensed carbon compounds. *Chemical Thermodynamics and Thermochemistry: The Journal of Physical Chemistry,* 2002. No. 3, pp. 424-428.

[7] Wild V. V., Kabo G. J. Thermodynamic properties of fullerenes C60 and C70. *Successes of Chemistry,* 2000. No. 2. s. 107-117.

[8] Zuo, T. New egg-shaped fullerenes: non-isolated pentagon structures of Tm3N@CS(51365)-C84 and Gd3N@CS(51365)-C84. T. Zuo, K. Walker, M. M. Olmstead, F. Melin, B. C. Holloway, L. Echegoyen, H. C. Dorn, M. N. Chaur, C. J. Chancellor, C. M. Beavers, A. L. Balch, A. J. Athans. *Chem. Commun*. – 2008. – P. 1067-1069.

[9] Olmstead, M. Sc3N@C68: folded pentalene coordination in an endohedral fuller-ene that does not obey the isolated pentagon rule. M. Olmstead, H. M. Lee, J. C. Duchamp, S. Stevenson, D. Marciu, H. C. Dorn and A. L. Balch. *Angew. Chem. Int. Ed*. – 2003. – V. 42. – No. 8. – P. 900-902.

[10] Fowler, P. *An Atlas of Fullerenes*. P. Fowler, D. Manolopoulos. – Oxford: Clarendon Press, 1995. – 392p.

[11] N. M. Barbin, D. I. Terentiev, S. G. Alekseev, Tuktarov M. A., Romenkov A. A. *Modeling of Radioactive Graphite Oxidation in Molten Salts. – Book of Abstracts*. The 33rd international symposium "Scientific Basis for Nuclear Waste Management". – St. Petersburg, 2009, p. 133.

[12] N. M. Barbin, D. I. Terentiev, S. G. Alekseev, Tuktarov M. A., Romenkov A. A. Modeling of radioactive graphite oxidation in molten salts: A computer experiment. – *Material Research Society Symposium Proceeding*, 2009, 1193, p. 359-366.

[13] Vatolin N. A. Moiseev G. K., Trusov B. G. Thermodynamic Modeling in High Temperature Systems. – *M.: Metallurgy*, 1994.-352 p.

[14] Alexeev S. G. Thermodynamic modeling of the behavior of americium, caesium and strontium during heating of irradiated graphite in nitrogen atmosphere. *Technosphere Safety: Internet Magazine* 2014. No. 2 (3). URL: http:www.uigps.ru.content.nauchnyy-zhurnal. .

[15] Gurevich L. V., Weitz I. V., Medvedev, V. A., *Thermodynamic properties of individual substances: Reference*. ed-e in 4 volumes. – M.: Nauka, 1982. -8540 s.

[16] Alemasov V. E., Dregalin A. F., Tishin A. P. *Thermodynamic and Thermophysical Properties of Combustion Products: Reference.* In 5 volumes. – M.: VNIITE, 1971. – 6350 s.

Smart Nanocomposites
Volume 8, Number 1
ISSN: 1949-4823

THE USE OF POROUS GALLIUM PHOSPHIDE AS SUBSTRATES FOR SUPERCAPACITORS

Anton O. Belorus[1,*], Boris D. Klimenkov[2], Veniamin L. Koshevoi[2], Nikolai S. Pshchelko[2], and Vyacheslav A. Moshnikov[1]

[1]Saint Petersburg Electrotechnical University "LETI"
Saint Petersburg, Russian Federation
[2]Saint Petersburg Mining University, Saint Petersburg, Russian Federation

ABSTRACT

Use of porous GaP is proposed as substrates for supercapacitors. Porous substrates are prepared by electrochemical etching. A method of producing of porous GaP is presented. Analysis of the morphology of resulting structures based on porous GaP is investigated. Obtained materials were assayed to evaluate the possibility of replacing activated carbon for electrodes of supercapacitors.

Keywords: semiconductors, porous semiconductors, supercapasitors, por-GaP, electro-chemical etching

INTRODUCTION

Supercapacitors are interesting for energy storage in hybrid electrical devices powered by batteries due to their high power density, excellent reversibility and a large number of rewrite cycles [1, 2]. Research in this area is aimed at the development of electrode materials, porous surface morphology and optimizing of specific parameters. Supercapacitor is a dielectric plate with the electrodes, where role of the plates carries a porous body, in which is a huge surface of the dielectric - gel (ionic liquid) that fills the cavities on the surface, the charge - ions, which are in the gel. Due to the fact that the surface is large, the capacity of the supercapacitor may be much more than the capacitance of capacitors.

Porous coal are conventionally used as the porous body. Nowadays, the manganese oxide is attracting the attention of scientists due to its low cost and environmental friendliness [3]. However, these materials have several drawbacks, among which a low conductivity and low

* Corresponding Author: PhD student Anton O. Belorus, Department of Micro- and Nanoelectronics, Saint Petersburg Electrotechnical University "LETI," Saint Petersburg, Russian Federation, Tel.: +7 931 291 69 85, E-mail: mop_92@mail.ru

specific capacity. Alternatively active semiconductor chips, namely porous structures grown on them are actively consideres. It is known that the ability to exhibit vapor formation have such semiconductors as Si, Ge, A_3B_5 structures. A special place in this listing takes gallium phosphide due to the ease of producing porous layers on the basis and ease of management of its morphological properties.

The use of porous materials in supercapacitors considerably increases the specific surface area, chemical and thermal resistance, conductivity, which leads to an increase in capacitance of supercapacitors to several thousands farads [3, 4].

Electrodes of supercapacitors are usually made of porous material, the inner specific surface area of which reaches 500—3000 m^2/g. What is important is the pore size of the electrode material (from 20 nm to 500 nm): at large active surface area decreases, at small — relatively large carriers (electrolyte ions) don't get in the pores pores, which are also often surrounded by solvent molecules.

Therefore, the present study was designed to evaluate the possibility of use of porous GaP as substrates for supercapacitors.

MATERIALS AND METHODS

To create a porous gallium phosphide (por-GaP) was used monocrystalline GaP, grown by Czochralski method. The thickness of the plates was 450 mm, the orientation (100). At the samples thin layer was formed by liquid phase epitaxy with thickness 20-50 μm, doped with Te.

Por-GaP was prepared in a single-chamber electrochemical cell by anodic etching using electrolyte solution based on hydrofluoric acid.

Preparation of the samples was conducted at the room temperature. During the experiment galvanostatic and potentiostatic regimes were used when selecting various process parameters: 1) the time of etching from 1.5 to 10 minutes 2) current density from 10 to 100 mA/cm^2.

Samples are thoroughly cleaned before the experiment. The purification process was consisted of the following steps: degreasing in acetone, with subsequent washing in distilled water and isopropanol. The morphology [5] of the porous structure investigated by the scanning electron microscope TESCAN MIRA II.

RESULTS AND DISCUSSION

From scanning electron microscopy (SEM) analysis for por-GaP:Te, it is seen that depending on various polishing surface, pore growth can be carried as in the surface regions with defects in the form of deepenings which are caused by chemical polishing, as well as with a developed pore system. Obtained porous semiconductor GaP:Te structures refers to macro- and mesoporous (pore size of 10 nm to 200 nm). The best parameters are observed in the samples which were etched for 10 minutes with current density 25 mA/cm^2 in galvanostatic regime (Figures 1, 2). The pores of these samples represent system of spongy columns system with crystallographic direction (100) with a square cross section. The pores form a circular system (Figure 1b), this effect requires further investigation the thickness of

the porous layer of these samples is about 28 microns. In consequence of that we can speak of a high specific surface area [6]. The pore size is about 20 - 30 nm, 30% porosity. The pores observed on the entire surface of the clusters. Irregularity of pore clusters areas are connected with access to the surface of the crystal dislocations and micro-defects.

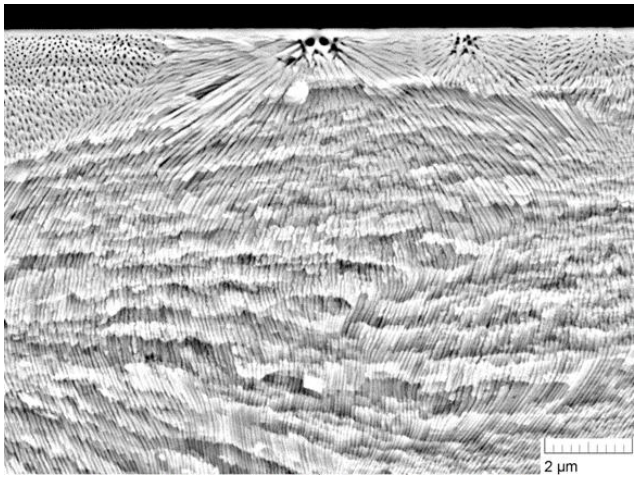

Figure 1. SEM cross-sectional image of obtained samples.

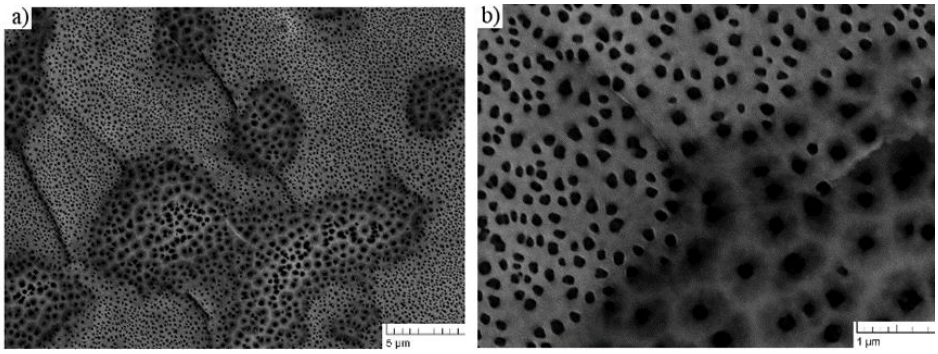

Figure 2. SEM images of obtained samples formed from secondary electrons:
a) view field 28.77 µm, b) view field 5.754 µm.

From earlier published works [7-12] it is known that with such pore size and thickness of the porous layer specific area reaches 800 m^2/g.

CONCLUSION

The paper presents a method of producing porous gallium phosphide. The morphology of the surface of the resulting structures and the possibility of the use of porous indium phosphide as a material for supercapacitor electrodes are analyzed. The study indicated the need for further research of porous materials before use of them for electrodes of supercapacitors instead of activated carbon. Further intensive study will focus on understanding of the mechanism of pore formation in porous semiconductors.

ACKNOWLEDGMENTS

The work was performed by the project contract code 0021109, competition UMNIK 15-12.

REFERENCES

[1] A. González, E. Goikolea, J. A. Barrena, R. Mysyk. Review on supercapacitors: Technologies and materials. *Renewable and Sustainable Energy Reviews*, Vol. 58, 2016. pp. 1189-1206.

[2] M. Vangari, T. Pryor, L. Jiang. Supercapacitors: Review of Materials and Fabrication Methods. *J. Energy Eng*. 2013. 10.1061. (ASCE)EY.1943-7897.0000102, pp. 72-79.

[3] A. F. Djadenchuk, V. V. Kidalov. Ispol'zovanie poristyh soedinenij A3B5 dlja obkladok superkondensatora (The use of porous compounds A3B5 for the supercondenser linings). *Journal of Nano and Electronic Physics*. 2015. vol. 7, № 1, 01021.

[4] F. Lufrano, P. Staiti Conductivity and Capacitance Properties of a Supercapacitor Based on Nafion Electrolyte in a Nonaqueous System. *Electrochem. Solid State Lett*. 2004. Vol. 7, A447.

[5] Lashkova N. A., Permyakov N. V., Maksimov A. I., et al. Local analysis of semiconductor nanoobjects by scanning tunneling atomic force microscopy. *St. Petersburg Polytechnic University Journal: Physics and Mathematics*. 2015. № 1. pp. 15-23.

[6] S. S. Nalimova, A. A. Bobkov, V. A. Moshnikov Fractal structure and electrical properties of percolation sensor layers. *Smart Nanocomposites*. 2016. vol. 7. № 1. pp. 21-26.

[7] Spivak Yu. M., Belorus A. O., Somov P. A., Tulenin S. S., Bespalova K. A., Moshnikov V. A. Porous silicon nanoparticles for target drug delivery: structure and morphology. *Journal of Physics*: *Conference Series*. 2015. vol. 643. p. 012022.

[8] Belorus A. O., Maraeva E. V., Spivak Y. M., Moshnikov V. A. The study of porous silicon powders by capillary condensation.. *Journal of Physics: Conference Series*. 2015. vol. 586. №1. p. 012017.

[9] P Belorus A. O., Koshevoi V. L., Spivak Yu. M., Levickij V. S., Moshnikov V. A. Photoluminiscence studies of porous silicon obtained by photoelectrochemical etching. *International Journal of Hydrogen Energy*. 2015. vol 23. (187). p. 126-132.

[10] Spivak Yu. M., Myakin S. V., Moshnikov V. A., Panov M. F., Belorus A. O., Bobkov A. A. Surface functionality features of porous silicon prepares and treated in different conditions. *Journal of Nanomaterials*. 2016. vol. 2016. p. 2629582.

[11] Bespalova K. A., Belorus A. O. Shaidarov L. V., Tret'akov A. V.. Izvestiya. Investigation of the influence of etch process upon the morphologe of the porous silicon particles. *SPbGETU «LETI»*. 2015. vol. 7. p. 10-13.

[12] Spivak Y. M., Maraeva E. V., Belorus A. O., Molchanova A. V., Nigmadzyanova N. R.. Preparation and investigation of porous silicon nanoparticles for targeted drug delivery. *Nanoscale-Arranged Syst*ems *for Nanotechnology*, 2015. p. 162-165.

Smart Nanocomposites
Volume 8, Number 1
ISSN: 1949-4823

NEW EMPIRICAL APPROACH FOR THE COVALENT BONDING CLASS OF (SYSTEM OF) ATOMS IN SIMULATION OBTAINING THIN FILMS PROCESS TECHNOLOGY

V. A. Tupik, V. I. Margolin, and Chu Trong Su*
Department of Radio Microelectronics and Radio Engineering
Saint Petersburg Electrotechnical University "LETI," Saint Petersburg, Russia

ABSTRACT

Obtaining thin films process technology to get high quality of a thin film or some specific coating is one of the actual challenges today. One promising way was shown in this paper. It's using a computer simulation with an appropriate calculation method. In more detail, using the numerical calculation "top-down" approach is more suitable to all classes of researchers including young ones, i.e., by using empirical and classic physics was shown. Based on the specific of atomic orbital for anisotropic bonding a new model of an atom and interatomic interaction of bonding were created in order to an adequate description of thin films growth process. In this work the results of computer simulation were shown, as well as limitations of the new given algorithm and a discussion of it.

Keywords: empirical interatomic potential, computer modeling, thin film process technology

INTRODUCTION

Obtaining thin films process technology plays a crucial role in many nowadays applications in various areas. Accordingly there were more new basic principles and new elements based on newfound materials created. For example, lasers based on heterostructure semiconductor, graphene, fullerene, diamond-like carbon, metamaterial, plasmonic, photonic, spintronic, terahertz material are actually discussed and it is also made use of in many applications in recent time. But synthesis and optimization for those obtaining process technologies most based on the result of natural experiments. One reason for these kind of studies is the difficulty in the occurring process (in nonequilibrium state, includes phase transmission, random and self-organization processes).

* Corresponding Author E-mail: chusu171@mail.ru

Today, based on a growing demand of thin films of high quality, the role of computer simulation is increasing in this area primarily for a better understanding of them. Furthermore experiments for synthesis and optimization in technological processes can be visualized more rapid and flexible by a computer simulation. Nowadays there are two approaches for solving this task by developing computer simulations. They are called the "top-down" and "bottom-up" approach. The "bottom-up" approach is based on the results of quantum physic at the first principles, and the "top-down" approach is based on the results of empirical approximating laws with classical physic. As is known, both of them have own advantages and disadvantages, but in author's opinion, owing to the limited access to use the power computation machine in the currently world for all researchers especially for young ones, the "top-down" approach plays a bigger role for the majority of them as a compromise of accuracy, reliability and an acceptable calculation time. So in this case we need to use more appropriate laws and rapid calculating algorithms to solve our tasks in trend of increasing requirement of target function, i.e., improving the quality of thin film.

Some regular numerical methods, which are used for this task, are molecular dynamics simulation, simulation based on Monte-Carlo method with pair potential energy like Lennard-Jones, Morse, Tersoff potential and their modification for many-body potential, etc. As is known, interacting bonds of a complex molecule are more dependent on influences of orbital configurations, the interaction between them. Then there are many problems of obtaining more various polymorphism and polytypicism and in the end make more structures with different physicochemical characteristics. In this case the above listed methods doesn't take into account sufficient specific characteristic of atoms or molecules, or in author's opinion it doesn't take visual process behavior of a system of atoms or have complex description for computational calculation or make hard to understand by conventional physical laws [1-3]. In this present paper we want to propose our new approach, which intend to improve above mentioned facts.

MODELS OF ATOM AND INTERATOMIC INTERACTION BONDINGS

As a result of x-ray radiation on atom and molecule shows that the role of their interatomic bondings is determined by the external electrons and their orbital configuration. For a simple atom, which can be described by an isotropic pair- interaction potential we can use all methods which are mentioned above for solving the problem of obtaining thin film processes. For example, we used many methods in many stages of this process. These are the mathematical calculation for macro index, the molecular dynamics simulation for taking into account the interatomic interactions in bell-jar in mass transfer process and the combination of Monte-Carlo method with quasi Newton's optimal method for modeling of thin film growth process [4-7]. One reason that taking the task became more difficult belongs to the specificity of obtaining thin film process. This means the number of particles will increase, many conditions and process parameters has to be taken into account and the number of substrate particles is large. Furthermore the periodic boundary conditions [3] cannot be used during the thin film growth process.

The object of this work is a new model, which is created for an adequate description of the anisotropic bonding of an atom. Especially for one, which has four bondings with another atom (hybrid orbital sp3), as shown in Figure 1a). However based on this model we can

realize many types of the hybridization as sp2, sp in a simple way [8]. The idea of this model is, that there are four identical orbitals in one atom, which repulse each other and form the angle φ_0^o, one orbital attract with the nucleus at determined distance r_1 (as shows in Figure 1. a). One atom relates (in this case attraction) isotropic with another one, when they have a certain distance r_2. This distance has to be longer than the given threshold length $d_{threshold}$ (as shows in Figure 1. c). In other words in this case we used a usual pair potential bonding. In the opposite case have an anisotropic relation, i.e., dependence on direction of two connected atoms, and presence of unconnected and connected orbitals (as depicted in Figure 1. b). The detailed description was shown beneath.

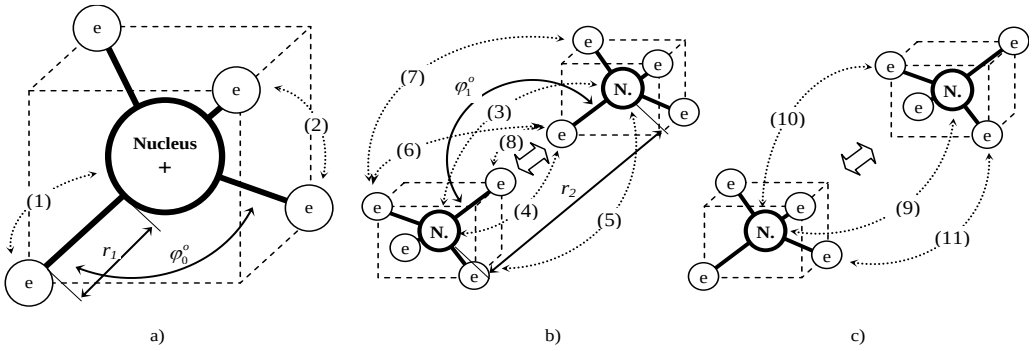

Figure 1. New model of an atom (a) and two cases of two related atoms: $d \geq d_{threshold}$ (b) and $d<d_{threshold}$ (c). There are shown 11 various types of bonds in this model.

Simplified Algorithm

1. Determine the hybridization orbital type sp3, sp2 or sp (in this work we will discuss just for hybrid sp3).
2. Describe the interaction external electron orbital (further it was shorten as electron) with electron, electron – nucleus (more accurately internal part of atom excluding external electron orbitals) and nucleus – nucleus (As shows in Figure 1) (i.e., empirical potential is given).
3. Generate particle with random orientation of orbital configuration. Give orbital and atom bonding length.
4. Determine the working particle with Monte-Carlo method; calculate the current distance to another particle.
5. Find the potential value for current particle according to the description of potential interaction (it will be proposed beneath).
6. Determine the optimal motion for all part of these particles (nucleus and four orbitals) with quasi-Newton's optimal method (quasi- means that it is worked with the lattice calculated coordinate) – as rotation motion, for particle – as forward motion, and for group related particle from 26 possible tentative lattice nodes, look for the direction, where this system have minimum system energy.
7. Exceeds the number of tentative the given number?
8. If "no" turn to step 4.
9. If "yes" end the program.

As a limitation of this algorithm it can be noted that: It is not possible to take the kinetic energy of a particle into account, this process is simulated in not real time, because we used the Monte-Carlo method and the type of orbital hybridization doesn't change during computer simulation process.

Description of the interaction of electron with one other, electron with nucleus and nucleus with nucleus - Empirical potential was proposed as following:

For internal atom:

Nucleus with electron (interacting line 1 – in Figure 1): $U1(r) = U_{01}\left(r^{-m} - r^{-n}\right)$;

Electron orbital with another electron (interacting line 2 – in Figure 1): $U2(r) = U_{02}r^{-2}$;

For interatomic interaction:

If the minimal distance between two particles is smaller than threshold length $d_{\min} \le d_{threshold}$:

Nucleus with nucleus (interacting line 3 – in Figure 1), nucleus with connected electron (interacting line 4 – in Figure 1), nucleus with unconnected electron (interacting line 5 – in Figure 1), connected electron with unconnected electron (interacting line 6 – in Figure 1) and unconnected electron with unconnected electron (interacting line 7 – in Figure 1) have the following equation of interacting type: $Ui(r) = U_{0i}r^{-2}$;

Connected electron with connected electron (interacting line 8 – in Figure 1): $U3(r) = U_{03}\left((r+\sigma_0)^{-m} - (r+\sigma_0)^{-n}\right)$;

The parameter σ_0 ($\sigma_0 > 0$) was given for the optimal distance between two connected electrons was zero.

If the minimal distance between two particles is bigger than threshold length $d_{\min} > d_{threshold}$:

Nucleus with nucleus (interacting line 9 – in Figure 1), nucleus with electron (interacting line 10 – in Figure 1), electron with electron (interacting line 11 – in Figure 1) have the next equation of interacting type: $Ui(r) = U_{0i}\left(r^{-m} - r^{-n}\right)$;

All linear dimensions are normalized by $r = r_{real}/\sigma_0$. Where, U_{0i}, $d_{threshold}$, m, n, σ_0 are adjustable parameters for the working material and each type of bonding, $d_{threshold}$ as usually offence the distance is longer than $3\sigma_0$, (m, n) as in the Lennard-Jones have the values (12, 6).

RESULTS AND DISCUSSION

In order to see how this model works, a computer simulation is carried out with the following conditions: 50 particles with given coordinates of atoms with random orbital configuration sp3. The initial structure was , which is shown in Figure 2a, where the coordinates of atoms were given so, that each atom has a distance to another that is longer than the threshold distance $d_{threshold}$ to be a connective atom. In Figure 2c the result of computer simulation for this case in the end of process is shown.

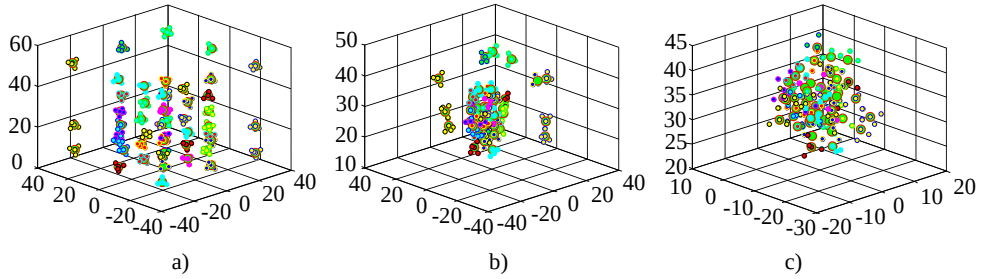

Figure 2. Tentative computer experiment for behavior of 50 unique atoms in initial moment (a), in intermediate moment (b) and obtained finished structure (c). The various colors of atoms or orbitals have been chosen for improving of visualization.

The calculation of some feature distributions of the obtained structure is shown in Figure 3 to give proof of the accuracy of this computer simulation and model.

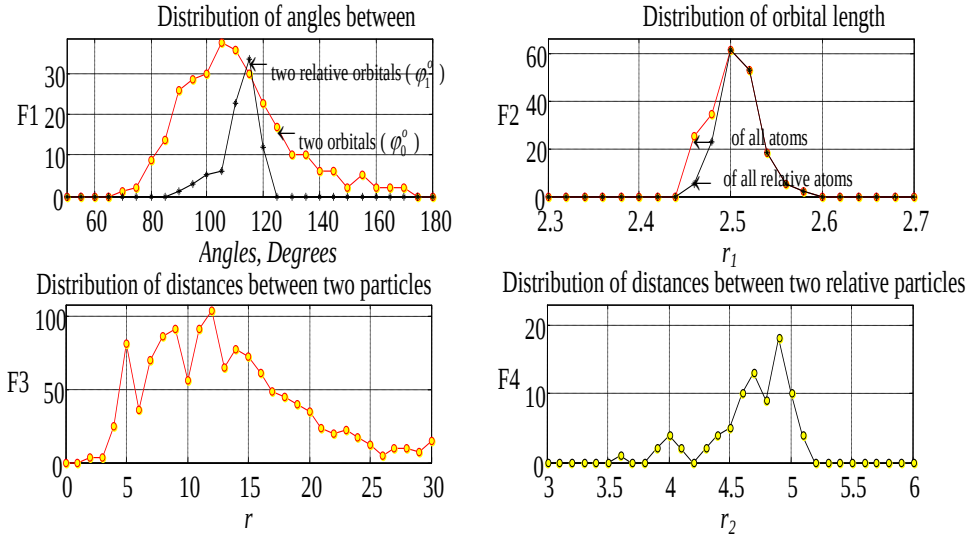

Figure 3. Some characteristic distributions of obtained structure (Figure 2. c). Fi (I = 1÷4) – It's qualities of orbitals or atoms have the distance or angle in x-axis.

CONCLUSION

The development of computer science and engineering is promising in the area of nanotechnology and thin film technology in particularly. For a large number of researchers, who have limited access to use the modern calculation machine, using the created numerical model with empirical interatomic potential is more actually. This model can take the anisotropic bonding, length and angular connection between two particles into account. Furthermore it is based on a new approach and an expansion for some kind of atom as sp and sp2 or more complex orbital hybridization is possible. Next the model has to be tested more detailed in many following computer simulations.

REFERENCES

[1] J. Tersoff, New empirical approach for the structure and energy of covalent systems, *Physical Review B*, Volume 37, Number 12 (1988) 6991-7000.

[2] Ximaowei Li, Peiling Ke, He Zheng, Aiying Wang, Structure properties and growth evolution of diamond-like carbon films with different incident energies: A molecular dynamics study, *Applied Surface Science* 273(2013) 670-675.

[3] M. Rieth, Nano-Engineering in Science and Technology: An Introduction to the World of Nano-Design, Series on the Foundations of Natural Science and Technology. Vol. 6. New Jersey: *World Scientific*. 2003. 163 p.

[4] Chu Trong Su, D. A. Babichev, *Mass transfer process simulation during thermal vacuum sputtering of thin films*. Book of reports of 67th sci-tech conference of higher-education teaching personnel of LETI University, pp. 29-33. (in Russian).

[5] V. I. Margolin, Chu Trong Su, *Computer simulation of thermal vacuum sputtering process using molecular dynamics method*. Public registration of computer program. Registration number 2015610057. (in Russian).

[6] V. I. Margolin, Chu Trong Su, *Computer simulation of thin films growth process in potential field (Thin film growth)* (Rost tonkih plenok)]. Public registration of computer program. Registration number 2015610052. (in Russian).

[7] Tupik V. A., Chu Trong Su, I. Steblevska, The simulation and the optimization of the quality function of the process of formation of functional coatings and films, *Proceedings of the Russian Universities*: *Radioelectronics*– 2015. – N. 5.15-19.

[8] Zvonimir B. Maksic, Symmetry, hybridization and bonding in molecules, *Computer & Mathematics with Applications*, V. 12, I. 3-4, Part 2 (1986) 697-723.

Smart Nanocomposites
Volume 8, Number 1
ISSN: 1949-4823

GROWTH AND PROPERTIES OF Al_2O_3 NANOLAYERS ON III–V SEMICONDUCTORS

Yu. K. Ezhovskii*
Saint Petersburg Technological Institute (Technical University),
Saint Petersburg, Russia

ABSTRACT

It describes the process of forming a nanolayers of aluminum oxide, obtained by atomic layer deposition (ALD-technology) on the surface of GaAs, InAs and InSb. The conditions for layer-by-layer growth of surface nanostructures are established, and some of their dielectric parameters are evaluated.

Keywords: atomic layer deposition, nanolayers of aluminum oxide, to obtain, the properties

INTRODUCTION

Advances in the fabrication of various nanodevices depend crucially on the development of processes for the synthesis of appropriate materials and knowledge of the fundamental mechanisms underlying the behavior of nanosystems [1]. In particular, intensive effort has been concentrated on novel electronic technologies for the atomic-scale fabrication of solid-state nanostructures.

The advent of molecular beam epitaxy [2] has considerably extended the possibilities of vacuum technology and has made it possible to overcome a number of challenges in microprocessor engineering. At the same time, though offering a number of indisputable advantages, molecular beam epitaxy requires very costly equipment, which has stimulated the search for alternative approaches.

In recent years, atomic layer deposition (ALD) has been the subject of intense attention as a process for growing high-quality ultrathin layers [3–5]. The advantages of this technology and its potential for fabricating submicron-sized components of integrated devices have been demonstrated in several studies [6-8]. ALD takes advantage of surface chemical processes previously referred to as molecular layering, whose physicochemical foundations were developed as early as the 1970 [9]. Chemical processes for the synthesis of low-

* Corresponding Author E-mail: ezhovski1@mail.ru

dimensional systems are an integral part of the rapidly growing chemical nanotechnology of novel materials for a variety of specialty applications, particularly for nanoelectronic systems.

MATERIALS AND METHODS

The use of surface chemical reactions, basic to the ALD process, allows one to grow low dimensional structures with their composition and thickness controlled on a monolayer scale. In this approach, the growth of oxide layers involves, as a key step, self-limiting chemisorption of a metal halide (MCl_n) and water vapor under limiting surface coverage conditions. For example, the process on hydroxylated surfaces (symbol |) can be run according to the schemes

$$|\text{-OH})_m + MCl_n \rightarrow |\text{-O-})_m MCl_{n-m} + mHCl. \quad (1)$$

$$|\text{-O-})_m MCl_{n-m} + (n-m)H_2O \rightarrow |\text{-O-})_m M(OH)_{n-m} + (n-m)HCl, \quad (2)$$

The value of m depends on the surface density of hydroxyls; e.g., $m \approx 2$ for silicon surfaces [10]. Repeating reactions (1) and (2) many times and intermittently removing the reaction products and excess reactants, one can grow an oxide layer of predetermined thickness. In such processes, two important conditions must be met. First, the growth temperature of AB film, T_s, must meet the relation $T_A^{\bullet}, T_B^{\bullet} \leq T_i \leq T_{AB}^{\bullet}$, where T^*_A , T^*_B and T^*_{AB}, are the critical condensation temperatures of components A and B and compound AB, respectively. This condition rules out direct condensation of component A or B, so that the process is limited to the formation of a chemisorbed layer.

Second, the surface reactions (1) and (2) should take place under nonequilibrium conditions in order to reach completion. To this end, surface hydroxyls must exhibit sufficiently high reactivity. Evaluation of their reactivity on gallium arsenide using the Taft inductive constants gives $\sigma_i = 5.1$ [11]. This value slightly exceeds that for silica, on which such reactions occur rather readily [9]. It is, therefore, reasonable to expect that hydroxyls on such surfaces will exhibit sufficient reactivity with silicon chloride and aluminum chloride vapors ($\sigma_{C\ l} = 2.88$). To raise the reaction yield in step (2), triethylamine can be used as an exchange activator, which is introduced together with water vapor. In addition, this approach makes it possible to stabilize the hydroxyl layer and to reduce the layer-by-layer growth temperature [12].

Oxide nanolayers were grown using reactions (1) and (2), by sequentially exposing the surface of the substrates to appropriate metal chloride (P = 1–10 Pa) and water ($P \approx 100$ Pa) vapors and intermittently removing the reaction products and excess reactants. The process was run in a flow reactor evacuated to a residual pressure no higher than 0.1 Pa.

The thickness of the deposited layers was evaluated from the ellipsometric parameters Δ and Ψ in the Drude–Tronston one layer model [13]. Δ and Ψ were measured using a fixed-compensator ellipsometer in the PQSA arrangement [14]. As a linearly polarized light source, we used a 632.8 nm LG-75 laser beam, which was magnetically modulated to improve the measurement accuracy. The uncertainty in the ellipsometric parameters was within ±0.01'. Ellipsometric determination of the refractive index of the grown structures was used to assess

their composition, which was also determined by X-ray photoelectron spectroscopy (XPS) on HP-5950A (AlK_α X-ray source, $E_{K\alpha}$ = 1486eV) and SER-1 (MgK_α X-ray source, $E_{K\alpha}$ = 1253eV) spectrometers. The dielectric parameters of the layers were determined on both the substrates and ~0.1 μm thick aluminum films grown on silicon by vacuum evaporation. The study of the electrical parameters of the layers was carried out by static and dynamic current-voltage characteristics (CVC) in a metal-insulator-metal when used as a substrate and one of the electrodes of the aluminum matrix. As used counterelectrode liquid gallium alloy of indium (In: Ga 5: 1). Static current-voltage characteristics were recorded using electrometers EM-1 and IT-12 with an input impedance of the $10^{15}\,\Omega$. Dynamic current-voltage characteristics were studied on a triangular waveform 0,1-2Hz frequency (G6-36 generator) through a measuring resistor with the registration on the storage oscilloscope S8-13.

RESULTS AND DISCUSSION

Our results on the growth kinetics of the oxides under consideration at various substrate temperatures (Figure 1) and reactant vapor pressures indicate that the thickness of Al_2O_3 layers, *d*, is a linear function of the number of deposition cycles, *N*. This indicates that the hydroxides involved retain their reactivity and that the same amount of the synthesized compound is deposited in each cycle. The effect of substrate orientation was insignificant. In all instances, the layer thickness was proportional to the number of surface processing cycles by reactions (1) and (2):

$$d = d_0 N. \tag{3}$$

Here, the proportionality factor d_0 is the average increase in layer thickness per cycle of surface processing with one of the reactants and characterizes the structure of the deposited layer. This parameter is a key characteristic of the deposition process and allows one to determine the surface coverage and to gain insight into the mechanism of film growth.

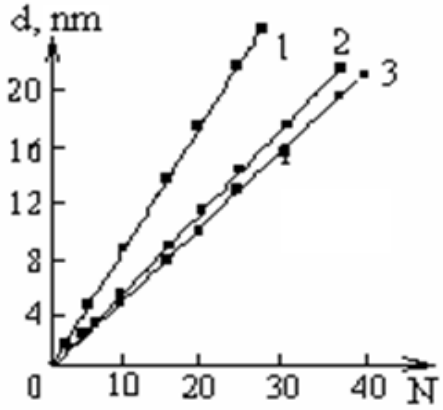

Figure 1. Layer thickness vs. number of deposition cycles for Al_2O_3 layers grown on (100) GaAs at a vapor pressure of 1.3 Pa and T = (*1*) 403, (*2*) 453, and (*3*) 523 K.

Analysis of the $d(N)$ data obtained at various substrate temperatures allowed us to assess the effect of thermal conditions on the layer growth parameter (Figure 2), to clarify the growth mechanism of the nanostructures, and to identify the layer-by-layer growth conditions.

The high d_0 values for alumina layers, far above the average size of aluminum–oxygen tetrahedra, are due to the fact that they grow through chemisorption of the Al_2Cl_6 dimer, which prevails in aluminum chloride vapor. Reactions (1) and (2) may then follow two major schemes (schemes 4a,b with the metal predominantly in fourfold coordination):

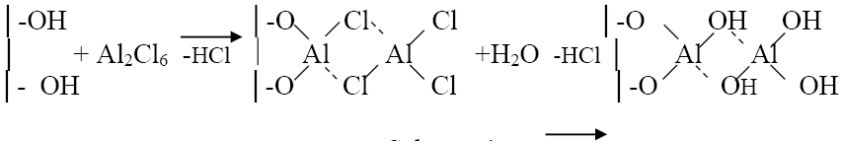

(4a)

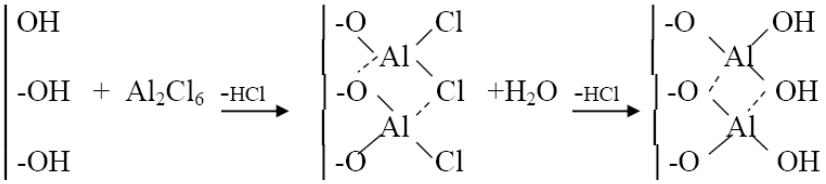

(4b)

Which of these surface-reaction paths prevails depends on the topography of the hydroxyl layer. At reduced substrate temperatures (T_s < 400 K), where conditions (I) are not met, the density of surface hydroxyls is high, and adsorbed water molecules may be present, Al_2O_3 layers grow predominantly through reactions in the adlayer. Aluminum chloride dimmers may then have various orientations, and the high d_0 values at T_s < 400K point to polymolecular sorption of reactants under such conditions. Only at T_s > 400K for InAs and InSb or T_s > 475K for GaAs does the layer growth parameter approach twice the size of the aluminum–oxygen tetrahedra. This gives grounds to assume that, under these conditions, Al_2O_3 layers grow in layer-by-layer mode and the process is dominated by reaction (Scheme 4a) with m = 2 (Figure 2).

The drop in d_0 at T > 473K for InAs and at T > 453K for InSb seems to be caused not so much by the reduction in the density of surface hydroxyls as by the thermochemical instability of these materials in the halide atmosphere. This is evidenced by the fact that the narrowing of the layer-by-layer growth ranges of Al_2O_3 correlates with the heats of formation of GaAs, InAs, and InSb (Figure 2). Note that the general trends in the ALD of Al_2O_3 on GaAs, InAs, and InSb are similar to those for silicon and other oxide substrates [13], indicating that these processes follow the same general mechanisms.

Structural characterization of the deposited films by electron diffraction showed that, over the entire temperature range studied, the Al_2O_3 layers less than 100nm in thickness were amorphous at T_s < 450K and contained α-Al_2O_3 at higher temperatures. In all cases, increasing the Al_2O_3 layer thickness and deposition temperature led to the formation of crystalline domains as supramolecular structures.

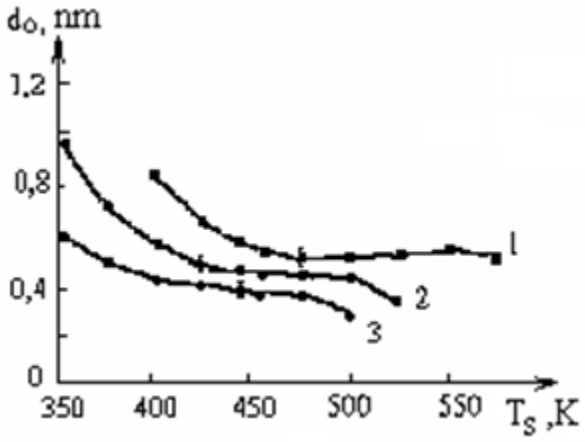

Figure 2. Effect of substrate temperature on d_0 for Al_2O_3 layers grown on (1) GaAs, (2) InAs, and (3) InSb at a vapor pressure of 1.3 Pa.

From the observed broadening of electron diffraction rings, the average crystallite size was evaluated to be 2 to 20 nm, depending on the layer thickness. The crystallites most likely consisted of oxide groups that had formed on periodic arrays of hydroxyl groups on homogeneous surface areas. Heat treatment of alumina layers on GaAs at 623K considerably increased the intensity of the electron diffraction rings from the layers and sharply increased the crystallite size, leading to almost complete oxide crystallization. Therefore, the polycrystalline layers contained an amorphous phase between the crystallites, which was involved in the crystallization process. This conclusion is supported by the fact that the deposited films showed no preferential orientation.

The XPS spectra of the oxide layers did not show any peaks at binding energies of 190–200 or 260–270 eV, characteristic of the Cl 2*s* and 2*p* levels. The observed broadening of the oxygen levels (530–531eV) indicated the presence of hydroxyl groups. Note that, at oxide layer thicknesses above 8 nm (electron escape depth), the XPS spectra showed no signal from the substrate, indicating that the layers more than 8 nm in thickness were continuous.

From the peak areas for oxygen (E_b =530–531eV) and aluminum (E_b = 74.6eV for Al2*p* and E_b = 118.8 eV for Al2*s*), we evaluated the oxygen-to-metal ratio in the oxide layers grown on GaAs at different temperatures. The results are presented in Table 1.

It seems likely that the increased oxygen content at low and elevated deposition temperatures is due to hydration of the oxides and to the contribution of the oxide layer of the substrate, respectively. The frustrated total internal reflection IR spectra of the alumina films grown on GaAs at *T*s = 553 K on the whole correlated with the XPS results. The spectra showed well-resolved absorption peaks at ν = 744 and 835 cm^{-1}, due to Al–O bonds with the aluminum in six- and fourfold coordination [16].

The dielectric properties of the nanolayers were studied at thicknesses above 10 nm, because the electrical conductivity was then essentially independent of the layer thickness and was determined by the deposition temperature (Figure 3). In all cases, increasing the substrate temperature reduced the conductivity to a level characteristic of layer-by-layer growth of the nanostructures. The increased conductivity of the layers at T_s <400K is most likely due to the hydration of the oxides and correlates well with the oxygen-to-metal ratios extracted from the XPS data for the layers (Table 1).

Table 1. Oxygen-to-metal ratio in alumina layers grown at different temperatures

T_s,K	423	473	523	553	573
[O]/[Al]	4	2,3	1,8	1,5	1,5

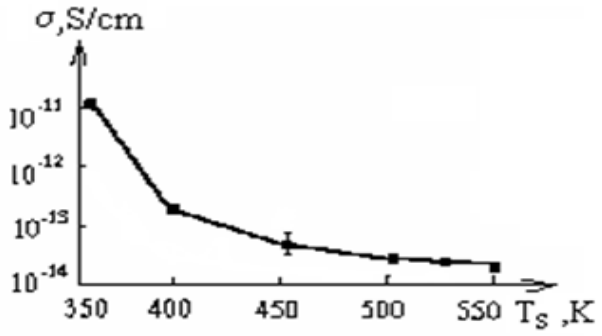

Figure 3. Electrical conductivity as a function of deposition temperature for Al_2O_3 layers; d = 25–30 nm, $E = 10^5$ V/cm.

Table 2 summarizes the main dielectric properties of the oxides grown in layer-by-layer mode.

Table 2. Dielectric properties of Al_2O_3 nanolayers

Oxide	σ, S/cm	$E \cdot 10^{-6}$, V/cm	ε	tgδ
Al_2O_3	10^{-13}–10^{-14}	5	8–10	0.005

CONCLUSION

Aluminum oxide nanolayers were grown on GaAs, InAs, and InSb substrates by ALD. Comparison of the present experimental data with previous results for other substrate materials and other oxides [13] shows that the growth of Al_2O_3 nanolayers on III–V semiconductor substrates follows the same general mechanisms, inherent in this process. In particular, analysis of the effect of deposition temperature indicates that the growth of oxide nanostructures via sequential chemisorption of metal halide and water vapors may follow three mechanisms: reaction between components in a polymolecular adsorbed layer, leading to the formation of hydrous oxides; sequential growth of monomolecular layers (layer-by-layer growth mechanism); and formation and subsequent growth of two-dimensional islands. Aluminum chloride chemisorbs in the form of dimers without thermal activation. This leads to high d_0 values for Al_2O_3 at any temperature.

Results of evaluation of the main characteristics of dielectric films obtained under layer growth showed that Al_2O_3 nanolayers have sufficiently high performance characteristic of aluminum oxide. This allows you to use the method of molecular layering to create a high-quality dielectric structures, including multilayer, in the sub-micron element base of micro- and nanoelectronic systems, for example, gate dielectric of MOS structure, capacitance elements and barrier layers.

REFERENCES

[1] M. C. Roco, S. Williams, and P. Alivisatos (Eds.) *Nanotechnology Research Directions: Vision for Nanotechnology in the Next Decade*. (Kluwer, Boston, 2000; Mir, Moscow, (2002).
[2] Chang, L. L. and Ploog, K., Eds., *Molecular Beam Epitaxy and Heterostructures*, Amsterdam: Nijhoff, (1985).
[3] Suntola, T., *Mater. Sci. Rep.*, vol. 4, no. 7, p. 261. (1989).
[4] Seidel, T., Londergan, A., Winkler, L., *Solid State Technol.*, no. 5, p. 67. (2003).
[5] Nishizava, J. and Kurabayash, T. *Chem. Sustainable Dev.*, no. 8, p. 5. (2000).
[6] Ming, X., *Solid State Technol.*, vol. 44, p. 70. (2001).
[7] Gelatos, J., Chen, L., Chung, H., Thakur, R, *Solid State Technol.* vol. 2, p. 44. (2003).
[8] Puurunen, R. L. *J. Appl. Phys.*, vol. 97, no. 12, p. 121301. (2005).
[9] Aleskovskii, V. B., *Vestn. Akad. Nauk SSSR*, no. 6, p. 48. (1975).
[10] Ezhovskii, Yu. K., Vainshtein, P. M., *Zh. Prikl. Khim.* (St. Petersburg), vol. 71, no. 2, p. 227. (1998).
[11] Ezhovskii, Yu. K., *Usp. Khim.* vol. 73, no. 2, p. 209. (2004).
[12] Ezhovskii, Yu. K., Klusevich, A. I., *Neorg. Mater.* vol. 39, no. 10, p. 1230. (2003), vol. 39, no. 10, p. 1062] (2003).
[13] Ezhovskii, Yu. K., *Khim. Fiz.* vol. 24, no. 4, p. 36. (2005).
[14] Azzam, R. and Bashara, N. *Ellipsometry and Polarized Light*, Amsterdam: North Holland, (1984).
[15] Gromov, V. K., *Vvedenie v Ellipsometriyu* (*Introduction to Ellipsometry*), Leningrad: Leningr. Gos. Univ., (1986).
[16] Tsyganenko, A. A., Mardilovich, P. P., Lysenko, G. M., and Trokhimets, A. I., *Usp. Fotoniki*, no. 9, p. 28. (1987).

Smart Nanocomposites
Volume 8, Number 1
ISSN: 1949-4823

SAXS AND WAXS INVESTIGATIONS AND THERMAL ANALYSIS OF STRUCTURAL TRANSFORMATION OF POLYORGANOSILOXANE AND OF THE SYSTEMS OF POLYORGANOSILOXANE – SILICATE AND POLYORGANOSILOXANE – OXIDE WITHIN THE TEMPERATURE RANGE FROM 20° TO 600°C

Irina B. Glebova*, MD, and Valery L. Ugolkov, PhD
Institute of Silicate Chemistry of the Russian Academy of Sciences,
Saint Petersburg, Russia

ABSTRACT

The structural transformations of polyorganosiloxane (PDMPhS) and of the systems of PDMPhS – silicate and PDMPhS – oxide were investigated by the SAXS and WAXS methods. For PDMPhS, within the temperature range from 20 to 300ºC, dependences of the scattering intensity on the scattering angle are fully reversible. At 150-160ºC, a clearly expressed kink connected with the structural unfreezing is observed. In the case of PDMPhS filled by silicates, this process shifts to higher temperatures and, in the case of oxide, this effect becomes less pronounced and depends on the concentration. According to data of the SAXS and WAXS investigations and of the thermal analysis, the intense destruction processes begin at the temperature higher than 350° - 450°C. Silicates decrease the loss in weight of composites by 15 – 20%, whereas Cr_2O_3 does not change it. Therefore, it is advisable to use about 50% of silicates and less than 12% of Cr_2O_3 for OCM synthesis.

Keywords: SAXS, WAXS polymers, polyorganosiloxanes, silicate, oxide

1. INTRODUCTION

The complex approach joining different methodologies of studies plays a significant role for investigation of polymer and of polymer composite materials [1-2]. Organosilicate materials (OSM) have long ago and confidently found their place among other composite

* Corresponding Author E-mail: iraglebova@mail.ru

materials [3-4]. They are successfully used in some different industry fields, building and developing of various metal constructions as thermo-stable, anticorrosive, deicing, isolating, radiation-stable coverings and materials. Polymers of silicone lacquers such as polyorganosiloxanes, silicates and metal oxides are obligatory components of OSM. One of the main properties of OSM is their thermo-stability. Therefore, of great interest is investigation of structural transformations both of polyorganosiloxane and of filled polyorganosiloxane during their heating in a wide temperature range, beginning from room temperature up to 600°C, with the help of devices of small-angle X-ray scattering, which were constructed in the Institute of Silicate Chemistry RAS. One of these two devices, due to the horizontal position of a sample, allows one to investigate samples in the liquid and melt phases. In both the devices, it is possible to heat a sample directly in the camera in which it is placed.

2. RESEARCH GOAL

The goal of this study is to research structural transformations of polyorganosiloxane and of polyorganosiloxane – silicate and polyorganosiloxane – oxide systems in the process of heating within the temperature range from 20° to 600°C and to reveal the effect of nature of different fillers on the thermal behavior of the polymer. This will allow one to choose proper fillers, their concentrations, as well as the regime of thermo-treatment and of industrial application of the composites.

3. EXPERIMENTAL PART

This study presents the results of investigation of polydimethylphenilsiloxane (PDMPhS), of some systems of PDMPhS with chrome oxide, kaolin and muscovite, taken at different concentrations.

Structures of the polymer and of the filled polymer were investigated by the small-angle X-ray apparatus with a high-temperature attachment. The CuKα - radiation was used. The SAXS intensity was measured at scattering angles from $q = 0.095\ nm^{-1}$ to $q = 5.28\ nm^{-1}$. The samples were investigated within the temperature range varying from 20 to 600°C. The SAXS curves were measured at temperatures which differ by 50-100°. The thermal analysis was performed with INSTRUMENT:NETZSCH STA 429 (CD), by using the sample mass about 10 mg, air as a protective gas, and a corundum crucible. The heating velocity was 10º/min up to 600ºC and 20º/min from 600ºC to 900ºC.

It should be noted that data on changes in the structure can be obtained from analysis of temperature dependences of the intensity (I) SAXS measured at fixed angles equal to $q = 0.12\ nm^{-1}$ и $q = 4.74\ nm^{-1}$. At the angle equal to $q = 0.12\ nm^{-1}$, I SAXS is sensitive to changes in the micro-heterogeneous structure, i.e., to changes in the regions of heterogeneity. At the angle equal to $q = 4.74\ nm^{-1}$ the changes of I SAXS are chiefly connected with changes in scattering by thermal fluctuations of density.

The change in the angle dependence of the SAXS intensity (I) of the PDMPhS sample with the increase in temperature shows that, within the temperature range of 20-300ºC, the dependence of I on the scattering angle is fully reversible.

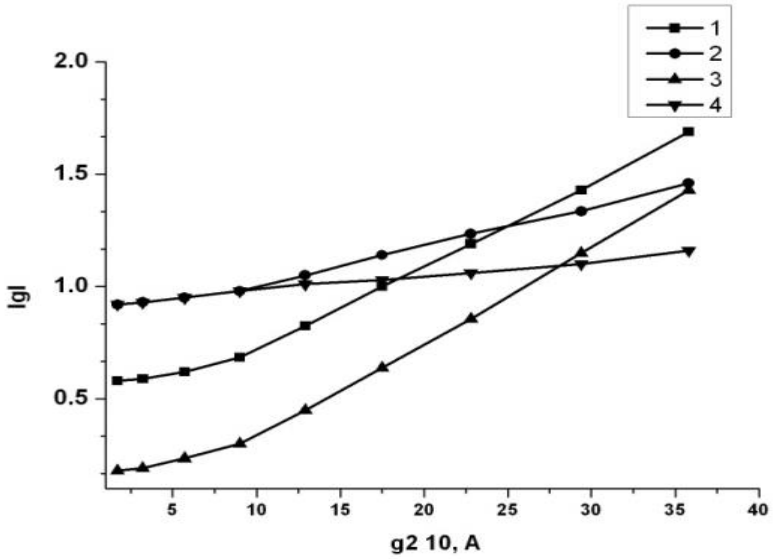

Figure 1. Dependence of lgI (SAXS) on q^2 at the different temperatures of the polymer heating: 1 – 210, 2 – 400, 3 – 550, 4 - 630°C.

Figure 1 shows the dependence of lg I SAXS on q^2 at the different temperatures for PDMPhS without fillers. At scattering angles larger than q = 2.37 – 2.96 nm^{-1}, lgI depends linearly on q^2, where wave vectors $q = 4\pi \cdot \sin\theta/\lambda$ (θ is the half angle of scattering and λ is the wavelength of X - ray radiation, equal to 0.154 nm for a copper anode). Such dependence is characteristic for homogeneous samples; this means that in the above range of scattering angles, the I SAXS is due to only scattering by thermal fluctuations of the density and to the contribution of large-angle scattering. In the range of small-angle scattering, one can see a deviation of the I SAXS from the values obtained by linear extrapolation of the dependence of lgI on q^2. This implies that, in the range of small-angle scattering, there exists an additional scattering that can be caused by the presence in the sample of heterogeneity regions with characteristic dimensions of the order of 5-10 A°.

When the temperature increases up to 400-450°C, the I SAXS increases within the all range of scattering angles, but the behavior of the curves remains relatively unchanged. With the following increase in the temperature, the intensity decreases at large angles and increases at small angles. Such behavior of the angular dependence of the I SAXS can be explained by an increase in the number of heterogeneities.

Figure 2 demonstrates the temperature dependence of I SAXS at the fixed angle of scattering equal to q = 4.74 nm^{-1}, I (q = 4.74 nm^{-1}), for polymer samples and for samples of the polymer with different fillers.

On the temperature dependence of the I SAXS of the polymer, one can clearly see a kink at 150-160°C. At temperatures 450-500°C, the increase in the I SAXS stops and then it decreases with the following increase in the temperature.

In the case of a sample containing kaolin, this kink on the temperature dependence of the I SAXS is also observed, but now at the temperatures ~ 200-210°C; whereas the temperature of the effect decreases by 75-100°C with the increase in the temperature. For the samples containing Cr_2O_3, this kink on the temperature dependence I (q = 4.74 nm^{-1}) is not observed.

The temperature corresponding to the maximum values I SAXS decreases at high content of Cr_2O_3, i.e., the temperature of the beginning of structural transformations in the polymer decreases.

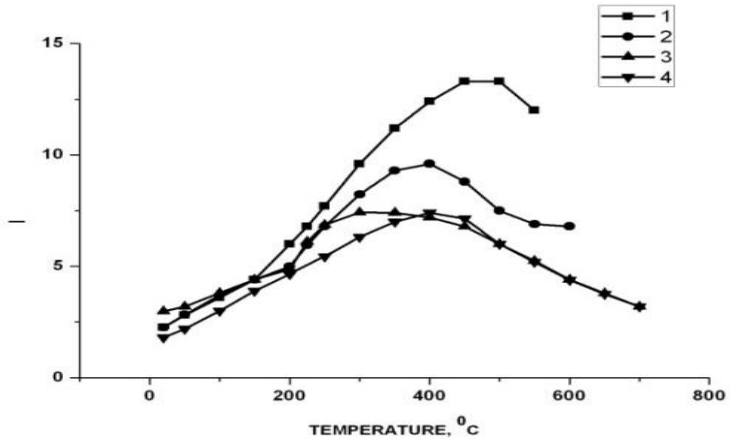

Figure 2. Temperature dependence of the intensity at the scattering angle 400′ by the samples: 1 – PDMPhS, 2 – PDMPhS +50% of kaolin, 3 – PDMPhS + 12% of Cr_2O_3, 4 – PDMPhS + 20% of Cr_2O_3.

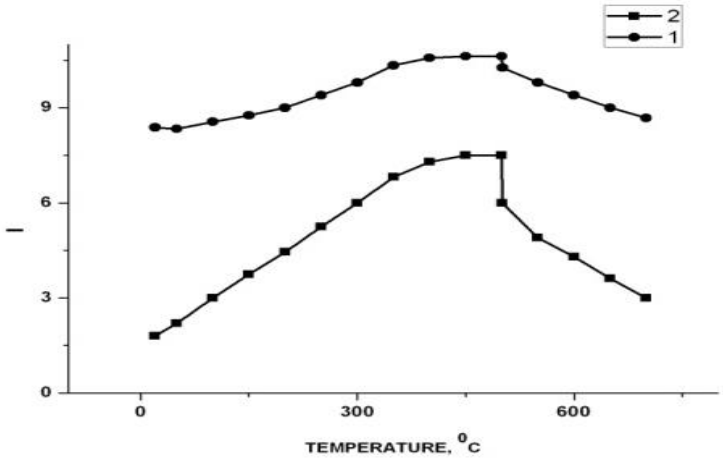

Figure 3. Temperature dependence of I SAXS for samples of PDMPhS + 12% of Cr_2O_3 at the scattering angles q = 0.12 nm^{-1} (1) and q = 4.74 nm^{-1} (2).

Figure 3 presents the temperature dependence of I SAXS at the scattering angles q = 0.12 nm^{-1} and q = 4.74 nm^{-1} for the sample containing 12% of Cr_2O_3 (the vertical line shows the decrease in the intensity at isothermal heating). The intensity of SAXS at the scattering angle equal to q = 0.12 $nm^{-1}$is caused by scattering from the interface between grains of Cr_2O_3 and PDMPhS. This intensity is proportional to difference in the densities of the polymer and Cr_2O_3. Its change is firstly connected with changes in the polymer density. As is evident from Figure 3, the temperature dependence I(q = 0.12 nm^{-1}) has a peculiarity in the range of temperatures close to 200°C, whereas the temperature dependence I (q = 4.74 nm^{-1}) has no deviations from linearity.

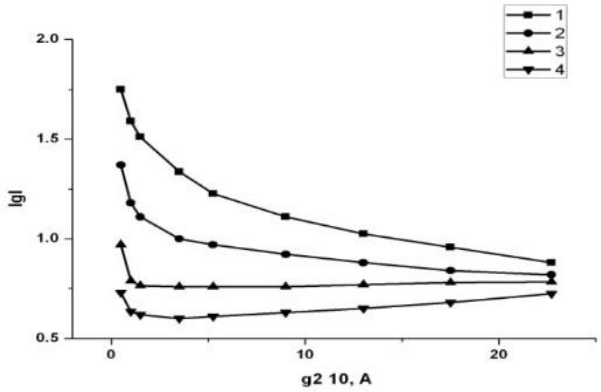

Figure 4. Dependence of lgI on q^2 at the temperature 550°C for the samples containing 50% of kaolin (I), 50% of muscovite (2), 12% of Cr_2O_3 (3), and 20% of Cr_2O_3 (4).

Figure 4 illustrates the dependence of lgI on q^2 for the samples heated at 550°C. For the samples containing Cr_2O_3, the angular dependence of I SAXS at the scattering angles exceeding 100-150′ is practically the same as for the polymer (Figure 1, curve 3). The increase of I SAXS with the scattering angle decrease in the region of small s is caused by scattering from the polymer-Cr_2O_3 interface. In the case of the polymer containing kaolin, a noticeable additional scattering appears within the whole interval of scattering angles, which cannot be connected with the scattering from the polymer-kaolin interface. This means that a large number of heterogeneity regions appear in the sample. The radii of these regions are approximately equal to 6-7 A°. At the present time, it is impossible to estimate their number. If we have deals with a microporous structure, as in the case of polymers, then the total volume of these pores exceeds that in the polymer by an order of magnitude.

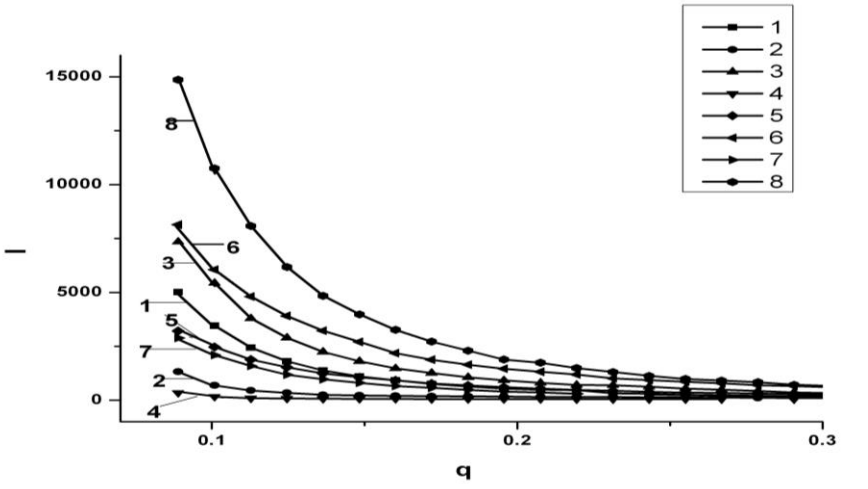

Figure 5. Dependence of I SAXS on q (nm^{-1}) for the samples: PDMPhS +12% of Cr_2O_3 (I), PDMPhS +20% of Cr_2O_3, (2), PDMPhS +12% of Cr_2O_3 +12% of muscovite (3), PDMPhS (4), PDMPhS +12% of muscovite (5), PDMPhS +50% of muscovite (6), PDMPhS +12% of kaolin (7), PDMPhS +50% of kaolin (8) kept at 100°C during 1 hour.

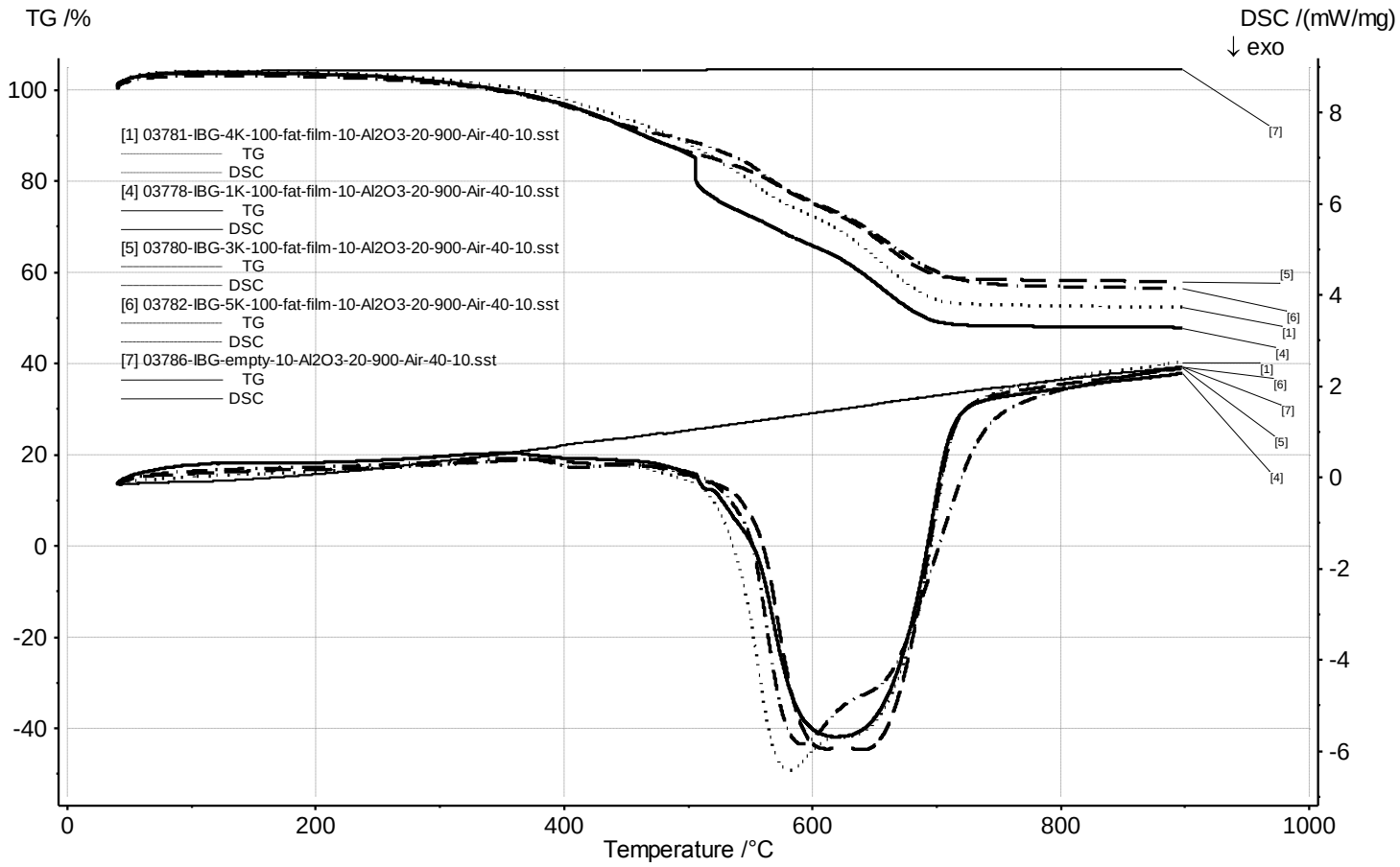

Figure 6. DSC and TG of the samples: DMPhS (1), PDMPhS +12% of Cr_2O_3 (4), PDMPhS +12% of Cr_2O_3 +12% of muscovite, (5) PDMPhS +12% of muscovite (6), the empty crucible (7); the heating at 100°C during 1 hour.

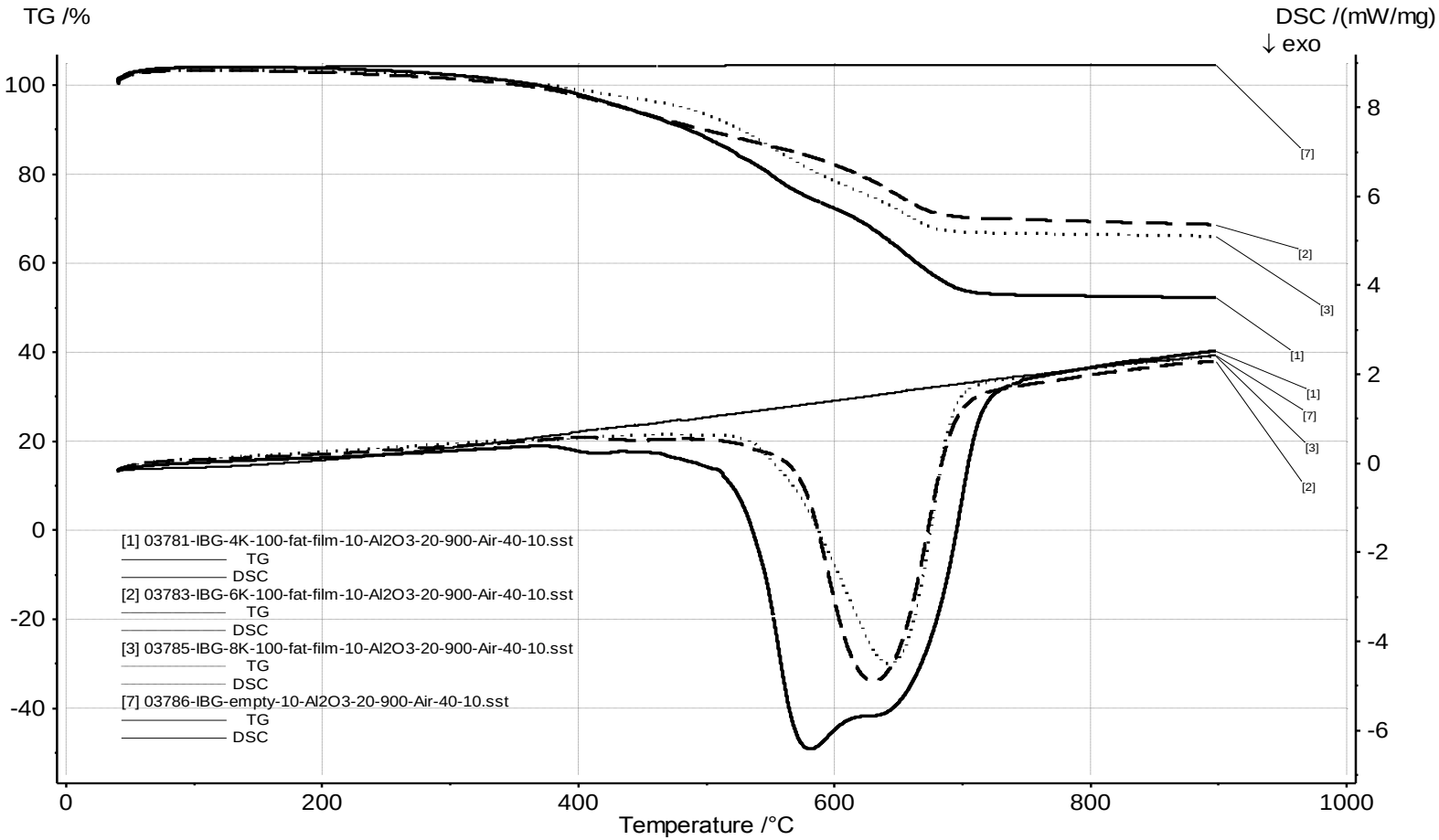

Figure 7. DSC and TG for the samples: DMPhS (1), PDMPhS +20% of Cr_2O_3, (2), PDMPhS +50% of muscovite (2), PDMPhS +50% of kaolin (3), empty crucible (7); the heating at 100°C during 1 hour.

A kink observed on the curve of temperature dependence of the ISAXS for the polymer (Figure 2) apparently corresponds to the temperature at which unfreezing of motion of molecules or of their parts takes place. When kaolin is used as filler, this kink also takes place but at somewhat higher temperature, whereas, in the case of Cr_2O_3, these effects become less pronounced or even are not observed.

Figure 5 demonstrates the dependence of I SAXS on q for the samples kept at 100°C during 1 hour. At scattering angles exceeding q = 1.18 – 1.78 nm^{-1}, the angular dependence of I SAXS for all the samples containing fillers has practically the same character as for PDMPhS. The increase in the I SAXS with the scattering-angle decrease in the region of small s is connected with the scattering from the polymer--Cr_2O_3 interface. In the case of the polymer containing muscovite or kaolin, a noticeable additional scattering appears within the whole interval of scattering angles, which cannot be caused by scattering from the polymer--muscovite or polymer–kaolin interfaces. This means that a large number of heterogeneity regions arise in the sample. The radii of these regions are approximately equal to 6-7 A°. The most intense additional scattering relates to silicates, for kaolin this scattering is considerably stronger than for muscovite. It should be noted that, with an increase in the silicate concentration, this additional scattering increases, whereas, in the case of Cr_2O_3, it decreases.

At temperatures above 350° - 450°C, a decrease in the I SAXS is observed for the polymer and for the polymer with filler, which can be connected with processes of their intense destruction.

On the WAXS curves of PDMPhS, an increase in the intensity of scattering with the increase of temperature from 250ºC to 400ºC is observed (the heat-treated samples were studied at the room temperature), while the destructive processes begin at the temperature of 220ºC. This testifies that, in this range, the structural changes in the polymer continue. The same processes occur in filled polymers but in other ranges of temperatures.

On can see from Figures 6 and 7 that Cr_2O_3, at both concentrations, practically has no effect on the weight loss, whereas silicates significantly decrease the weight loss of composites: muscovite by 20%, and kaolin by 15% at their concentrations equal to 50%. All the silicates moderately transform the shape of two slightly expressed peaks of exothermal effects, which are related to the intense destruction of the polymer at lower concentrations. At higher concentrations, the first exoeffect fully disappears and the maximum on the curves of DSK shifts to higher temperatures. Thus, for synthesis of OCM it is recommended to use approximately 50% of silicates and less than 12% of Cr_2O_3.

4. EXPECTED RESULTS

For all the samples, both an increase in the temperature and in the silicate concentration leads to an increase in the number of heterogeneities, whereas an increase in the Cr_2O_3 concentration decreases their number. Within the range of temperatures from 20 to 300ºC, the dependence of intensity of scattering on the angle is fully reversible. At 150-160ºC, a pronounced kink is observed, which is caused by unfreezing of the structure. In the case of PDMPhS filled by silicates, this process shifts to higher temperatures and, in the case of the concentration decreases their number. Within the range of temperatures from 20 to 300ºC, the dependence of intensity of scattering on the angle is fully reversible. At 150-160ºC, a pronounced kink is observed, which is caused by unfreezing of the structure. In the case of

PDMPhS filled by silicates, this process shifts to higher temperatures and, in the case of the oxide, the effect disappears. The process of intense destruction of the samples begins at temperatures above 350° - 450°C. The silicates decrease the weight loss of composites by 15 – 20%, and Cr_2O_3 does not change it. For synthesis of OCM we recommend to use approximately 50% of silicates and less than 12% of Cr_2O_3.

REFERENCES

[1] Todorov, Lyudmil V.; Martins, Carla I.; Viana, Julio C., *In situ WAXS* / *SAXS* structural evolution study during uniaxial stretching of poly(ethylene terephthalate) nanocomposites in the solid state: Poly(ethylene terephthalate)/titanium dioxide and poly(ethylene terephthalate)/silica nanocomposites (2014) *Journal of Applied Polymer Science* (131) 3: 39752/1-39752/9.

[2] Yuta Saito, Moriya Kikuchi, Yuji Jinbo, Atsushi Narumi and Seigou Kawaguchi, Determination of the Chain Stiffness Parameter of Molecular Rod Brushes Consisting of a Polymethacrylate Main Chain and Poly(n‑hexyl isocyanate) Side Chains (2015) *Macromolecules* (48): 8971–8979.

[3] D. W. Mccarthy, J. E. Mark, S. J. Clarson, D. W. Schaefer, Synthesis, Structure, and Properties of Hybrid Organic – Inorganic Composites Based on Polysiloxanes. II. Comparisons between Poly(Methylphenylsiloxane) and poly(Dimethylsiloxane), and between Titania and Silica (1998) *Journal of Polymer Science: Part B: Polymer Physics*, (36): 1191–1200.

[4] Okhlopkova, T. A.; Okhlopkova, A. A.; Spiridonov, A. M.; Nikiforov, L. A. UHMWPE structural changes under the influence of ceramic nanodispersions (2014) *Voprosy Materialovedeniya* (3): 145-153.

Smart Nanocomposites
Volume 8, Number 1
ISSN: 1949-4823

CALCULATION OF AN EXPERIMENTAL PSEUDOCAPACITOR SELF-DISCHARGE RATE WITH THE USE OF CYCLIC VOLTAMMOGRAMS

Alexandra G. Ivanova*, Oleg A. Zagrebelnyy, Maria S. Masalovich, Irina Yu. Kruchinina, and Olga A. Shilova
Institute of Silicate Chemistry of Russian Academy of Sciences,
Saint Petersburg, Russia

ABSTRACT

In this report we consider the usage of a previously developed computational method of self-discharge evaluation on the basis of a cyclic voltammogram (CVA) for such an energy storage device as a pseudocapacitor (PC). The CVAs of testing PCs with different types of electrodes in organic and inorganic electrolytes are analyzed. It has been revealed that the SDRs depend on the potential window of an electrochemical system, the electrode and electrolyte composition and the synthesis conditions of a PC electroactive coating. Complementary match of the electrolyte and the electrode compositions and the rational choice of potential window significantly diminish the SDR of an experimental PC. The elaborated calculation procedure is the express method which facilitates the SDR estimation.

Keywords: a pseudocapacitor, self-discharge, cyclic voltammograms, transition metal oxides, electrically conducting organic polymers

1. INTRODUCTION

The self-discharge phenomenon is known to play a crucial role in the deterioration of PCs performance. Despite numerous publications on the development of materials for energy storage devices in which much attention is paid to the specific capacity, cyclic stability and charge/discharge rate, there is little known about the self-discharge. Self-discharge is literally a spontaneous voltage drop in open circuit after charging the device. The self-discharge rate (SDR) of a battery is known to be lower than of a supercapacitor. Besides, supercapacitors

* Corresponding Author -Email: agp-13@inbox.ru

solely based on electric double layer with specially treated coal electrodes possess lower SDR than the PCs operating mainly due to reversible surface redox reactions. Unlike batteries the thermodynamic instability of a supercapacitor system, and of a PC system in particular, is caused by electrochemical reactions taking place on the surface of PC electrodes rather than in the bulk. On the whole, the thermodynamic instability of such electrochemical systems as a supercapacitor or a PC is caused by possible side Faraday reactions at the electrode/electrolyte interface as well as by time-limited ion diffusion leading to some potential redistribution in the electrode bulk and overcharge of the devices. The charge redistribution is also possible in the pores of the PC electrode. Besides, when the electrochemical device constructed with defects, ohmic leakage significantly increases the SDR [1-3]. Thus, to clarify the means of eliminating these phenomena, especially for PCs, it is further necessary to study the electrode/electrolyte interface processes with the use of diverse electrode, electrolyte and support materials.

Multiple cyclic voltammetry experiments are known to be conducted in the course of studying the electrochemical properties of a model PC. The cyclic voltammetry method provides information about kinetics and thermodynamics of electrochemical processes at the electrode/electrolyte interface in the working voltage range. Meanwhile, the estimation procedure of a PC capability to collect and store the energy received from outer sources which is the testing of electrodes by means of open circuit method, takes long time (an hour at least). Hence, the development of a procedure facilitating the objective estimation of electrochemical properties of a model PC is quite an important problem.

We found the following regularity when testing a PC: asymmetry of the CVA determines the SDR, the more asymmetry, the more the SDR. Therefore, we suggest an alternative express method to calculate the SDR of a PC using CVAs. This method is based on the compare of the energy irreversibly absorbed by an electrode as a result of conversion into heat or chemical energy and the total energy transferred to the electrode. It was previously shown that the results obtained by the express calculation method complied with the ones registered by the classic long-term open circuit method. The high correlation index (0.71) was achieved [4].

2. RESEARCH GOAL

The goal of the research is to test the experimental PCs with different types of electrodes in organic and inorganic electrolytes and estimate the SDR of the electrochemical systems with the help of the elaborated method.

3. EXPERIMENTAL PART

Electrochemical experiments were carried out in a three – electrode cell (a half - cell). Two groups of working electrodes were tested. The first one is pieces of steel mesh covered with a WO_{3-x} layer (tungsten oxide of variable valency) (75%), carbon black (20%) and a polymeric binder (5%). Then the prepared electrodes were electrochemically covered with manganese (IV) oxide (0.001 g). Depending on the composition the electrodes were marked 3a and 4akB. These electrodes differ by the tungsten oxidation state.

The second group of electrodes is platinum plates with a layer of electrically conducting polymer (eg. polythiophene). Films of polythiophene were formed by the electrochemical deposition method in different modes.

The recorded CVAs were processed with the software package Mathcad 15.0. The SDR values were calculated automatically according to the consequent set of previously derived formulas [4].

4. Results and Discussion

Figure 1and 2 show that the SDR values directly depend on the potential window width used while registering the CVAs of the experimental PCs. The window getting wider up to (-500 ÷ +1000 mV), the self-discharge increases, and the efficiency factor EF falls down from 38 to 16%. The difference between the SDRs is probably provoked by side electrochemical reactions (e.g., molecular hydrogen formation at the potential less than -300 mV; irreversible reduction of manganese (IV) and tungsten oxides) affecting the SDR of the electrochemical system.

Moreover, potential sweep rate also influences the SDR. Thus, on the rise of the potential sweep rate up to 50 mV c^{-1} (Figure 3), the SDR falls, and therefore, the EF of the electrochemical system increases. It is most likely that the increase of the potential sweep rate inhibits the side chemical reactions due to the rising limitation of the electrolyte transport towards the electrode surface. Noteworthy, that in this case the SDR has not been affected by the enlarging of the potential window from 0÷ +700 mV (Figure 1) to -20÷ +1000 mV (Figure 3).

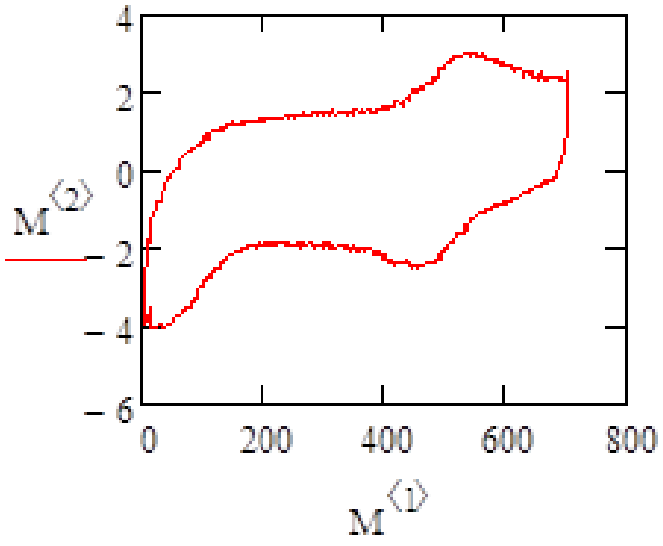

Figure 1. The CVA of the electrode 3a in the electrolyte (1M H_2SO_4/1M HNO_3 = 1:1); sweep rate 10 mV C^{-1}; the potential range from 0 to +700 mV); $M^{<2>}$ - current matrix (mA), $M^{<1>}$ - voltage matrix (mV). The equilibrium potential of the electrode 3a is 247 mV. SDR = 62%; EF = 38%.

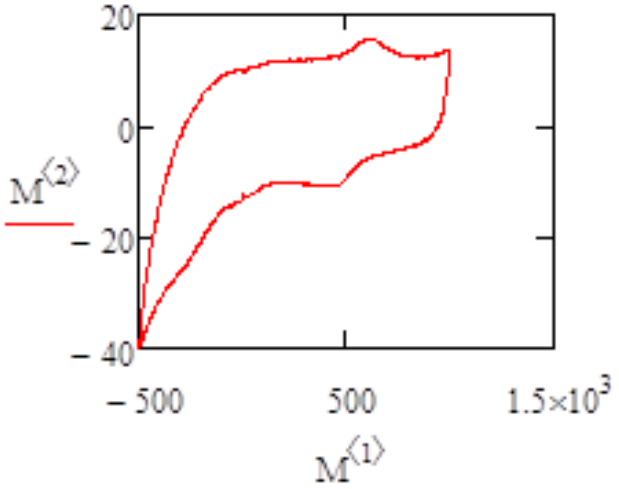

Figure 2. The CVA of the electrode 3a in the electrolyte (1M H_2SO_4/1M KNO_3 = 1:1); sweep rate 10 mV C^{-1}; the potential range from -500 to +1000 mV); $M^{<2>}$ - current matrix (mA), $M^{<1>}$ - voltage matrix (mV). The equilibrium potential of the electrode 3a is 247 mV. SDR = 83%; EF = 17%.

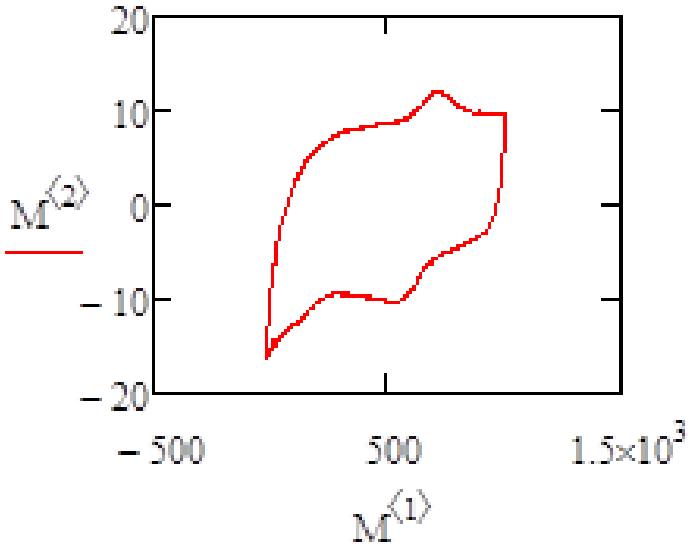

Figure 3. The CVA of the electrode 3a in the electrolyte (1M H_2SO_4/1M KNO_3 = 1:1); sweep rate 50 mV C^{-1}; the potential range from -20 to +1000 mV); $M^{<2>}$ - current matrix (mA), $M^{<1>}$ - voltage matrix (mV). The equilibrium potential of the electrode 3a is 247 mV. SDR = 56%; EF = 44%.

Figure 4 reflects the smallest SDR value among the discussed above. Thus, the potential range +200 ÷ +1000 mV (ΔE = 800 mV) and the sweep rate 50 mV c^{-1} are optimal for the experimental PC with the electrodes 3a and the electrolyte (1M H_2SO_4 / 1M HNO_3 = 1:1) where the SDR is less than 40%.

Meanwhile, the EF of the experimental PC with the electrode 4akB in the similar electrolyte, the potential window ΔE = 800 mV and the sweep rate 50 mV c^{-1} is twice lower. Hence, the potential window of the PC with the electrodes 4akB is likely to be reduced to ΔE = 600 mV as the electrode composition has been altered by the addition of WO_3 (Figure 5).

Therefore, the potential window, electrode composition and electrolyte influence the SDR of supercapacitors with pseudocapacitive effect in the inorganic aqueous electrolyte. Complementary match of the electrolyte and the electrode compositions, the rational choice of the potential window and sweep rate diminish the SDR of an experimental PC.

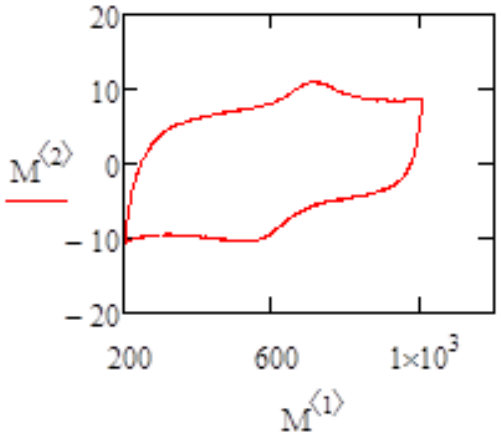

Figure 4. The CVA of the electrode 3a in the electrolyte (1M H_2SO_4/1M HNO_3 = 1:1); sweep rate 50 mV C^{-1}; the potential range from +200 to +1000 mV); $M^{<2>}$ - current matrix (mA), $M^{<1>}$ - voltage matrix (mV). The equilibrium potential of the electrode 3a is 247 mV. SDR = 39%; EF = 61%.

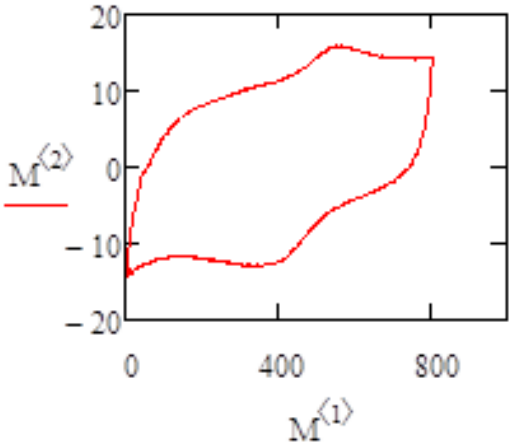

Figure 5. The CVA of the electrode 4akB in the electrolyte (1M H_2SO_4/ 1M HNO_3 = 1:1); sweep rate 50 mV C^{-1}; the potential range from 0 to +800 mV); $M^{<2>}$ - current matrix (mA), $M^{<1>}$ - voltage matrix (mV). The equilibrium potential of the electrode 4akB is 259 mV. SDR = 75%; EF = 25%.

The model PC with a platinum electrode covered with a polythiophene film, and the organic electrolyte solution (tetraethylammonium tetrafluoroborate – 0.1 M $TEABF_4$ in acetonitrile solution) [5] represent the electrochemical system similar to the PCs with the aqueous electrolytes.

It may be seen from Figure 6 and 7 that the SDR grows drastically on the enlarging the potential window from ΔE = 900 mV to ΔE = 1250 mV while the EF being significantly reduced. This implies that the electrochemical system is unstable in this potential range. Moreover, it has been revealed that the SDRs depend on the electrode composition and synthesis conditions of the electroactive material for the electrochemical systems of PCs with either aqueous inorganic or non-aqueous organic electrolytes. Thus, the galvanostatic mode is the best mode of polythiophene electrochemical synthesis which complies with the published data [6].

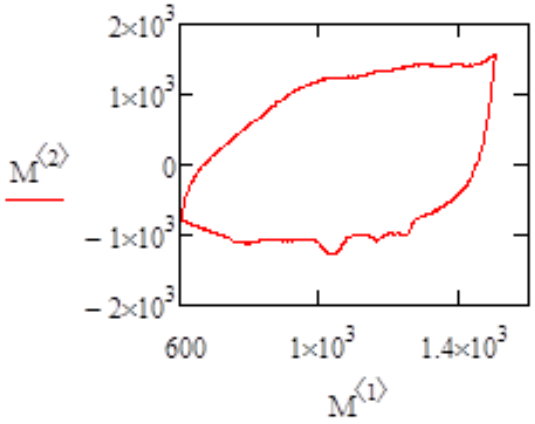

Figure 6. The CVA of the electrode covered with polythiophene in the electrolyte 0.1 M $TEABF_4/CH_3CN$; sweep rate 10 mV C^{-1}; the potential range from +600 to +1500 mV); $M^{<2>}$ - current matrix (mA), $M^{<1>}$ - voltage matrix (mV). The equilibrium potential of the electrode is 800 mV. SDR = 55%; EF = 45%.

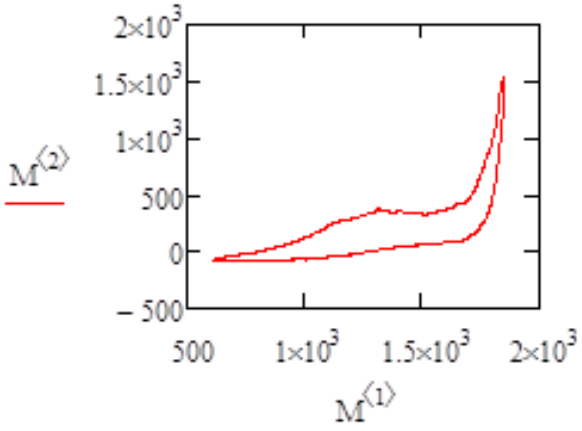

Figure 7. The CVA of the electrode covered with polythiophene in the electrolyte 0.1 M $TEABF_4/CH_3CN$; sweep rate 10 mV C^{-1}; the potential range from +500 to +1750 mV); $M^{<2>}$ - current matrix (mA), $M^{<1>}$ - voltage matrix (mV). The equilibrium potential of the electrode is 800 mV. SDR = 99%; EF = 1%.

Therefore, the developed calculation procedure provides the fast and thorough estimation of the electrochemical properties (self-discharge and electrochemical stability) of an experimental PC.

The research has been supported by the funding programs of Chemistry and Material Sciences Department of Russian Academy of Sciences (№2, №7).

REFERENCES

[1] Conway, B. E., *Electrochemical Supercapacitors: Scientific Fundamentals and Technological Applications* (1999). Kluwer Academic, New York: 685.

[2] Andreas, H. A., Self-Discharge in Electrochemical Capacitors: A Perspective Article (2015) *J. Electrochem. Soc*. (162) 5: A5047-A5053.

[3] Lewandowski A., Jakobczyk P., Galinski M., Biegun M. Self-Discharge of Electrochemical Double Layer Capacitors (2013) *Phys. Chem. Chem. Phys*. (15): 8692-8699.

[4] Zagrebelnyy, O. A., Ivanova, A. G., Masalovich, M. S., Kruchinina, I. Yu., Shilova, O. A., Electrochemical Pseudocapacitor Self-Discharge Estimation Procedure Based on the Electrode Cyclic Voltammograms (2017) *Glass Physics and Chemistry* (43) 3: 267-271.

[5] Masalovich, M. S., Shevtsova, Yu. A., Ivanova, A. G., Zagrebelnyy, O. A., Kruchinina, I. Yu., Shilova, O. A., Electrochemical Synthesis of Polythiophene-Polyacrylamide Composite Coatings Used for Pseudocapacitors (2016), *Glass Physics and Chemistry* (42) 6: 635-636.

[6] Shopf, G., Kobmehl, G., *Polythiophenes – Electrically Conductive Polymers* (1997). Springer, Germany: 153.

Smart Nanocomposites
Volume 8, Number 1
ISSN: 1949-4823

HYDROPHOBIC AND SUPERHYDROPHOBIC COATINGS BASED ON FLUOROSILOXANE BLOCK COPOLYMERS

Yu. V. Khoroshavina[1,*], Yu. V. Frantsuzova[1], I. N. Tsvetkova[2], O. A. Shilova[2], and G. A. Nikolaev[1]

[1]Institute of Synthetic Rubber, Saint Petersburg, Russia
[2]Institute of Silicate Chemistry of the Russian Academy of Sciences, Saint Petersburg, Russia

ABSTRACT

The kinetically and sedimentation stable sols were synthesized on the basis of methyltriethoxysilane and additives of polyphenylsilsesquioxane-polymethyl-(3,3,3-trifluoropropyl)siloxane block copolymers and hydrogenated aerosil. The method of obtaining hydrophobic and superhydrophobic coatings based on the sol-gel compositions was developed. The resulting coatings are transparent; they have got an improved adhesion to glass.

Keywords: hydrophobic and superhydrophobic coatings, sol-gel synthesis, polyphenyl-silsesquioxane – polymethyl-3,3,3- trifluoropropylsiloxane

INTRODUCTION

Currently, the much for new technologies of preparing hydrophobic and superhydrophobic coatings is constantly growing. Thus, the use of such materials during buildings in megalopolises with high level of harmful gas emissions allows to reduce significantly the severity of the problem of cleaning windows and facades from dirt, protects them from destruction in conditions of high moisture at cyclic temperature changes. When using superhydrophobic coatings effect of water repellency allows minimizing the damaging effects.

The relevance of the works aimed to create such coatings for the power engineering are caused with the corrosion problems of metal poles, rebar and cracking the ferroconcrete transmission towers; damage or disruption of poles, wires, insulators and ground wires due in excess deposits of ice or snow. Hydrophobic and superhydrophobic coatings provide

* Corresponding Author: Yulia Khoroshavina, Senior scientific researcher, Institute of Synthetic Rubber, Saint-Petersburg, Russia. Tel.: + 79112913931, E-mail: julhor@yandex.ru

protection from atmospheric corrosion, reducing the rate of corrosion processes even in harsh environments [1]. These materials are demanded in aviation, optics, energy, the textile industry.

It's actively carried out a development of materials having high water resistance and resistance to icing, as well as biological stability.

In practice various kinds of hydrophobisatoris are mainly used. The organic-silicon and silicone hydrophobisatoris based on alkylsilanes potassium, alkoxysilanes, hydrosiloxanes are the most widespread. Various kinds of polyorganosiloxanes liquids (polymethylmethyl-hydrosiloxane), elastomers (polymethylphenyl- and polydimethylsiloxane) can distinguish as a base for modern hydrophobic materials [2].

Weatherproof protective coatings for timber based on the sol-gel composition and polyphenylsilsesquioxane-polydimethylsiloxane block copolymer formula $\mathbf{D_{320}T_{70}}$, where **D** - dimethylsiloxane link [$(CH_3)_2SiO$], **T** – phenylsilsesquioxane link [$C_6H_5SiO_{3/2}$] was obtained earlier [3]. This type of block copolymers combines the properties of linear siloxanes: flexibility, elasticity, processability and stair silsesquioxane - hardness, wear resistance [4]. These polymers were introduced into the sol-gel composition on the basis of hydrolyzed tetraethoxysilane (TEOS) and the texturizing filler - finely dispersed amorphous silica with hydrophobic surface with a specific surface area of 130 m²/g (aerosil). Such coatings were deposited on samples of wood of coniferous species without prior grinding or polishing. As a result of processing the sol-gel composition with the addition of polyphenylsilsesquioxane – polydimethylsiloxane the surface of the wood purchased as smooth and silky as hydrophobic properties (wetting angle – 110-140^0).

Superhydrophobic coatings have several advantages over hydrophobic. However, poor adhesion to the substrate is a common problem for them. As a consequence frequent update of the applied layer is usually required. Therefore the search of special additives, for example, new polyorganosiloxanes which will give superhydrophobic properties to the treated surface and will improve the properties of the sol-gel compositions, for example, the adhesion of coatings to the substrate, is a very important task.

It is known that coatings obtained from compositions based on fluorosiloxanes have higher values of the contact wetting angle (~120 – 130^{0}C) in comparison with coatings obtained on the basis of non-fluorinated siloxanes [5]. This is because the presence of fluorine atoms in the polymer chain ensures low surface energy due to the weakness of intermolecular effects, as well as a higher hydrophobicity than their non-fluorinated analogues. The aim of this work is to study the possibility of creating hydrophobic and superhydrophobic coatings with improved adhesion properties on the basis of specially synthesized new fluorosiloxane block copolymers and sol-gel compositions with the additives of such polymers.

MATERIALS AND METHODS

For this study of a number of polyphenylsilsesquioxane – polymethyl (3,3,3- fluoro-propyl)siloxane block copolymers of the general formula $\mathbf{M_nF_{300}T_{70}}$, where **F** is methyl(3,3,3- trifluoropropyl)siloxane link [$(CH_3)(CF_3CH_2CH_2)SiO$], **T** – phenylsilsesqui-oxane link [$C_6H_5SiO_{3/2}$], **M** – trimethylsiloxy - link [$(CH_3)_3SiO_{1/2}$-] were synthesized by hydrolytic polycondensation.

The number of hydroxyl groups was regulated by the introduction of monofunctional trimethylsiloxy-links M to the process of synthesis in the ratio **M/T** = 0,09 ÷ 0,6 (mol.). The presence of hydroxyl- groups in silsesquioxane fragment from one side will provide interaction with polysiloxane matrix, which is formed in the sol, in which it is added, on the other hand will improve the adhesion of the coating to the surface. However, hydrophobic coatings can significantly worsen. Therefore, the influence of content of hydroxyl groups on the properties of coatings was investigated.

Synthesis of silica sols was carried out by successive mixing of methyltriethoxysilane (MTEO), acetone, 0.1 M HCl solution and aminopropyltriethoxysilane (AGM-9) in a weight ratio of (1:2:0,2:0,5). The maturation of the sol was carried out for 1 day. Then block copolymers $M_6F_{300}T_{70}$, $M_{21}F_{300}T_{70}$, $M_{42}F_{300}T_{70}$ was introduced in silica sol. The mixture was thoroughly mixed for 20 min. To make a special structure (rough terrain) to the surface coating hydrogenated aerosil was introduced as a suspension in acetone (compounds 5, 6 and 7 Figure 1) in sols. Scheme of the synthesis of the sols is shown in Figure 1. Marking and compositions of the resulting sols are shown in Table 1.

The obtained sol-gel compositions (compositions 5, 6 and 7) and block copolymers (compositions 1, 2, 3), previously dissolved in butyl acetate, were applied to degreased glass slides-substrate by an airbrush. Coatings were dried in air and after - at 100-150 ^{0}C.

The surface condition of the coatings was estimated phenomenologically with the aid of a microscope Bresser LCD Micro. Wetting angle was determined by goniometer LK-1. Adhesion to the substrate was determined by scarification by the method GOST 15140.

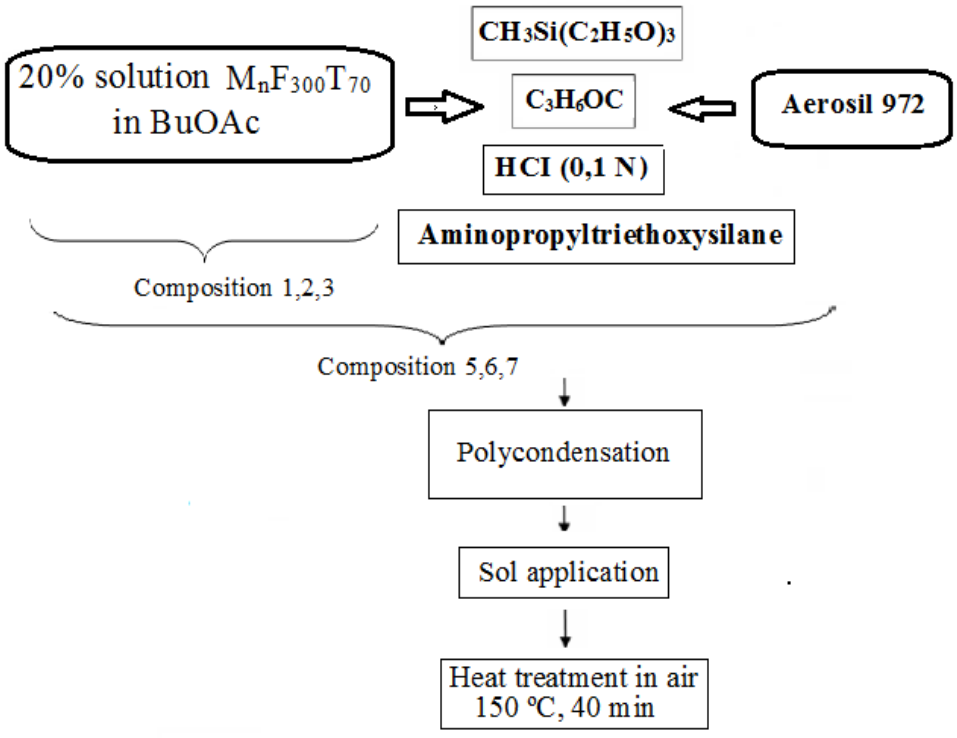

Figure 1. The scheme of the sol-gel synthesis of coatings obtained on the basis of polyphenylsilsesquioxane - polymethyl(3,3,3- trifluoropropyl)siloxane block copolymers.

RESULTS AND DISCUSSION

The surface condition and the degree of hydrophobization of the coatings based on polyphenylsilsesquioxane – polymethyl (3,3,3- trifluoropropyl)siloxane block copolymers can be estimated from the data of Table 1.

Table 1. The surface condition and the degree of water repellency of coatings obtained from solutions of the polymers

№ of composition	Polymer formula	Wetting angle	Wetting angle, after heat treatment *(150 ^{0}C, 40 min.)*	Observations
1	$M_6F_{300}T_{70}$	97	100	Transparent cover; drops flow off leaving no a trace; the cover is easy to wash
2	$M_{21}F_{300}T_{70}$	95	98	
3	$M_{42}F_{300}T_{70}$	122	120	

As it can be seen from the above data, decreasing the content of hydroxyl groups (the increase in the proportion of M-units) leads to an increase of the wetting angle values until the hydrophobic coating (120^0). A small proportion of M-units ($M_6F_{300}T_{70}$) increases the strength of the coating compared to films cast from the original block copolymer, without affecting its hydrophobicity.

It is known the higher a contact angle the more hydrophobic the surface is considered. A rough surface having a low value of the surface energy with the boundary contact angle more than 150^0 and the angle of sliding less than 10^0 is related to superhydrophobic. In our case, the superhydrophobic surface was formed by controlled aggregation during the sol-gel synthesis and coating of the substrate (in situ) particles of hydrogenated aerosil. The results of the study are given in Table 2.

As it can be seen from Table 2 the formation of multimodal surface takes place when used hydrogenated aerosil. It can be noted that the adhesion to the substrate is improved by the combined effect of a macromolecular siloxane component built-in ladder silsesquioxane structure of the polymer, which together with hydrogenated aerosil in situ form a distinct surface topography that gives it superhydrophobic properties.

Table 2. Properties of coatings based sols with additives polymers and aèrosil

№ of composition	Polymer formula	Wetting angle	Wetting angle, after heat treatment (250^0C, 40 min.)	Observations
5	$M_{42}F_{300}T_{70}$ - sol MTƏOS -Aèrosil 972	103	120	A transparent coating adhesion 2 points
6	$M_{21}F_{300}T_{70}$ – sol MTƏOS -Aèrosil 972	116	150	
7	$M_6F_{300}T_{70}$ sol MTƏOS -Aèrosil 972	138	146	

CONCLUSION

The possibility of the synthesis of kinetically and sedimentation stability of the Sols on the basis of methyltriethoxysilane and supplements of polyphenylsilsesquioxane-polymethyl-(3,3,3-trifluoropropyl)siloxane block copolymers and hydrogenated aerosil is shown. The introduction of polyphenylsilsesquioxane-polymethyl-(3,3,3-trifluoropropyl)siloxane block copolymer $M_{21}F_{300}T_{70}$, where M is trimethylsiloxy- link, T – phenylsilsesquioxane link, F – methyl-(3,3,3- trifluoropropyl)siloxane link, and hydrogenated aerosil allowed to obtain a superhydrophobic coating with a good adhesion to glass.

This project was supported by Federal Target Program (grant 14.576.21.0028), code - RFMEFI57614X0028.

REFERENCES

[1] Shilova O. A., Tsvetkova I. N., Krasil'nikova L. N., Ladilina E. J., lubova T. S., Kruchinina I. Y. "Synthesis and study of superhydrophobic, deicing hybrid coatings." *Network Electronic Journal Transport Systems and Technologies.* Vol. 1 (1). 2015. S. 91-98.

[2] Stoye D., Freitag W., Itsko E. F. *Paints, Coatings and Solvents*– St. Petersburg.: Profession, 2012. – 528 p.

[3] Tsvetkova I. N., Krasil'nikova L. N., Kozhin P. K., Khoroshavina J. V., Frantsuzova Y. V., Petrova I. V., Shilova O. A. Composition formation for weather-protective and decorative coatings. International Symposium: Chemistry for Biology, Medicine, Ecology and Agriculture. *ISCHEM* 2015 Abstracts. 2015. pp 230-231.

[4] Khoroshavina Yu. V.; Frantsuzova Yu. V.; Nikolaev G. A., *International Polymer Science and Technology.* 2016. V. 42. № 9. P. T/13-T/15.

[5] P. Fabbri, M. Messonri, M. Montecchi, F. Pilati, R. Taurino, C. Tonelli, M. Toselli. Surface Properties of Fluorinated Hybrid Coating. *J. of Appl. Pol. Sci*. 2006. V. 102. P. 1483-1488.

Smart Nanocomposites
Volume 8, Number 1
ISSN: 1949-4823

IMPURITY CENTERS U-MINUS TIN IN CHALCOGENIDE SEMICONDUCTORS A4B6 AND A5B6

***M. Yu. Kozhokar*[1,*]**
[1]Saint Petersburg Mining University,
Saint Petersburg, Russia
[2]21st Line of the Vasilyevsky Island,
Saint Petersburg, Russia

ABSTRACT

This article presents a study on the identification by emission Mössbauer spectroscopy parent isotopes ^{119mm}Sn (^{119m}Sn), ^{119}Sb (^{119m}Sn) and ^{119m}Te (^{119m}Sn) impurity U-minus tin centers in chalcogenide crystal (PbS, PbSe) and vitreous (Ge_xS_{1-x}, Ge_xSe_{1-x}, As_xS_{1-x} and As_xSe_{1-x}) semiconductors, said centers are formed by nuclear reactions in the respective parent atom lattice sites PbS, PbSe (i.e., at positions of lead and chalcogen) and structural glass network nodes (in positions of arsenic, germanium and chalcogens). X-Ray Fluorescent spectroscopy was used to determine the number of members of the studied glasses and crystals.

Keywords: Mössbauer spectroscopy, U-minus centers

INTRODUCTION

Conduct of impurity atoms in semiconductors based on the idea that the introduction of the impurity center in a crystal lattice, or a disordered structure of glass mesh in the forbidden band of the semiconductor is formed a single-electron donor (or acceptor) level. When you change the position of the Fermi level, this level gives (takes) one electron. However, there may be cases in which the impurity centers are formed in the forbidden band of the semiconductor two bands of localized states (two-electron centers), and the magnitude of the correlation energy:

$$U = W_2 - W_1, \quad (1)$$

* Corresponding Author E-mail: m-kozhokar@mail.ru

(where W_1 and W_2 center -first and second ionization energies) may be either $U > 0$ (with a positive center two-electron correlation energy) and $U < 0$ (two-electron centers with a negative correlation energy, U-minus centers). The concept of the existence of the impurity U-minus centers in chalcogenide glassy semiconductors (CGS) is widely used to explain the electrical, thermal and magnetic properties of these materials (the absence of extrinsic conductivity, chemical fixation potential near the middle of the gap, the lack of electron spin resonance signal).

The concept of the existence of the impurity U-minus centers in chalcogenide stack loobraznyh semiconductors (CGS) is widely used to explain the electrical, thermal and magnetic properties of these materials (no impurity conduction bridges, fixation of the chemical potential near the middle of the gap, the lack of electron spin resonance signal).

An effective method of identifying the impurity U-minus centers is Mössbauer spectroscopy, which allows you to determine the charge states of the centers, the symmetry of the local environment, the nature of the electrical activity in semiconductors.

EXPERIMENT

The objects of research were glassy and crystalline alloys Ge_xS_{1-x} systems, Ge_xSe_{1-x}, As_xS_{1-x}, As_xSe_{1-x}, $Pb_{1-x}Sn_xS$ and $Pb_{1-x}Sn_xSe$. The compositions of these samples are given on the composition of the initial charge, with certain accuracy ± 0.005. The spectra were measured in the industrial instrument X-Art M x-ray fluorescence excitation of atoms is carried out X-ray tube. To obtain quantitative information on the chemical composition of the test sample spectra were processed using the software of the spectrometer. The spectrometer can detect impurities with a threshold of detection of ~ 10^{-4} at.%. X-ray fluorescence spectra were measured at values of the anode voltage U of 12 to 50 kV.

To determine the method for concentration of tin in lead chalcogenides was also used standard (the standard used $Pb_{0.98}Sn_{0.02}Se$ - defined area under Lα1,2-line lead for him and Kα1,2 - tin line, determined by atomic fraction of tin and then constructed calibration curve xRFA = f (x), which is approximated by a polynomial of the second degree (Figure 1)). This polynomial and its schedule were calibrating ratios for determining the composition of the targets on the obtained spectra xRFA value with an error of ± 0.0007. To demonstrate such a possibility in Figure 1 further shows the experimental values xRFA solid solutions and $Pb_{0.99}Sn_{0.01}$ $Pb_{0.983}Sn_{0.017}Se$. It can be seen that for all samples the experimental data fit well to the calibration relation between the values of x and xRFA [1]. The spread data is due to a large error in determining the value of x for the initial charge (no better than ± 0.005).

The developed method to determine the number of members of glassy alloys Ge_xS_{1-x}, Ge_xSe_{1-x}, As_xS_{1-x}, As_xSe_{1-x}, as well as the concentration of tin impurities in solid solutions $Pb_{1-x}Sn_xS$ and $Pb_{1-x}Sn_xSe$, used in the future for the certification of the samples.

Mössbauer spectra were measured with a spectrometer SM 4201 TerLab. For caliber-ki-speed spectrometer scale used absorption Mössbauer spectroscopy on isotope ^{119}Sn (source served $Ca^{119mm}SnO_3$, and sinks $CaSnO_3$, SnS, SnS_2, SnSe, $SnSe_2$, SnAs and Sn_3As_4 - for all of these compounds are known values of the isomer shift and quadrupole splitting).

Emission Mössbauer Spectroscopy ^{119mm}Sn (^{119m}Sn)

Subsidiaries atoms ^{119mm}Sn in lattices of PbS and PbSe form donor centers with a negative-tive correlation energy, the centers Sn_6^{2+} and Sn_6^{4+} correspond respectively to neutral and doubly ionized state donor center, then once ionized impurity U-minus center (Sn_6^{3+}) is unstable.

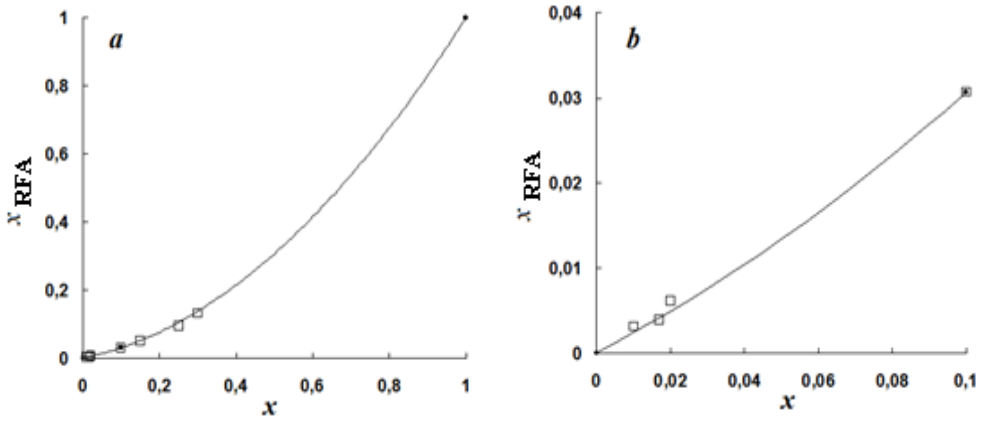

Figure 1. (a) The dependence xRFA = f (x) for the $Pb_{1-x}Sn_xSe$ in compositions from 0 to 1. The point is the value of x and cauldrons xRFA used to construct the calibration curve (it is held by a solid line). (B) Dependence xRFA = f (x) $Pb_{1-x}Sn_xSe$ for a range of compositions from 0 to 0.1. Square box shows the values of x and xRFA for $Pb_{1-x}Sn_xSe$ compositions. (B) spectra were measured at U = 50 kV.

Tin atoms formed after the disintegration of radioactive ^{119mm}Sn in the structure of vitreous germanium chalcogenides are stabilized in the form of Sn_6^{4+} ions and Sn_3^{2+} nodes in Germany, have in their local environment only atoms chalcogens and their population depend on the composition of glass and technology of its receipt. These ions are singly ionized acceptor (Sn_6^{2+}) and singly ionized donor states amphoteric U-minus tin center.

Motherboard ^{119mm}Sn atoms in the structural grid of glassy arsenic chalcogenides form their own structural units so that the daughter atoms ^{119m}Sn stabilized tin structural units in the form of electrically inactive ions coordinated six tetravalent tin Sn_6^{4+} (Model Gubanov-Mott) [2].

Emission Mössbauer Spectroscopy ^{119}Sb (^{119m}Sn)

Antimony impurity atoms in the lattice of lead chalcogenides are distributed between the cationic and anionic sublattices - in electronic samples of the bulk of the antimony is localized in the anion sublattice, while the bulk of the sample hole antimony localized in the cation sublattice (Figure 2). Tin atoms formed after ^{119}Sb radioactive decay in the anion sublattice of PbS and PbSe are electrically inactive, whereas in the cation sublattice of tin atoms form a U-minus donor centers (Sn_6^{2+} centers and Sn_6^{4+} correspond respectively to neutral and doubly ionized state donor center). There has been a process of electron exchange between neutral and doubly ionized U-minus tin centers, using state of the allowed bands.

Antimony atoms in the structure of germanium chalcogenide glassy form their own structural units. Tin atoms formed after the disintegration of radioactive ^{119}Sb form Sn_6^{4+} ions and Sn_3^{2+}, the populations of which are dependent on the composition of glass and technology of its receipt. These ions are singly ionized acceptor (Sn_6^{2+}) and singly ionized donor states amphoteric U-minus tin center.

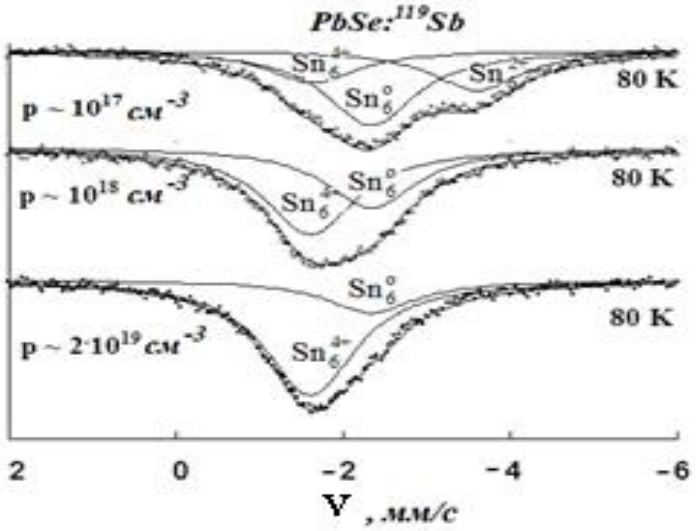

Figure 2. Emission Mössbauer spectra at 80 K hole samples PbSe: ^{119}Sb with different carrier concentration. Displaying the expansion of the experimental spectra into components corresponding to Sn_6^0, Sn_6^{2+} and Sn_6^{4+}.

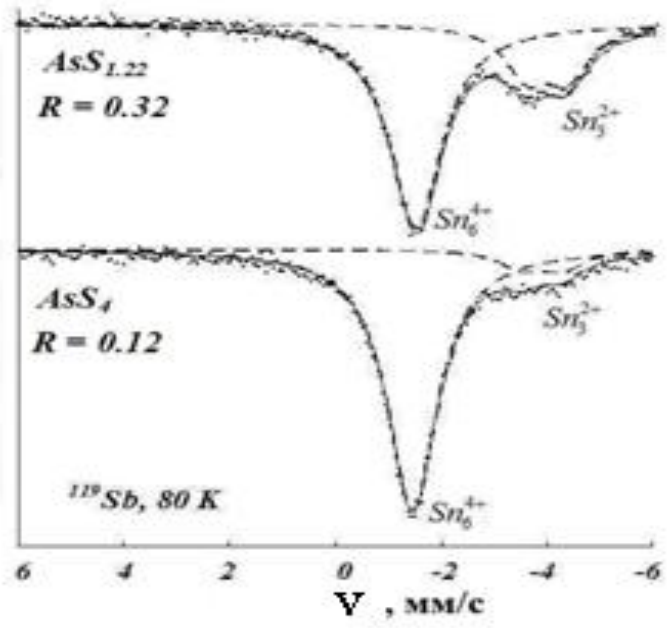

Figure 3. Mössbauer spectra ^{119}Sb (^{119m}Sn) glassy $AsSe_{0.4}$ at 80 K. The position of the lines corresponding to the centers and Sn_6^{4+} Sn_3^{2+}. Quenching the melt from 700°C in air.

Antimony atoms of arsenic chalcogenides coordinating state and two-rehvalentnogo couple different tin (Sn_3^{2+} and Sn_6^{4+}) and tin plays the role of impurity centers minus U-amphoteric type (Figure 3) [3].

Emission Mössbauer Spectroscopy ^{119m}Te (^{119m}Sn)

Motherboard 119 mTe atoms in the structural grid glassy chalcogenides germanium and arsenic occupy anion chalcogen components, so that most of daughter atoms ^{119m}Sn, stabilized in the anionic sites in the form of Sn^0 centers are electrically inactive, while their smaller part shifted to cationic units, forming amphoteric U-minus centers.

CONCLUSION

On the basis of spectroscopic data messbaueroskoy it found that the impurity of tin atoms in the cation sublattice crystalline and glassy chalcogenide semiconductors form electrically active centers U-minus, and in crystalline semiconductors doped tin minus U-donor centers exhibit activity, and in vitreous semiconductors - amphoteric activity. The anionic sublattices impurity tin atoms are electrically inactive.

Electrical activity of tin impurity atoms in the cation sites, and the lack of it for impurity tin atoms in the anion sublattice due to the fact that:

- Tin in the lithium cation sublattice forms covalent bonds with the chalcogen atoms in their local environment, typical semiconductor compounds A4B6, and realized the possibility of forming the forbidden band local energy levels for it;
- In the anion sublattice tin intermetallic forms chemical bonds with atoms in its local environment, typical of metals and intermetallic compounds in which there are no conditions for the formation of local energy levels.

Electronic configuration 4d105s25p2 tin atoms. When entering into the net glass tin forms chemical bonds with the chalcogen atoms using two electron-5p (sold state Sn^{2+}), and remain unused paired 5s on the back of two-electron (“single pair of electrons” or “lone pair of electrons”). According to the ideas of Anderson spin interaction of the two 5s-electrons prevents single ionization of impurity tin atoms electrons and, as a result, formed two centers Sn_6^{4+} and Sn_6^{2+} (“a pair of variable-valence”), which are singly ionized acceptor and donor states - amphoteric U-centers tin.

The difference between the nature of the electrical activity of the tin in the crystalline and glassy-chalcogenide semiconductors is explained as follows:

- Tin crystalline PbS and PbSe is lattice sites and is unable to change their coordination state (both center Sn_6^{4+} and Sn_6^{2+} are in the same state and coordination naturally tin can form only donor levels); - Tin chalcogenide glasses can rebuild their coordination state of compliance of the structural glass network, the center of two charge states are in various states of coordination and, of course, only a tin can form amphoteric U-minus centers.

REFERENCES

[1] M. Yu. Kozhokar. Proceedings of the Conference on Physics and Astronomy for Young Scientists of St. Petersburg and North-West. *Fizik A. SPB.* St. Petersburg, 2010. - pp. 19-20.

[2] M. Yu. Kozhokar, A. V. Zaitseva. *XLIX International Scientific Student Conference on Student and Technological Progress*. Novosibirsk, 2011. - p. 362.

[3] M. Yu. Kozhokar. Proceedings of the Conference on Physics and Astronomy for Young Scientists of St. Petersburg and North-West. *Fizik A. SPB.* St. Petersburg, 2012. pp. 106-107.

Smart Nanocomposites
Volume 8, Number 1
ISSN: 1949-4823

MECHANICAL PROPERTIES OF POLYACRYLIC ACID - POLYVINYL ALCOHOL HYDROGELS AT COMPRESSION AND EXTENSION

I. S. Kuryndin, I. Yu. Dmitriev, N. V. Bobrova, Z. F. Zoolshoev, and G. K. Elyashevich*
Institute of Macromolecular Compounds, Russian Academy of Sciences,
Saint Petersburg, Russia

ABSTRACT

Cylinder and ring shaped samples of hydrogels were prepared by polymerization of acrylic acid in the solution of polyvinyl alcohol. The swelling degree and mechanical properties of the hydrogels were determined. The two-components hydrogels are characterized by a higher breaking strength and elasticity than the polyacrylic acid gels. It was found that the hydrogels demostrate the electromechanical response.

Keywords: hydrogels, polyacrylic acid, polyvinyl alcohol, swelling degree, mechanical properties

INTRODUCTION

Hydrogels are of great interest to researchers as elements of artificial muscles. At present the hydrogels prepared of polyelectrolyte polymers are promising materials for the soft robotic applications due to easy manufacturing and low voltages for their actuation [1]. The application of hydrogels as artificial muscles is caused by their ability to the considerable changes of swelling degree under the small variations of external conditions (electric field, pH medium, ionic force, light and heat exposure) [2, 3]. The deformation (compression, tension, bending) of polyelectrolyte hydrogels in an electric field is the result of the pronounced changes in their swelling degree at displacement of ionic equilibrium in the volume of hydrogel, the transport of ions through hydrogel and electrochemical reactions on electrodes [4-7]. Earlier the swelling systems with electromechanical response based on polyacrylic acid and polyvinyl alcohol were investigated in [2, 8]. The problem is to provide

* Corresponding Author: Prof. G.K. Elyashevich, Dr. Sci. (Polymer Physics), Institute of Macromolecular Compounds, Russ. Acad. Sci, 199004 Saint Petersburg.Tel./Fax: +7 812 3286876; E-mail: elya@hq.macro.ru

the polyelectrolyte gels a sufficient level of breaking strength and elasticity. It may be solved by the preparation of two-components interpenetrating networks containings trong polyelectrolyte and also the component to optimize the mechanical properties of hydrogels. The goal of this work was to synthesize the electroactive hydrogels based on polyacrylic acid and polyvinyl alcohol and to investigate the dependence of their swelling degree and mechanical properties on the preparation conditions.

MATERIALS & METHODS

The preparation technique of polyacrylic acid (**PAA**) - polyvinyl alcohol (**PVA**)hydrogels of required shape has been elaborated. The hydrogels were synthesized by free-radical copolymerization of acrylic acid in water solution of PVA (M_w = $7 \cdot 10^4$) at 30^0C. Methylenebisacrylamide was used as crosslinker. Concentrations of PVA in solution were chosen as 5, 10 and 15%. Three-component initiator (ammonium peroxydisulfate/ Mohr's salt/sodium sulfite) was used to synthesize PAA - PVA hydrogels [9]. As a result the semi-interpenetrating network of PAA and PVA was formed. Cylinder and ring shaped samples were prepared. Swelling degree of the hydrogels and their mechanical properties under compression and extension have been measured.

RESULTS AND DISCUSSION

It was observed that equilibrium swelling degree of hydrogel PAA-PVA in distilled water decreases (from 4.0 to 3.2 g/g) as the concentration of PVA in solution increases (Figure 1). All of the PAA-PVA samples demonstated a swelling degree lower than one of PAA hydrogel (13.8 g/g).

The swelling degree of the samples PAA-PVA in 5% water solution of Na_2SO_4 is about 20% lower than in distilled water (Figure 1) because the degree of dissociation of PAA in water is higher than in sodium polyacrylate.

The cylinder shaped hydrogels swollen in distilled water were tested under compression (Figure 2). It was found that all the PAA-PVA hydrogelsexhibit a higher breaking strength than PAA gels (160 kPa). Maximal value (250 kPa) was observed for the PAA-PVA gels synthesized in 5% solution of PVA, and it decreases as the concentration of PVA increases. When PVA content grows from 5 to 15% the elastic modulus diminishes (from 75 to 50 kPa) and breaking deformation rises (from 60 to 80%). All of the PAA-PVA gels are characterized by a higher breaking deformation and lower elastic modulus than PAA ones (40% and 207 kPa, respectively).

The ring shaped PAA-PVA gels swollen in distilled water were used for mechanical tests at extension (Figure 3). It was shown that the increasing of PVA concentration from 10 to 15% results in the increase of breaking strength from 60 to 65 kPa and elongation at break from 125 to 168%; at the same time elastic modulus decreases from 63 to 46 kPa.

The ring-shaped PAA-PVA gels synthesized at PVA concentration equal to 10% and swollen in 5% water solution of Na_2SO_4 are characterized by a higher deformation at break (375%), a higher breaking strength (70 kPa) and a lower elastic modulus (23 kPa) than these samples swollen in distilled water (Figure 3).

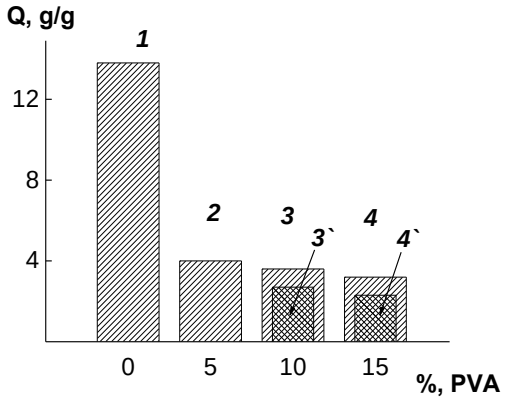

Figure 1. Equilibrium swelling degree of hydrogels PAA (1) and PAA-PVA in distilled water (2 – 4) and in 5% Na_2SO_4 water solution of (3`, 4`) on content of PVA.

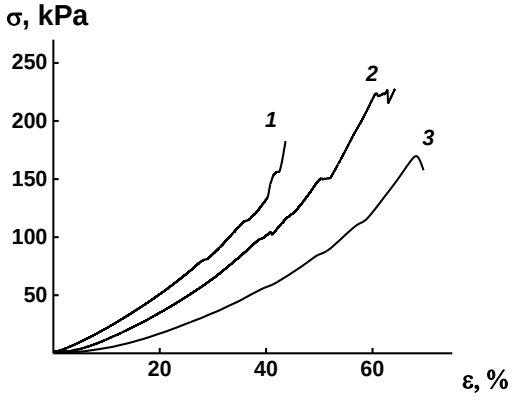

Figure 2. Stress-strain curves at compression after equilibrium swelling in water for the hydrogels PAA (1) and PAA-PVA: PVA content 5% (2) and 15% (3).

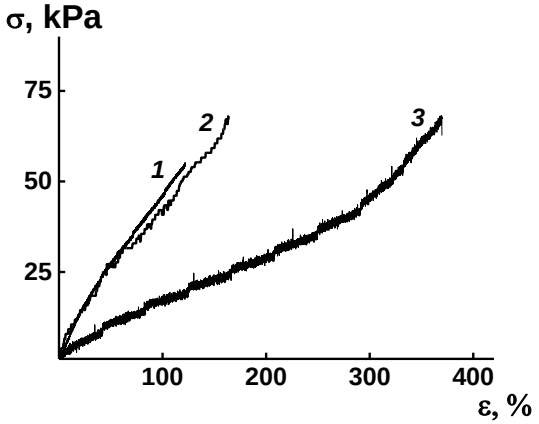

Figure 3. Stress-strain curves at extension for the hydrogels PAA-PVA: PVA content 10% and 15% (1, 2) after equilibrium swelling in water:; PVA content 10% after equilibrium swelling in 5% water solution of Na_2SO_4 (3).

It was found that the elastic rings of the PAA-PVA hydrogels demonstrate the electromechanical response (compression) under electric voltage. The effect is more pronounced when the rings swell in Na_2SO_4 solution as compared with their swellingin water. These results evidence that the PAA-PVA gels may be used as linear electric actuators (artificial muscles).

ACKNOWLEDGMENTS

This work was supported by The Programme of the Division of Chemistry and Material Science, Russian Academy of Sciences № 7 "The Elaboration of Scientific Fundamentals of Ecologically Safe and Resource Saving Technological Processes" (2015-2017), the Russian Foundation for Basic Research (Project № 16-03-00265a) and Project of Collaborative Research of the Russian Academy of Sciences and the University of Ljubljana (Slovenia) (ARRS-BI-RU/16-18-017).

REFERENCES

[1] Bar-Cohen Y., *Electroactive polymer (EAP) actuators as artificial muscles: Reality, potential, and challenges*. Bellingham: SPIE Press, 2004. 765 p.
[2] Osada Y., Gong *J., Prog. Polym. Sci*., 18, (1993), 187-226.
[3] Shiga T., *Adv. Polym. Sci.,* 134 (1997), 131-163.
[4] Elyashevich G. K., Smirnov M. A., Bobrova N. V., Dmitriev I. Yu., Bukošek V., *Smart Nanocomposites,* 3 (2), (2012), 123-136.
[5] Otake M., Kagami Y., Inaba M., Inoue H., *Robotics and Autonomous Systems*, 40, (2002), 185-191.
[6] Budtova T., Suleimenov I., Frenkel S., *Polymer Gels and Networks*, 3(3), (1995), 387-393.
[7] Rasmussen L., Erickson C. J., Meixler L., Ascione G., Gentile C. A., Tilson C., Abelev E., *Polym. Int.,* 59, (2010), 290–299.
[8] Byun H., Hong B., Nam S. Y., Jung S. Y., Rhim J. W., Lee S. B., Moon G. Y., *Macromol. Research,* 16(3), (2008), 189-193.
[9] Bel'nikevich N. G., Bobrova N. V., Elokhovskii V. Yu., Zoolshoev Z. F., Smirnov M. A., Elyashevich G. K., *Russian Journal of Applied Chemistry,* 84(12), (2011), 2106-2113.

Smart Nanocomposites
Volume 8, Number 1
ISSN: 1949-4823

SOLUBILITY, THERMAL ANALYSIS, AND ASSOCIATION IN WATER SOLUTIONS OF THE ADDUCTS OF FULLERENE C_{60} WITH LYSINE, L-THREONINE, L-HYDROXIPROLINE

Dmitry G. Letenko[1,*], Konstantin N. Semenov[2], Nikolay A. Charykov[3,4], Viktor A. Keskinov[3], Natalya A. Kulenova[5], Nikolay M. Saf'yannikov[4], Natalya N. Duryagina[3], Polina V. Garamova[3], Vyacheslav V. Klepikov[3], Andrey A. Zolotarev[3], and Alexey S. Ivanov[6]

[1]Saint Petersburg State University of Architecture and Civil Engineering (SPSUACE) Saint Petersburg, Russia
[2]Saint Petersburg State University, Saint Petersburg, Russia
[3]Saint Petersburg State Technological Institute (Technical University), Saint Petersburg, Russia
[4]Saint Petersburg State Electrotechnical University (LETI), Saint Petersburg, Russia
[5]East Kazakhstan State Technical University, Ust-Kamennogorsk, Kazakhstan
[6]Saint Petersburg Mining University, Saint Petersburg, Russia

ABSTRACT

This work devoted to the synthesis, identification and investigation of physical-chemical properties (including solubility in binary water containing systems, association processes and complex thermal analysis) of the derivatives of light fullerene (C_{60})of Light Fullerene C60and Essential Amino-acids: Lysine, L-Threonine, L-hydroxyproline, namely: Bis-Adduct$C_{60}(C_6H_{13}N_2O_2)_2$, $C_{60}(C_4H_8NO_3)_2$, $C_{60}(C_5H_9NO_3)_2$ at 25ºC.

Keywords: Bis-Adduct, Light Fullerene C_{60}, Essential Amino-acids: Lysine, L-Threonine, L-hydroxyproline, synthesis, identification, investigation of physical-chemical properties

* Corresponding Author E-mail: dletenko@mail.ru

INTRODUCTION

This article is the continuation of the cycle of the authors articles [1-16], devoted to the synthesis, identification and investigation of physical-chemical properties (including solubility in binary, ternary systems, association processes and complex thermal analysis) derivatives of light fullerenes (C_{60}andC_{70}) and: complex ethers of two-base carbon acids (malonates, oxalates), hydroxylated forms (fullerenols), amino-acids (arginine, β-alanine). As was shown earlier, the properties of this compounds are unique practically for all types of solutions. The relevance of the investigation is connected with such well-known fact, that fullerenes themselves are not practically soluble in water, water solutions, in particular physiological (blood, gastric juice, lymph etc). So, this fundamentally restricts its use in medicine, pharmacology, food industry. Synthesis and investigation of well soluble fullerene derivatives is actual.

MATERIALS AND METHODS

Amino acid derivative of the C_{60} fullerene with the Essential Amino-acids: Lysine, L-Threonine, L-hydroxyproline, namely: Bis-Adducts$C_{60}(C_6H_{13}N_2O_2)_2$, $C_{60}(C_4H_8NO_3)_2$, $C_{60}(C_5H_9NO_3)_2$ at 25ºC L- threonine (C_{60}-Thr) - $C_{60}(C_4H_9NO_3)_2$ of mass fraction purity 99.8% were used for the physico-chemical investigation of water solutions. The reagent was produced in Ltd ZAO "ILIP" (St. Petersburg). Additionally we have carried out the identification of the purchased C_{60}-bis adducts using the complex of physico-chemical methods (IR and UV – spectroscopy, mass-spectrometry, elemental analysis).

The measurements of the concentration dependence of density of the C_{60}-bis adducts aqueous solutions were performed by picnometer method. We used quartz picnometer, volume calibration was performed with distilled water, the accuracy of temperature control during the density measurement was ΔT = ± 0.1 ÷ 0.2 K degrees, the accuracy of densities determination was equal to $\Delta\rho = \pm 0.001$ g·cm^{-3}. The series of the C_{60}-bis adducts water solutions were prepared by dilution of the basic solution at 298.15 ± 0.05K.

The concentration dependence of refractive index of the C_{60}-bis adducts derivatives water solutions (n_D^{20}) was measured by refractometry, using Abbe refractometer IRF-454B2M (measurement limits in transmission light n_D^{25} = 1.3-1.7, $\Delta n_D^{20} = \pm 0.0001$, the accuracy of temperature control $\Delta T = \pm 0.2$ K).

The temperature dependence of the C_{60}-bis adducts derivatives solubility in water in the temperature range 293.15 – 353.15 K was carried by the method of isothermal saturation in ampoules. The saturation time was equal to 8 hours, temperature was maintained with accuracy equal to $\pm$ 0.05 K. For the C_{60}-Thr water solutions saturation the LAUDA ET 20 thermostatic shaker was used at a shaking frequency $\omega \approx 80$ c^{-1}, quantitative determination of the C_{60}-bis adducts concentrations in water was performed using spectrophotometric technique at 330 nm (after the dilution and cooling of saturated solutions). The relative uncertainty of the solubility determination was equal to ± 5%. Relative air humidity was 40-50%.

For the thermal investigation of the C_{60}-bis adducts we have used Netzsch STA 449 F1 Jupiter and Netzsch QMS 403CAeolos apparatus, the temperature range was 303.15 – 1300.15 K at the air, the heating rate was 5 $K \cdot min^{-1}$.

RESULTS AND DISCUSSION

Solubility and Saturated Solutions Density of Bis-adducts of Light Fullerene C_{60} and Essential Amino-Acids: lysine, l-threonine, l-hydroxyproline: $C_{60}(C_6H_{13}N_2O_2)_2$, $C_{60}(C_4H_8NO_3)_2$, $C_{60}(C_5H_9NO_3)_2$

Diagrams of solubility in all three systems consist 2 branches of crystallization of crystal hydrates: $C_{60}(C_6H_{13}N_2O_2)_2*5H_2O$, $C_{60}(C_4H_8NO_3)_2*6H_2O$, $C_{60}(C_5H_9NO_3)_2*2H_2O$ (low temperature branches) and non-water bis-adducts: $C_{60}(C_6H_{13}N_2O_2)_2$, $C_{60}(C_4H_8NO_3)_2$, $C_{60}(C_5H_9NO_3)_2$, (high temperature branches). All invariant points O of crystal hydrate de hydration correspond to close temperatures: $T(O)_{C60(C6H13N2O2)2}$ = 44°C, $T(O)_{C60(C4H8NO3)2}$ = 55°C, $T(O)_{C60(C5H9NO3)2}$ = 50°C. Solubility (S) of all bis-adducts is great and is from tens to thousands g/dm^3. At all temperatures: $S_{C60(C6H13N2O2)2} < S_{C60(C4H8NO3)2} << S_{C60(C5H9NO3)2}$.

With the help of quartz picno-meters in the same conditions temperature dependence of density of saturated solutions was investigated (thermostat accuracy $\Delta T = \pm 0.1$ K, density accuracy $\Delta\rho = \pm 0.0002 \div 0.0005$ g/sm^3).

Examples of solubility diagram is represented lower in Figure 1, 2 for bis-adduct with threonine. Terminology, concerning invariant points – eutonics, peritonics etc. is given for example in the monograph [17].

Temperature dependences of solubility (S) (Figure 1) and density (ρ) (Figure 2) of the C_{60}-Thr water solutions. Low-temperature line corresponds to crystallization of $C_{60}(C_4H_9NO_3)_2*6H_2O$, high-temperature line corresponds to crystallization of non-hydrated fullerene derivative - $C_{60}(C_4H_9NO_3)_2$. O is a nonvariant eutonics point.

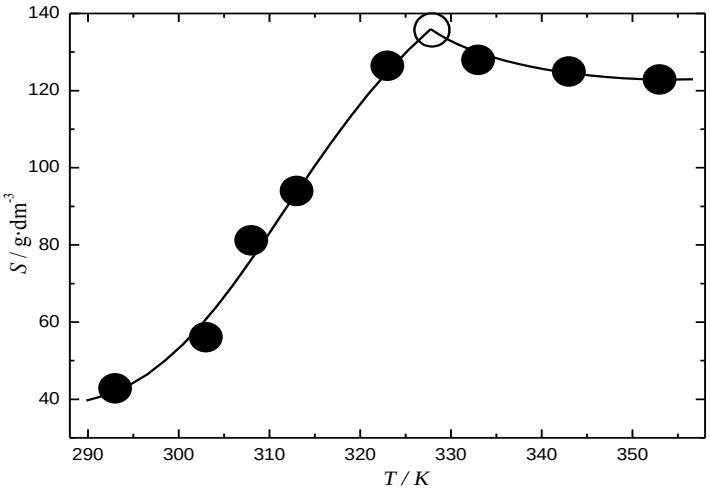

Figure 1.

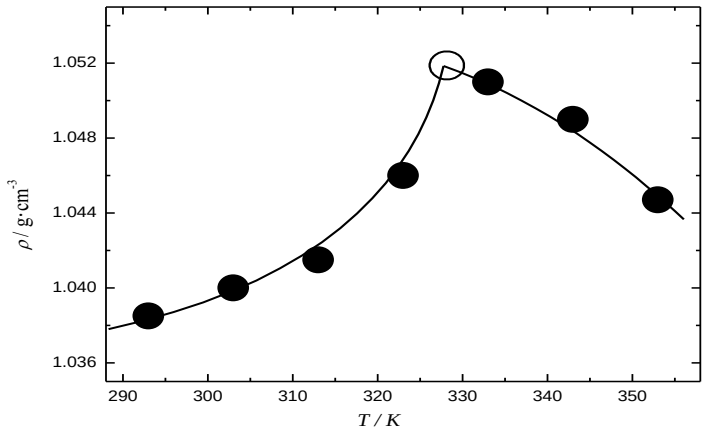

Figure 2.

Complex Thermal Analysis of Bis-adducts of Light Fullerene C_{60} and Essential Amino-Acids: lysine, l-threonine, l-hydroxyproline: $C_{60}(C_6H_{13}N_2O_2)_2$, $C_{60}(C_4H_8NO_3)_2$, $C_{60}(C_5H_9NO_3)_2$

By the method of complex thermal analysis the investigation of $C_{60}(C_6H_{13}N_2O_2)_2*5H_2O$, $C_{60}(C_4H_8NO_3)_2*6H_2O$, $C_{60}(C_5H_9NO_3)_2*2H_2O$ was provided at the temperatures 40 ÷ 1100°. All crystal hydrates first of all lose crystal water, then at T≈170÷220°C oxidation thermal destruction of amino-acids groups starts (consequent dehydration ($-H_2O$), de-nitrogen process ($-N_2$), decarboxylation ($-CO_2$ and - CO). These stage processes continue at ≈720 ÷ 830°C, i.e., fullerene core stabilize amino-acids essentially. Finally at T≈750÷850°C starts destruction of fullerene core. An example for the derivative with threonine-bis-adduct is represented lower in Figure 3.

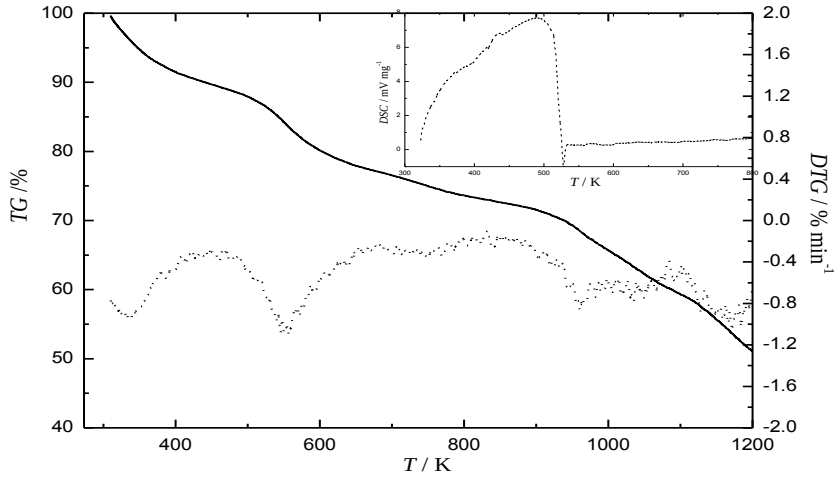

Figure 3. Thermal analysis of the $C_{60}(C_4H_9NO_3)_2*6H_2O$ derivative.

Dynamic Light Scattering of Water Solutions of Bis-adducts of Light Fullerene C_{60} and Essential Amino-Acids: lysine, l-threonine, l-hydroxyproline: $C_{60}(C_6H_{13}N_2O_2)_2$, $C_{60}(C_4H_8NO_3)_2$, $C_{60}(C_5H_9NO_3)_2$

By the method of dynamic light scattering the concentration dependencies of associate dimensions was investigated in the binary systems: $C_{60}(C_6H_{13}N_2O_2)_2 - H_2O$, $C_{60}(C_4H_8NO_3)_2 - H_2O$, $C_{60}(C_5H_9NO_3)_2 - H_2O$at 25°C, concentration range C = 0.01 ÷ 10 g/dm^3). In all cases while concentration increases, we have seen consequent formation from monomers (diameter $\delta_0 \sim 2$ nm) the associates of I order (diameter $\delta_I \sim 20 \pm 10$ nm), from them the associates of the II order form ($\delta_{II} \sim 200 \pm 100$ nm), from them III order associates form ($\delta_{III} \sim 5000 \pm 1000$ nm). Last associates are micro-heterogeneous. Such hierarchical association we have observed earlier for other C_{60}derivatives [1, 3, 4, 16].

CONCLUSION

So, authors have provided original investigations, concerning synthesis, identification and water solution properties of novel bis-adducts of fullerene C_{60} and some essential amino-acids. The synthesis and all investigations, as authors know, were provided for the first time. The solubility of all adducts in all natural temperature range are relatively high (tens – first hundreds g/dm^3) and they are perfectly compatible with water and water solutions. All adducts in water solutions are hierarchically associated and are even micro-heterogeneous in the solutions with high concentrations.

ACKNOWLEDGMENTS

Investigations were fulfilled with the support of Russian Found of Fundamental Investigations (Projects NN: 15-08-08438, 16-08-01206, 15-29-05837) and Russian Found of the Support of Small Forms of Business in Science and Technology (Contract N24357).

REFERENCES

[1] K. N. Semenov, N. A. Charykov, V. N. Postnov, V. V. Sharoyko, I. V. Murin. *Uspechi Khimii* (Russian Chemical Reviews). 2016. V. 85. N1. P. 38-59.

[2] G. G. Panova, I. N. Ktitorova, O. V. Skobeleva, N. G. Sinjavina, N. A. Charykov & K. N. Semenov. *International Journal on Plant Growth and Development*, Volume 79, Number 3, P. 309-318.

[3] K. N. Semenov, N. A. Charykov, I. V. Murin, Yu. V. Pukharenko. *J. of Molecular Liquids.* 2015. V. 202. P. 50-58.

[4] K. N. Semenov, N. A. Charykov, I. V. Murin, Yu. V. Pukharenko. Physico-chemical properties of the fullerenol-70 water solutions. *J. of Molecular Liquids*. 2015. V. 202. - P. 1-8.

[5] K. N. Semenov, N. A. Charykov, V. A. Keskinov, Fullerenol Synthesis and Identification. Properties of the Fullerenol Water Solutions, *J. Chem. Eng. Data*. 56(2011) - P. 230-239.

[6] I. A. Pestov, V. A. Keskinov, K. N. Semenov, N. A. Charykov, D. G. Letenko, V. A. Nikitin. Rus. *J. of Phys. Chem*. 2015. V. 89. N6. P. 990-992.

[7] O. S. Manyakina, K. N. Semenov, N. A. Charykov, N. M. Ivanova, V. A. Keskinov, V. V. Sharoyko, D. G. Letenko, V. A. Nikitin, V. V. Klepikov, I. V. Murin. *Journal of Molecular Liquids.* 2015. V. 211. P. 487-493.

[8] K. N. Semenov, I. G. Kanterman, N. A. Charykov, I. V. Murin, A. S. Kritchenkov. *Russian Journal of Physical Chemistry*. 2014. V. 88. N 6. P.1073-1076.

[9] K. N. Semenov, N. A. Charykov, V. A. Keskinov. *J. Chem. Eng. Data*. V. 56. 2011. P. 230-239.

[10] D. G. Letenko, V. A. Nikitin, K. N. Semenov, S. A. Ivanov. *Rus. J. Phys. Chem.* 2012. V. 86. N12.P. 1806-1813.

[11] K. N. Semenov, N. A. Charykov. *Rus. J. Phys. Chem*. 2012. V. 86. N10. P. 1636-1639.

[12] A. I. Lushin, N. A. Charykov, K. N. Semenov, V. I. Namazbaev, V. A. Keskinov, A. S. Kritchenkov. *Industrial and Engineering Chemical Research*. 2013. V. 52. P. 14583-14591.

[13] K. N. Semenov, V. A. Keskinov, N. A. Charykov, A. S. Kritchenkov, I. V. Murin. *Industrial and Engineering Chemical Research*. 2013. V. 52. P. 16095-16100.

[14] K. N. Semenov, N. A. Charykov. Phase Equilibria in Fullerene – Containing Systems. In: *Handbook on Fullerene: Synthesis, Properties and Applications*. Editors R. F. Verner and C. Benvegny. P. 1-91. 2011. Nova Sciences Publishers, Inc.

[15] K. N. Semenov, N. A. Charykov. Solubility of Light Fullerenes and Fullerenol in Biocompatible with Human Beings Solvents. In: *Handbook on Grapes*. Editors R. P. Murphy et al. P. 1-48. 2011. Nova Sciences Publishers, Inc.

[16] A. A. Shestopalova, K. N. Semenov, N. A. Charykov, V. N. Postnov, N. M. Ivanova, V. V. Sharoyko, V. A. Keskinov, D. G. Letenko, V. A. Nikitin, V. V. Klepikov, I. V. Murin. *Journal of Molecular Liquids*. V. 211. 2015. P. 301–307.

[17] M. V. Charykova, N. A. Charykov. *Thermodynamic Modelling of the Processes of Evaporate Sedimentation*. St. Petersburg. Nauka. 2003. 237 p.

Smart Nanocomposites
Volume 8, Number 1
ISSN: 1949-4823

THERMAL DESORPTION OF INERT GASES IN METAL-OXIDE NANOMATERIALS

Evgeniya V. Maraeva[1,*], Anton A. Bobkov[1], Vyacheslav A. Moshnikov[1], and Igor A. Averin[2]
[1]Saint Petersburg Electrotechnical University "LETI," Russian Federation
[2]Penza State University, Russian Federation

ABSTRACT

The specifics of applying the inert gas thermal desorption method for studying the porous structure parameters of nanomaterials based on SiO_2 – SnO_2 for vacuum sensors are studied. The possibilities for modifying the metal oxide layers to manage the parameters of their porous structure, and selection of modifying agents are discussed.

Keywords: Porous nanoparticles, sol-gel synthesis, pore size distribution

INTRODUCTION

The manufacturers of modern instruments and devices currently show great interest in porous nanostructured materials. Thus, the grade of surface development and availability of a multi-layer system of pores play a defining role in technology of semiconducting metal oxide gas sensors, where different pore types can facilitate different functionality. The structure features (pore size, size distribution, pore volume, specific surface area) are combined under the term "porous body texture." As it was recommended by IUPAC, the porous systems are classified by predominant pore size into microporous (pore diameter up to 2 nm), mesoporous (2 to 50 nm), and macroporous (over 50 nm). In metal oxide sensors, the macropores can facilitate the feed of gas or liquid materials to nanoreactors, as well as carry away the reaction products. The micropores appear to be a key player in adsorption processes of semiconducting gas sensors. In mesh structures, there is a micropore system that blocks and unblocks the conductivity.

Currently, there are several groups of research methods for porous structure parameters of materials [1-3]. When studying the materials with multi-layer pore system, it is definitely

* Corresponding Author: PhD. Evgenia V. Maraeva, Assistant, Department of micro- and nanoelectronics, Saint Petersburg Electrotechnical University "LETI", 197376, Russian Federation, Saint Petersburg, Prof. Popova Street. 5, Russian Federation, Tel.: + 7 812 234 3164, E-mail: jenvmar@mail.ru

interesting to look into the adsorption and desorption processes in wide range of relative partial pressures, including the cases with capillary condensation of inert gases. This allows us to obtain data not only on specific surface area, but also on the pore size distribution, as the pore content nature for physical adsorption can be judged particularly by the initial section of adsorption isotherm and the section exposed to high pressures. However, despite the progress made in application of nanoporous materials over the recent decades, the task of evaluating their fractality remains unresolved.

MATERIALS AND METHODS

In this study the sol-gel technology was used to synthesize the porous nanomaterials based on silicon dioxide and stannic oxide. Tetraethoxysilane served as a source (precursor) of silicon dioxide, and inorganic water-soluble tin salt $SnO_2 \cdot 2H_2O$ was used as a source of stannic oxide. The propyl and butyl alcohols served as solvent. To obtain powders, 10% aqua ammonia (NH_4OH) was added to the solutions-sols. Adding ammonia is accompanied by changes in pH of the solution ranged from 2 to 8, and an immediate condensation of the hydrolysis products takes place resulting in a much faster gelation process. After the gelation, evaporation of the solvent at the indoor temperature was performed, and then the powders received were heat-treated for 30 minutes at the temperature of 600°C.

To control properties of the synthesized nanomaterial surface, the nitrogen thermal desorption and atomic force microscopy were used. Specific surface area and pore distribution measurements were made using Sorbi MS (CJSC «META», Novosibirsk, Russia). Before the measurements, all the samples were pretreated in the SorbiPrep preparation station. The operating principle of the station is based on the degassing dispersed and porous materials by heating in a stream of an inert gas (helium). The station allows one to set the temperature and time of heating in the range of 50–400°C, 0–99 minutes.

RESULTS AND DISCUSSION

The main purpose of this work was to research the specifics of applying the inert gas thermal desorption method for studying the porous structure parameters of nanomaterials based on SiO_2 – SnO_2 for vacuum sensors. The stated purpose implies the following objectives:

1. to develop the process solutions for synthesizing the porous metal oxide nanomaterials in a system based on SiO_2 – SnO_2 with controlled morphology and mesopores size distribution;
2. to identify the correlation between the synthesis process modes and the parameters of porous structure of metal oxide systems, which respond to the atmospheric composition and gas pressure.

The earlier researches of metal oxide sensor systems responding to the atmospheric composition and gas pressure [4-9] show that the porous nanostructured films based on metal oxides and silicon dioxide actively react with the atmosphere, which leads to adsorption of

different gases on their surface, including oxygen, carbon dioxide, water vapor, etc. When the pressure drops below the atmospheric pressure, gas desorption occurs, causing the resistance of such films to reduce significantly. Therefore, the porous nanostructured materials based on SiO_2-SnO_2 can be used for producing the highly sensitive, miniature, power efficient, and reliable vacuum sensors. The maximum sensitivity to pressure drop below atmospheric is offered by vacuum sensors, which are based on percolation mesh structures with 85% mass fraction of stannic oxide.

For research purposes, a set of specimens with different component ratio was prepared. The work scope included analysis of possibilities for modifying the metal oxide layers to manage the parameters of their porous structure, and selection of modifying agents. The modifying agent of choice was the carbon-bearing materials, including the amorphous carbon.

For all the patterns pore distribution measurements were made using Sorbi MS that realizes physical adsorption and desorption of noble gas by the sample to be studied [3]. For the measurement of absorbed gas volume the thermal desorption method was applied. In this method a thermal conductivity sensor is a detector of gas mixture composition. The signal of thermal conductivity sensor (TCS signal) is a desorption curve. The measurements were made under variation of the relative partial pressure (P/P_0) of gas-adsorbate. For example the nitrogen desorption curves for the sample containing $50\%SiO_2$–$50\%SnO_2$ are shown in the Figure 1.

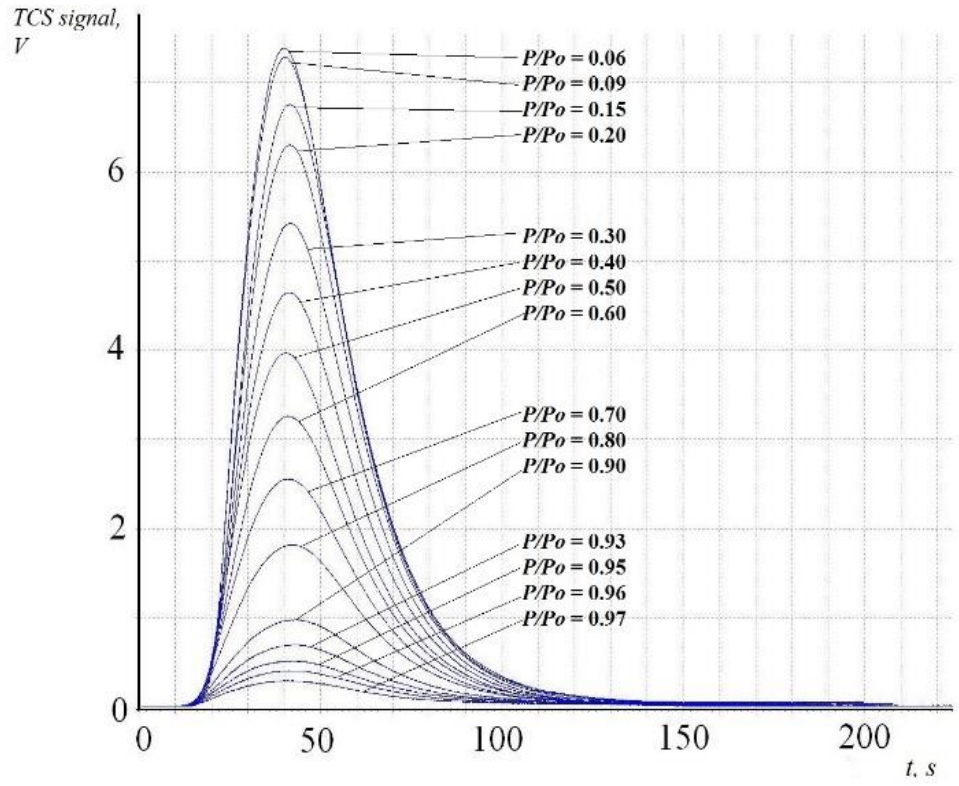

Figure 1. Nitrogen desorption curves for the sample containing $50\%SiO_2$–$50\%SnO_2$ modified with carbon-bearing material.

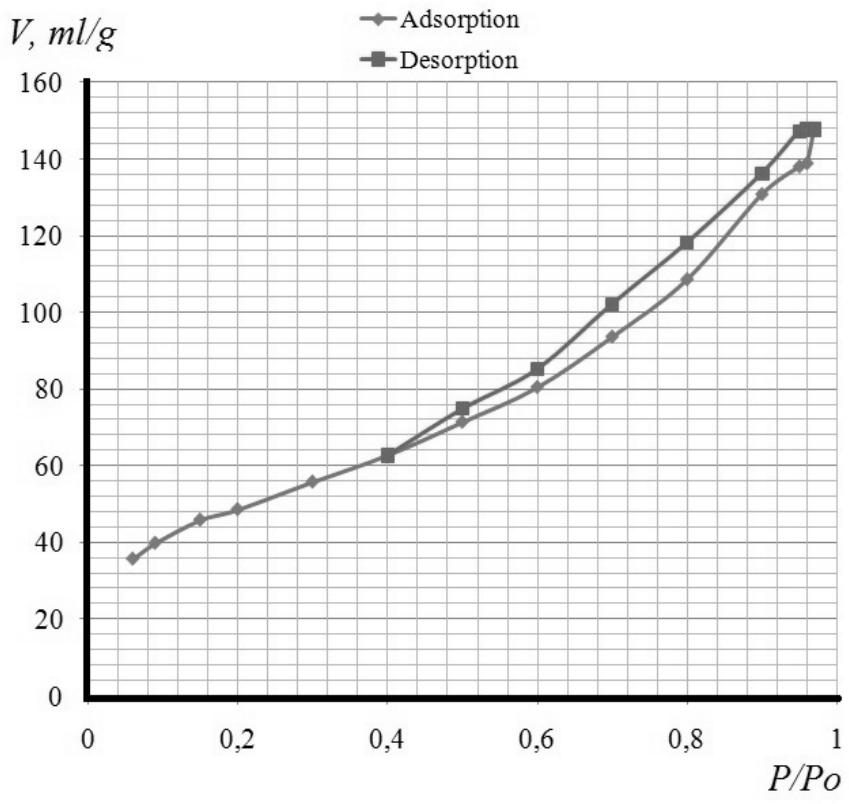

Figure 2. Full adsorption/desorption isotherm for the pattern containing 50%SiO_2 – 50%SnO_2 modified with carbon-bearing addition.

In terms of studying the capillary condensation processes in nanomaterials based on SiO_2 – SnO_2, it was established that there is the so-called sorption hysteresis in the middle adsorption isotherm of all specimens. In the Figure 2 the full nitrogen adsorption/desorption isotherm for the pattern containing 50% SiO_2 – 50% SnO_2 modified with carbon-bearing addition is shown for example. The assessment of porous structure parameters showed that in all cases the introduction of carbon-bearing modifying agent leads to formation of an additional system of pores with average radius of 15 to 20 nm. The obtained results correlate with the findings of research [6]. Most likely, this is driven by carbon removal from the porous structure during the thermal annealing.

Thus, the work defines the process modes for synthesizing the porous metal oxide materials in the system “silicon dioxide - stannic oxide” with various modifying agents with controlled morphology and 2 to 50 nm pore size distribution. The technology has been worked out for production of nanomaterials based on SiO_2 – SnO_2 with the required component ratio and the set pore size, using the carbon-bearing agents. The methods for studying the gas capillary condensation processes in metal oxide nanomaterials based on SiO_2 – SnO_2 with the set pore size have been developed for evaluation of parameters of porous structure. The findings allow us to optimize the technology of metal oxide structure synthesis for gas-sensing probes and of porous matrices for optoelectronic devices based on metal chalcogenides [10, 11].

ACKNOWLEDGMENTS

This study was supported by the Ministry of Education and Science of the Russian Federation within the framework of the project № 16.897.2017/ПЧ.

REFERENCES

[1] Maex K., Baklanov M. R., Shamiryan D., et al. Low dielectric constant materials for microelectronics. *Journal of Applied Physics*, 2003. Vol. 93, №. 11. PP. 8793-8841.

[2] Gidley D. W., Frieze W. E., Dull T. L., Sun J., Yee A. F., Nguyen C. V., Yoon D. Y. Determination of pore-size distribution in low-dielectric thin films. *Applied Physics Letters*, 2000. Vol. 76, № 10. PP. 1282- 1284.

[3] Belorus A. O., Maraeva E. V., Spivak Y. M., Moshnikov V. A. The study of porous silicon powders by capillary condensation. *Journal of Physics: Conference Series*, 2015. Vol. 586. P. 012017.

[4] Gracheva I. E., Moshnikov V. A., Maraeva E. V., et al. Nanostructured materials obtained under conditions of hierarchical self-assembly and modified by derivative forms of fullerenes. *Journal of Non-Crystalline Solids*, 2012. Vol. 358. PP. 433–439.

[5] Abrashova E. V., Gracheva I. E., Moshnikov V. A. Functional nanomaterials based on metal oxides with hierarchical structure. *Journal of Physics: Conference Series*, 2013. Vol. 461. P. 012019.

[6] Maraeva E. V., Istomina M. S., Moshnikov V. A., etc. Study of porous sol-gel nanocomposites based on silicon dioxide and tin dioxide modified by fullerenol C_{60}(OH)n (n = 22–24). *Journal of Physics: Conference Series*, 2016. Vol. 690. P. 012031.

[7] Pronin I. A., Averin I. A., Yakushova N. D., etc Theoretical and experimental investigations of ethanol vapour sensitive properties of junctions composed from produced by sol-gel technology pure and Fe-modified nanostructured ZnO thin films. *Sensors and Actuators A: Physical*, 2014. Vol. 206. PP. 88-96.

[8] Averin I. A., Igoshina S. E., Karmanov A. A., etc. Sensitive elements of vacuum sensors based on porous nanostructured SiO_2-SnO_2 sol-gel films. *Technical Physics. The Russian Journal of Applied Physics*, 2015. Vol. 60. № 6. PP. 928-932.

[9] Abrashova E. V., Kononova I. E., Moshnikov V. A. Metal oxide SnO_2 - ZnO - SiO2 films prepared by sol-gel. *Smart Nanocomposites*, 2013. Vol. 4. № 2. PP. 1-7.

[10] Chesnokova D. B., Moshnikov V. A., Gamarts A. E., etc. Structural characteristics and photoluminescence of $Pb_{1-X}Cd_XSe$ (x = 0-0.20) layers. *Journal of Non-Crystalline Solids*, 2010. Vol. 356. № 37-40. PP. 2010-2014.

[11] Moshnikov V. A., Gamarts A. E., Chesnokova D. B., etc. Growth and properties of nanostructured layers based on $Pb_{1-X}Cd_XSe$ (x = 0-0.20) solid solutions. *Inorganic Materials*, 2011. Vol. 47. № 1. PP. 18-22.

Smart Nanocomposites
Volume 8, Number 1
ISSN: 1949-4823

DATA INCONSISTENCY ON TRANSPORT PHENOMENA IN $A_2^V B_3^{VI}$ MATERIALS WITH THE HOLE CONDUCTIVITY

Sergey A. Nemov[1,2,*], Ali A. Allahkhah[1], and Arseny A. Rulimov[1]
[1]Peter the Great Saint Petersburg Polytechnic University, Saint Petersburg, Russia
[2]Zabaikal'skii State University, Chita, Russia

ABSTRACT

It is shown that accounting of interband scattering allows eliminating contradictions in the literature between interpretations of the electrical properties of $A_2^V B_3^{VI}$ materials with the hole conductivity and describing observed temperature dependences of the kinetic coefficients as well as the parameters of the band spectrum.

Keywords: $A_2^V B_3^{VI}$ materials, Interband scattering, Scattering parameter, Kinetic coefficients, Acoustic mechanism of hole scattering, $Sb_2Te_{2,9}Se_{0,1}$

INTRODUCTION

Investigations of layered semiconductor $A_2^V B_3^{VI}$ materials have been being carried out since the middle of last century.

Constant interest in these materials is caused by their wide usage in thermoelectric energy converters (in the form of ternary and quaternary solid solutions based on bismuth and antimony chalcogenides).

DISCUSSION

The experimental data obtained in the middle of the 20th century were summarized and systematized in Gol'tsman monograph [1]. However, the features of the energy spectrum of $A_2^V B_3^{VI}$ materials and the mechanisms of charge-carrier scattering are still discussed. Also the differences in the interpretation of experimental data of transport phenomena at low

* Corresponding Author: Prof. Sergey Aleksandrovich Nemov, Professor of the Department "Materials Science and Technology of Materials," Peter the Great Saint Petersburg Polytechnic University, Saint Petersburg, Russia, Tel.: +7 (921) 347-30-33, E-mail: nemov_s@mail.ru

(T = 4.2 K) and medium (77 - 300 K) temperatures are stored. Results of the quantum oscillations research at liquid-helium temperatures have confirmed the Drabble-Wolfe one-band six-ellipsoidal model [2] for crystals with low hole concentration. There are some features, which are associated with the existence of the secondary extremes in the valence band in the samples with a higher Fermi energy [2, 3].

The secondary extremum parameters are discussed so far. In addition, the unique view of the Fermi surface of a crystal with high hole concentration is not defined [2, 3]. Specifically, in [2] an ellipsoidal shape is assumed, and in [3] the authors suggest a hyperbolic tubes connecting ellipsoids of light holes.

Anyway, holes of different varieties involved in the quantum oscillations. Therefore, in the analysis of experimental data the two-band model is used at low temperatures.

Most of experimental investigations of transport phenomena in $A_2^{V}B_3^{VI}$ compounds are related to the temperature range 77 - 300 K.

Unlike the low-temperature data, the kinetic coefficients (the conductivity σ, the thermopower α, the transverse Nernst-Ettingshausen effect Q) do not have any differences from the nature of the temperature dependences predicted by the theory within one-band model (at the temperature range 77 – 450 K). Therefore, the one-band model is widely used for analysis of the electrical properties of materials, estimates of energy spectrum parameters and for the calculations of the thermoelectric efficiency.

EXPERIMENTAL

It should be noted that the temperature dependences of the Hall coefficient (R) are characterized by a significant increase of R, the ratio between the Hall coefficients achieves a value $R_{300}/R_{77} \approx 2$. At the same time, in the experiment in the two-band model in the case of ordinary scattering mechanisms of light and heavy holes (scattering at acoustic phonons and the Coulomb potential of impurities and point defects) the thermopower coefficient has no expected significant increase (see Figure 1). In the physics of semiconductors this effect is commonly explained by the complex structure of the valence band.

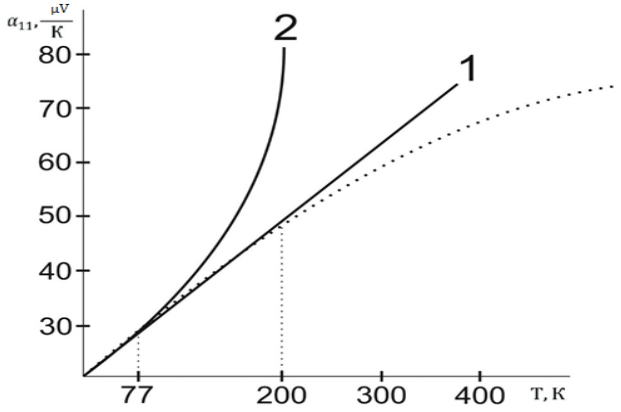

Figure 1. Temperature dependence of the thermopower (α_{11}) in the cleavage plane in the $Sb_2Te_{2,9}Se_{0,1}$ crystal. Dots – experiment; 1, 2 curves – the calculations in the one-band model for degenerate statistics and in the two-band model, respectively.

To explain the observed increase of the Hall coefficient with the temperature growth the two-band model is used, in which the valence band contains two non-equivalent extremes with the different density-of-state effective masses, separated by an energy gap with a width ΔE_v [4, 5].

RESULTS AND DISCUSSION

From our point of view, the above-mentioned contradictions in interpretation of the experimental data can be eliminated by correction of the mechanisms of hole scattering. $A_2^V B_3^{VI}$ crystals are characterized by rhombohedral symmetry, so the Nernst-Ettingshausen coefficient (Q) is a tensor quantity having three independent components Q_{123}, Q_{132} and Q_{321}.

According to available literature data all three components of the Nernst-Ettingshausen tensor are negative numbers at temperatures $T \geq 77$ K in all investigated $A_2^V B_3^{VI}$ materials.

The $Sb_2Te_{2,9}Se_{0,1}$ solid solution crystal has the hole concentration $p \simeq 8{,}2 \cdot 10^{19}$ cm^{-3} according to the Hall effect at T = 77 K. Such a high charge-carrier concentration allows analyzing the experimental data using degenerate quantum statistics. In this case the components of the Nernst-Ettingshausen tensor are described by the following formula:

$$Q_{ikl} = \frac{k_0}{e} \cdot \frac{\pi^2}{3} \cdot \frac{k_0 T}{\mu} R_{ikl} . \sigma_{kk} . r_{kk}, \quad (1)$$

where: k_0 – the Boltzmann constant;

e – the elementary charge;

R_{ikl} – the component of the Hall tensor;

σ_{kk} – the component of the conductivity tensor;

T – the absolute temperature;

μ – the chemical potential;

r_{kk} – the effective scattering parameter which characterizes the scattering mechanisms.

The Nernst-Ettingshausen coefficient is determined by the following expression [6, 7]:

$$Q = \frac{k_0}{e} (R\sigma) \frac{\pi^2}{3} \frac{k_0 T}{\mu} (r - \frac{1}{2}), \quad (2)$$

where r is the scattering parameter.

In the one-band model such behavior of the Nernst-Ettingshausen coefficient clearly indicates the dominance of the acoustic mechanism of hole scattering. According to the two-band model of the band structure the Nernst-Ettingshausen coefficient is determined by the contributions of the both extremes of the valence band in accordance with the expression [4]:

$$Q = Q_1 \frac{\sigma_1}{\sigma} + Q_2 \frac{\sigma_2}{\sigma} + Q_{12} \frac{\sigma_1 \sigma_2}{\sigma^2}. \quad (3)$$

Here, the subscripts 1 and 2 denote the corresponding partial kinetic coefficients for two bands and Q_{12} is a mixed term defined as:

$$Q_{12} = (\alpha_1 - \alpha_2)(u_1 - u_2), \quad (4)$$

where u_1 and u_2 are the hole Hall mobilities in the primary and the secondary extremes of the valence band, respectively.

In the two-band model in the samples with the Fermi level located closely to the top of the secondary extremum of the valence band ($\varepsilon \approx \varepsilon_F \approx \Delta E_v$) the channel of additional scattering of kinetic moment of charge carriers appears. Without energy change electrons can move from the primary extremum to the secondary extremum with momentum change.

This mechanism is called interband scattering. The concepts of interband scattering were originally introduced by N. V. Kolomoets [8] to explain anomalies in the concentration dependences of the thermopower in iron group alloys. In [8] from a combination of four kinetic coefficients according to the formula [6]:

$$\frac{Q}{R\sigma\alpha} = \frac{r - 0.5}{r + 1} \quad (5)$$

for three components of the Nernst-Ettingshausen tensor Q_{123}, Q_{132} and Q_{321} from the experimental data the scattering parameter (r) was calculated at the temperature range 77 – 450 K. It should be noted that the dependence of the relaxation time τ on charge-carrier energy ε describes as the power function $\tau \sim \varepsilon^{r-0.5}$ for the most important and used scattering mechanisms. It turned out that the values of scattering parameter found in this way are close to zero up to 200 K in the cleavage plane of crystals and in the direction of trigonal axis C_3. These results confirm the dominant character of hole scattering at acoustic phonons in different crystallographic directions. At higher temperatures the scattering parameters become negative and are growing rapidly in absolute value. This fact indicates the appearance of additional mechanism of hole scattering with a strong energy dependence of the relaxation time. This scattering mechanism is the above-mentioned interband scattering.

CONCLUSION

Produced estimates show that accounting of interband scattering allow describing observed temperature dependences of the kinetic coefficients and determining the parameters of the band spectrum more correctly.

REFERENCES

[1] B. M. Gol'tsman, V. A. Kudinov, I. A. Smirnov. *Semiconductor Thermoelectric Bi_2Te_3 Based Materials*. Nauka, Moscow (1972). 320 p.

[2] Von Middendorff, G. Landwehr. *Sol. State Com.,* 11, 203, 1972.

[3] V. V. Sologub, R. V. Parfen'ev, A. D. Goletskaya. *JETP Letters*, 21, (12), 711 (1975).

[4] I. A. Chernik. *The Research of the Transverse Nernst-Ettingshausen Effect and Transport Phenomena in Lead Chalcogenides.* Th. Candidate of Physical and Mathematical Sciences. I. A. Chernik. – L., 1968. – 242 p.

[5] D. A. Pshenai-Severin. The Influence of the Band Structure Features on Thermoelectric Properties of Semiconductor. D. A. Pshenai-Severin, M. I. Fedorov. *SSP*. - 2007, - T. 49, vol. 9. - 1559 - 1562 p.

[6] B. M. Askerov. *Electronic Transport Phenomena in Semiconductors*. - M.*:* Nauka. - 1985. 320 p.

[7] B. M. Gol'tsman. Film Thermoelements: Physics and Application. B. M. Gol'tsman, Z. M. Dashevskii, V. I. Kaidanov, N. V. Kolomoets. *Film Thermoelements*: *Physics and Application.* Nauka, Moscow, 1985

[8] N. V. Kolomoets, *SSP*, 1966, t. 8, N 4, 997 p.

Smart Nanocomposites
Volume 8, Number 1
ISSN: 1949-4823

SOL-GEL SYNTHESIS AND CHARACTERIZATION OF TUNGSTEN OXIDE NANOLAYERS FOR ELECTROCHROMIC DEVICES

Vera S. Zemko, Elena V. Kolobkova, Evgenia V. Sokhovich*, and Sergey V. Mjakin
Saint Petersburg State Institute of Technology (Technical University),
Saint Petersburg, Russia

ABSTRACT

Optimal conditions are determined for α-WO_3 layer deposition onto glass supports with different conductive coatings using a sol-gel synthesis from polyperoxotungstic acid alcosols to obtain electrochromic devices with improved coloration-bleaching efficiency.

Keywords: electrochromism, sol-gel, tungsten, peroxotungstic acid, WO_3

INTRODUCTION

Smart glass with various adjustable properties and performances is a promising type of modern materials featuring with a rapidly growing worldwide market currently approaching $500 million [1]. For the recent decades low emission glass with special coatings including selective transmission, sunlight protection, anti-glare, conductive and other specific layers attract increasing attention of manufacturers, designers and researchers, especially in view of specific requirements to energy efficiency, power and heat saving. Particularly, one of the most intensively developing directions in this field relates to the manufacture of "smart" (photo-, thermo-, electrochromic) sunlight protection glasses with controllable transmission. The most promising among them are electrochromic devices affording a precise reversible adjustment of light transmission by the application of low electric voltages (0.5-5 V) and currents (about 1 mA/cm^2) with variable intensity and polarity [2].

Hydrated tungsten oxide (α-WO_3) is an important inorganic material combining electronic and ionic conductivity that determines its effective application in electrochromic (EC) devices as an active cathode layer undergoing a reversible coloration activated by electric current [3]. EC device consists of a support with a transparent conductive coating and

* Corresponding Author E-mail: sokhovitchevg@gmail.com

α-WO_3 layer, a similar support with a counter-electrode and an electrolyte layer between these supports [4]. The main requirements to EC systems include intensive coloration followed by a complete bleaching upon the application of electric voltage of reverse polarity, stability at numerous coloration-bleaching cycles as well as the electrochromic efficiency determined by the coloration contrast in combination with minimized power consumption.

The enhancement of these performances requires the study and optimization of α-WO_3 synthesis and deposition conditions as well as the structure, properties and compatibility of all functional and auxiliary layers in EC devices [3, 4]. In this study α-WO_3 layer formation is studied at all steps of its synthesis and deposition using various physicochemical characterization techniques in comparison with the target performances of EC devices obtained therefrom.

MATERIALS AND METHODS

α-WO_3 layers were deposited onto glass supports with indium-tin oxide (ITO, supplied by Polytech Co., St. Petersburg, Russia, surface resistance ρ_s = 15-20 Ohm/□) or SnO_2:F (FTO, Pilkington Co., ρ_s = 25-30 Ohm/□) conductive layers via a procedure involving the following steps:

(1) reacting powdered metal W (W05-10, Wolfram, Germany, particle size 0.5-0.7μm) or tungsten carbide WC (CRC035U, Wolfram, Germany, particle size 0.5-0.7μm) with hydrogen peroxide (30%, chemical purity grade) via an approach similar to that described in [5] affording the preparation of peroxotungstic acid (PTA) H_2WO_5 of the required high purity. The optimal values for the ratio between the initial components (W:H_2O_2) and hydrogen peroxide concentration (above 25% wt.) were determined and used in the syntheses. The determination of free H_2O_2 concentration by titration with 0.1 N $KMnO_4$ solution indicated that a slight excess (10-12%) of hydrogen peroxide provides a durable stabilization of the target reaction products. The formation of PTA was confirmed by XRD data.
(2) PTA polycondensation yielding polyperoxotungstic acid (PPTA) $H_2W_2O_5$ [O-O] , $H_2W_4O_9$ [O-O] followed by drying to form a hydrated xerogel;
(3) dissolving hydrated PPTA xerogel in an ethyl alcohol to obtain an alcosol subsequently maintained within 7-10 days for comlete maturing;
(4) PPTA alcosol deposition onto the support by centrifugation followed by annealing at different temperatures from 150 to 450°C within 1 hour.

The prepared PPTA xerogels and α-WO_3 layers were characterized using Raman spectroscopy and DSC techniques.

Another support with the same conductive layer was coated by TiO_2 counter-electrode via a sol-gel synthesis from tetrabutoxytitanium (TBT) in combination with an isopropanol – ice acetic acid (15%) mixture (NAc). Then the above supports with α-WO_3 and TiO_2 layers were sticked together with the addition of $LiClO_4$ or $LiBF_4$ electrolyte between them. Thus obtained 5x5cm EC device samples were subjected to coloration by the application of about 1.5-4.0 V voltage and about 0.8-1.0 mA/cm^2 current density followed by bleaching upon the

application of reverse polarity 1.2-3.2 V voltage. The coloration-bleaching kinetics was studied by measuring the changes in optical transmission at the wavelength 670 nm (characterizing the blue coloration intensity) with time.

Electrochromic efficienct was calculated as

$$\eta = (D - D_0)\cdot S/\int I(\tau)d\tau = \lg(T_0/T)\cdot S/\int I(\tau)d\tau$$

where D and Do are optial densities in colored and bleached states, T and To – corresponding transmission coefficients (%), S is the electrochromic "window" sample area, $\int I(\tau)d\tau$ is overall electric charge consumed for the coloration defined as the numerically calculated integral of the electric current vs time in the course of coloration [6].

RESULTS AND DISCUSSION

The results of performed comparative studies indicate that the most important parameters of α-WO_3 layer synthesis responsible for the quality of the target EC devices include:

(1) Optimal temperature (75-80°C) and time (about 1 hour) of PTA polycondensation;
(2) Method and temperature of PPTA solution drying to form a uniform xerogel with optimal hydration degree. DSC characterization of the prepared products indicated that drying conditions affect the concentration of various OH-groups. Particulatly, drip drying on a flat glass support at optimal temperature about 60-70°C at the support surface yields a xerogel with 12-15%wt. of bound water that is mostly favorable for the subsequent dissolving in ethyl alcohol (due to the sufficient hydration and hydroxylation) and formation of electrochromic layers. DSC study also allowed us to determine the temperature regions of α-WO_3 glass transition (300-350°C) and crystallization (410-440°C);

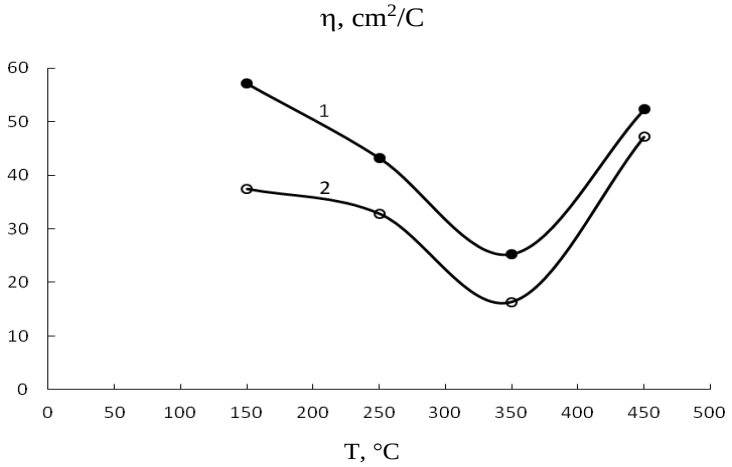

Figure 1. Effect of annealing temperature on electrochromic efficiency of EC devices comprising α-WO_3 layer on glass supports with ITO (1) and SnO_2:F (2) transparent electrodes.

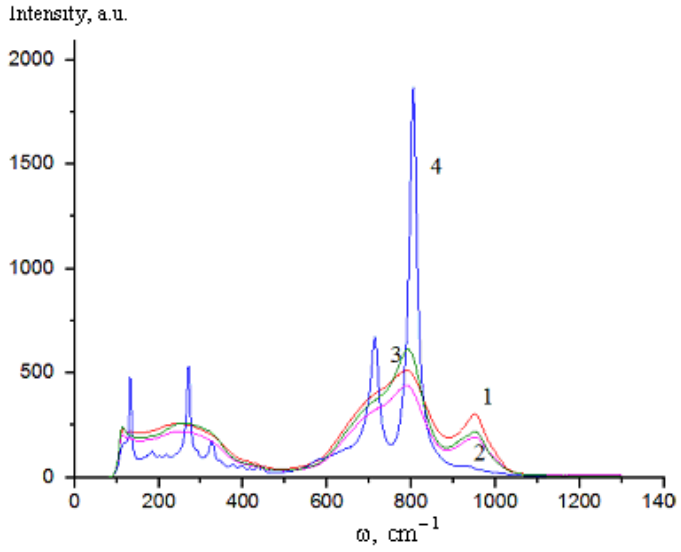

Figure 2. Raman spectra of α-WO_3 samples annealed at 150 (1), 250 (3), 350 (3) and 450°C (4).

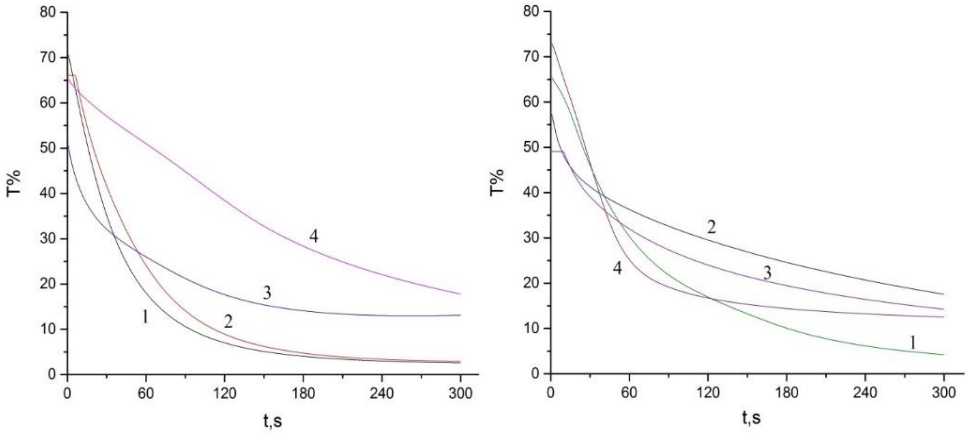

Figure 3. Coloration kinetics of EC device samples annealed at 150 (1), 250 (2), 350 (3) and 450°C (4). Transparent electrodes - SnO_2:F (a) and ITO (b).

(3) Optimal temperature (about 50°C) of the solvent at PPTA alcosol preparation and resulting alcosol concentration (12-15 wt.%);

(4) Annealing temperature of PPTA alcosol layers (Figure 1) providing a high electrochromic efficiency either at about 150°C due to retaining a relatively high α-WO_3 hydration degree (responsible for increased conductivity and decreaed power consumption) or at about 450°C due to WO_3 nanocrystallization as confirmed by Raman spectroscopy (Figure 2) featured with prominent peaks corresponding to the formation of monoclinic crystal structure upon treatment at this temperature.

(5) Transparent electrode material. Although ITO conductive layer provides about 1.5-fold increased electrochromic efficiency relating to FTO (Figure 1) due to a higher conductivity and consequently reduced power consumption at similar coloration intensity (Figure 3), FTO layer affords more complete bleaching after coloration (Figure 4).

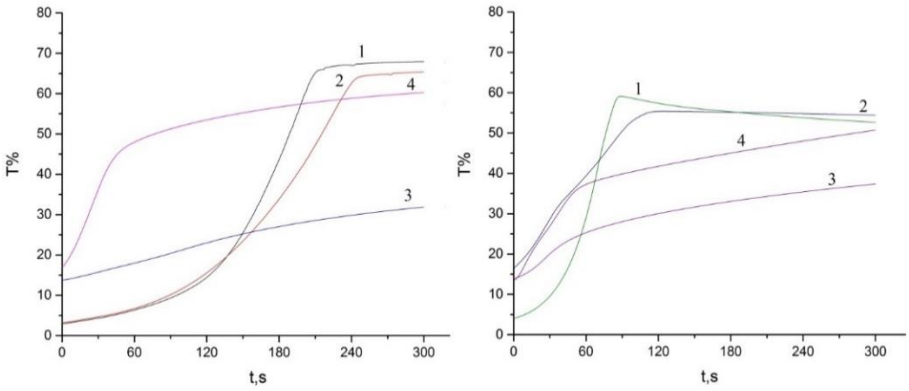

Figure 4. Bleaching kinetics of EC device samples annealed at 150 (1), 250 (2), 350 (3) and 450°C (4). Transparent electrodes - SnO_2:F (a) and ITO (b).

Taking into account these comparative data and a significantly lower cost of FTO compared with ITO, FTO can be considered as a promising material for variuos EC devices.

CONCLUSION

The considered sol-gel approach provides the synthesis of stable (up to 12 months) PPTA alcosols from metal tungsten and 30% hydrogen peroxide and subsequently affords the formation of target α-WO_3 EC layer of high purity free of any side products. Upon the optimization of the synthesis parameters this method featuring with a significantly lower cost compared with such conventional techniques as magnetron sputtering is promising for the development of processes for the manufacture of EC devices for various applications including house and vehicle windows.

REFERENCES

[1] Pike Research. *Smart Glass. Electrochromic, Suspended Particle, Thermochromic, and Liquid Crystal Glass Technologies for Architectural and Transportation Applications: Global Market Analysis and Forecasts*. http://www.navigantresearch.com/wp-content/uploads/2012/06/SGLASS-12-Brochure.pdf.

[2] Makaryan I. A., Efimov O. N., Gusev A. L. At the world market of smart electrochromic devices. *Alternative Energy and Ecology* (ISJAEE). 2014 (3):81-93.

[3] Granqvist C. G.. Electrochromic tungsten oxide films: Review of progress 1993-1998// *Sol. Energy Mater. Sol. Cells*, 2000 (60):201-262.

[4] Granqvist C. G.. Avendano E., Azens A. Electrochromic coatings and devices: Survey of some recent advances. *Thin Solid Films*, 2003 (442):201-211.

[5] Kudo T., Matsumoto K. Peroxopolytungstic acids synthesized by direct reaction of tungsten carbide with hydrogen peroxide. *Inorg. Chim. Acta*. 1986 (111): L27-L28.

[6] V. Sorokin, O. Oleneva, E. Nodova, N. Shastova, D. Krylsky. An equipment set and software for measurement and calculations of the basic characteristics of electrochromic devices. *Molekulyarnye Technologii* (*Molecular Technologies*). 2010 (4): 212-223.

Smart Nanocomposites
Volume 8, Number 1
ISSN: 1949-4823

CHARGE CARRIERS AND CONDUCTIVITY MECHANISM IN VO_2 FILMS

E. A. Tutov[1,*], H. I. Al-Khafaji[2], and V. P. Zlomanov[3]
[1]Voronezh State Technical University, Voronezh, Russia
[2]Department of Chemistry, College of Engineering,
Al-Nahrain University, Baghdad, Iraq
[3]Moscow State University, Moscow, Russia

ABSTRACT

Resistance of commercial thermoresistor (*TP-68*) based on vanadium dioxide film, and tablet pressed from the synthesized VO_2 powder is measured on direct and alternating current. For the thermoresistor at measurements on alternating current expansion of a hysteresis loop is revealed. It is established that in conductivity of a semiconductor phase of vanadium dioxide give a contribution both activation, and the hopping mechanism. Temperature dependence of *TP-68* resistance in area of phase transition under gases adsorption is studied. The energy zone model is offered for explaining "anomalous" response to the adsorption of donor gases due to inversion of conductivity type in surface layers of vanadium dioxide.

Keywords: chromogenic materials, chemichromism, vanadium dioxide, semiconductor-metal phase transition, conductivity mechanism, chemisorptions, zone model

INTRODUCTION

Fundamental and applied investigations of the semiconductor–metal phase transition in vanadium dioxide (VO_2) proceed more than half of century with not decreasing interest. During transition along with conductivity of vanadium dioxide its optical characteristics also considerably change, that is attractive for elaboration the termochromic "smart" glasses [1]. One of effective ways of impact on surface states of vanadium dioxide and, consequently, on transition parameters is use of field effect arising at chemisorptions of various gases on its surface [2, 3]. Complex nature of structural and electronic transformations during phase transition in VO_2 leads to that the microscopic picture of the phenomenon still remains debatable. Concerning a type of charge carriers in VO_2 still there is no consensus. The majority considers the main carriers electrons, however, some authors develop idea about a

* Corresponding Author E-mail: tutov_ea@mail.ru

role of holes in phase transition [4, 5]. So, the study [5] of *p*-type vanadium dioxide films used the Hall Effect to demonstrate a change of the carriers sign at the transition from the semiconductor to metallic state. Now as for the transition of a hole semiconductor into the metallic state with degenerate electron gas, there are no reliably established relations, and the question of the transition mechanism has fundamental importance. It is obvious that change of electrophysical characteristics of material thus can't be monotonous.

In the work [6] devoted to the analysis of conductivity of monocrystal VO_2 on the basis of linear dependence of conductivity on temperature in $ln\sigma - T$ coordinates the conclusion about the hopping mechanism of conductivity for a low-temperature (dielectric) phase of vanadium dioxide is drawn. Studying of electronic properties of vanadium dioxide during phase transition has certain difficulties as bulk monocrystals collapse for some cycles of heating – cooling because of thermo-mechanical stresses. Therefore research of mechanisms of a charge transfer in practical important area of temperatures near phase transition in ceramic and film materials represents special interest.

At the hopping mechanism along with the specified temperature dependence of conductivity also a certain dependence on the frequency of alternating current, as a rule, $\sigma \sim \omega^{0.8}$ has to be observed [7]. In this direction of researches the most essential new results are received by use of impedance spectroscopy for the high-ordered thin films of vanadium dioxide [8, 9].

The detailed analysis of electrophysical characteristics of VO_2 films allowed authors to draw a conclusion on coexistence of the semiconductor and metal phases not only in the field of phase transition, but also at lower temperatures. Thus, in work [8] decreasing of films resistance was observed with frequencies of alternating current over 10 kHz whereas in work [9] conductivity of films to frequencies ~ 500 kHz remained almost constant, and with higher frequencies decreased. Authors explain such unusual result with inductive impedance of ultrathin inclusions of the metal phase VO_2 of a threadlike form (filaments). Comparison of phase transition parameters on direct and alternating current in work [8] showed insignificant shift of a hysteresis loop heating branch towards decrease in temperature, almost identical to all studied frequencies; the cooling branch for alternating current isn't given in work.

Characteristics of ceramic and film materials in strong degree depend on conditions on their external and internal surfaces. The situation becomes complicated due to various defects of a non-stoichiometry of surface layers and volume of crystallites (grains, film) VO_2 and, as a result, distinctions in nature of their conductivity.

The present work is aimed at refining the conductivity mechanism of polycrystalline (powder) and film vanadium dioxide in temperature region near phase transition on the basis of measurement of conductivity frequency dependence and its temperature dependence on direct and alternating current. Influence of chemisorptions of ethanol and water vapors on parameters of the semiconductor – metal phase transition in vanadium dioxide films is also investigated.

EXPERIMENTAL

Powder of polycrystalline vanadium dioxide (*n*-type on measurements of Seebeck effect), was synthesized by reduction of vanadium pentoxide with oxalic acid when heating on air up to the temperature of 600 – 700°C according to reaction: $V_2O_5 + H_2C_2O_4 = 2VO_2 + H_2O +$

$2CO_2$. The phase analysis of oxide powder was carried out with a DRON-4.0 X-ray diffractometer operated with filtered K_α radiation of cobalt (wavelength λ = 0.179021 nm). On a diffractogram of vanadium oxide powder after reducing reaction (Figure 1) there are reflexes of vanadium dioxide of a stable monoclinic phase α-VO_2. Results of diffractometric analysis are given in the table.

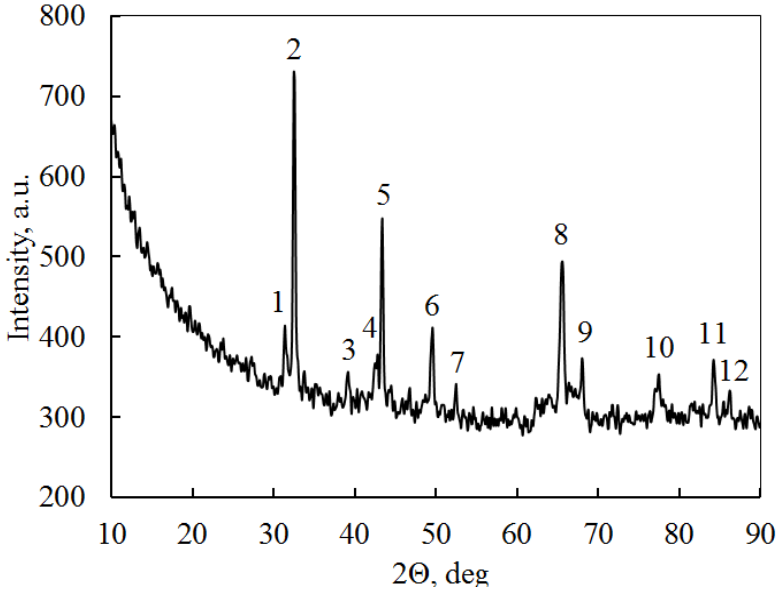

Figure 1. Diffractogram of synthesized powder of vanadium dioxide.

Table. Diffractometric analysis of synthesized powder of monoclinic vanadium dioxide

Reflection number	Angle, deg	Relative intensity	d, nm	*(hkl)*
1	31.50	11.58	0.330	$(11\bar{1})$, (110)
2	32.50	100.00	0.320	(011)
3	39.10	8.38	0.268	$(10\bar{2})$
4	43.40	8.58	0.242	$(21\bar{1})$, (200)
5	44.80	50.90	0.235	(002)
6	49.60	27.74	0.213	(210)
7	52.60	8.78	0.202	(012), (021)
8	65.60	47.31	0.165	(220)
9	68.10	17.76	0.160	(022)
10	77.30	14.17	0.143	(013)
11	84.20	19.76	0.134	$(23\bar{1})$, (202)
12	86.10	8.18	0.131	$(41\bar{3})$

On a direct current and alternating current (12 Hz – 100 kHz, INSTEK *LCR*-meter, model 819) are measured resistance of the tablet pressed from the synthesized VO_2 powder and serially released thermoresistor (*TP-68*) on the basis of VO_2 film, both in the closed case, and with the open case was used. For the thermoresistor on a direct current and at a frequency of 100 kHz temperature dependence of resistance is measured in the range of temperatures including area of phase transition. The measurements were carried out in a tubular heater in the microcompressor-produced air flow with saturated ethyl alcohol vapor and water vapor. The rate of heating and cooling of samples was approximately one degree a minute.

RESULTS AND DISCUSSION

Typical dependence of resistance of vanadium dioxide (the tablet pressed from powder and the film thermoresistor) versus the frequency of alternating current in logarithmic coordinates is presented in Figure 2. In both cases conductivity with frequencies up to 10 kHz is almost constant that testifies to prevalence of the delocalized charge carriers in conductivity of VO_2 at the room temperature. At the same time for higher frequencies decreasing of resistance with growth of frequency owing to "turning on" of the hopping mechanism of charge transfer is observed. Therefore at temperatures near phase transition in vanadium dioxide, apparently, the mixed conductivity mechanism takes place.

The contribution of the hopping mechanism to the conductivity of vanadium dioxide, nevertheless, can be shown in features of electric characteristics of VO_2 upon phase transition; therefore we measured temperature dependence of resistance for samples of both types on a direct current and alternating current of the maximum frequency (100 kHz). Such dependence for the film thermoresistor is given in Figure 3. In the region of temperatures from room to beginning of phase transition dependence of resistance on temperature on a direct current stronger, than on alternating current that qualitatively coincides with shown in [8] data.

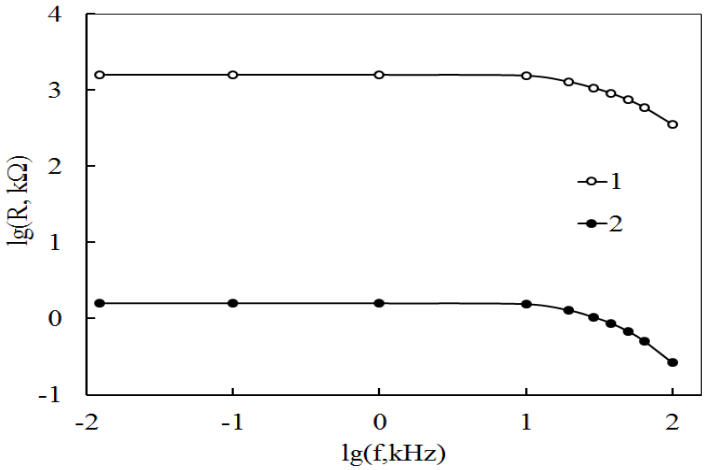

Figure 2. Dependence of the resistance of powder and film vanadium dioxide on frequency at the room temperature (1 – *TP-68* thermoresistor, 2 – a tablet from the VO_2 powder).

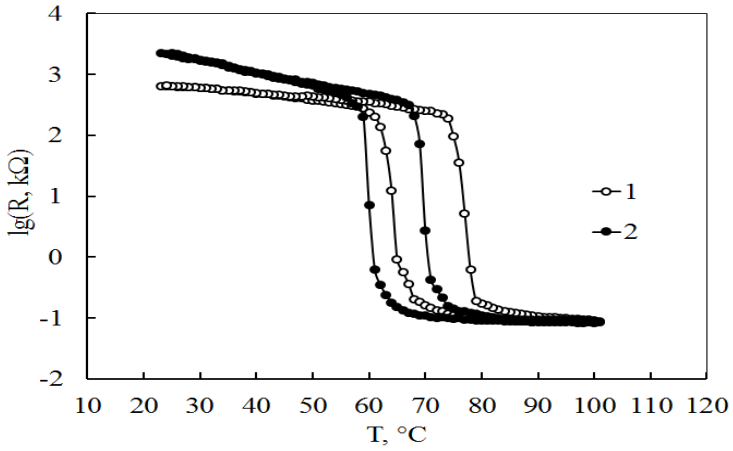

Figure 3. Dependence of the resistance of the *TP-68* thermoresistor on the temperature (1 – alternating current, 2 – direct current). The right branch of a hysteresis loop – heating, the left – cooling.

The main distinctions in measurements on direct and alternating current are observed in the field of a hysteresis loop, characteristic for the semiconductor-metal phase transition in vanadium dioxide. For the *TP-68* thermoresistor phase transition with change of resistance approximately on four orders occupies a temperature interval about ten degrees, unlike results of work [8] where process of resistance change on three orders occupies forty degrees on a temperature scale. For the *TP-68* thermoresistor at measurements on alternating current the loop of a hysteresis extends on some degrees and is displaced towards more high temperatures, and the heating branch is displaced more considerably, than cooling.

It is known that the semiconductor – metal phase transition in ceramic and film vanadium dioxide represents percolation process. The loop of a thermal hysteresis observed in experiments on conductivity reflects process of formation of the infinite carrying-out cluster near a percolation threshold [10, 11]. Actually, there is a transition the semiconductor – metal in each crystallite and percolation transition on all set of crystals in general. Therefore, at measurements of conductivity on alternating current the thermal position of a transition threshold can depend on the frequency of a measuring signal.

In general, the analysis of a conductivity hysteresis loop at measurements on alternating current for ceramic and film vanadium dioxide represents extremely complex challenge. Nevertheless, we suppose that in percolation transition in vanadium dioxide give a contribution as the charge carriers localized on the defect centers, and the delocalized (zone) charge carriers.

Unlike films, the pressed tablets from powder of polycrystalline vanadium dioxide when heating on air up to the temperatures above phase transition lost ability to sharp change of resistance for one-two cycles. The general resistance of samples thus considerably decreased. Fast degradation of phase transition in powder vanadium dioxide in the oxidizing atmosphere (in air) is caused by a large number of grain surfaces available to oxygen molecules, that leads to the oxide V_6O_{13} formation (confirmed by X-ray analysis). Thermo-cycling of such degrading samples in the atmosphere of donor gases (ethanol, ammonia) was followed by decreasing of quantity of V_6O_{13} phase and partial restoration of the semiconductor – metal phase transition in vanadium dioxide.

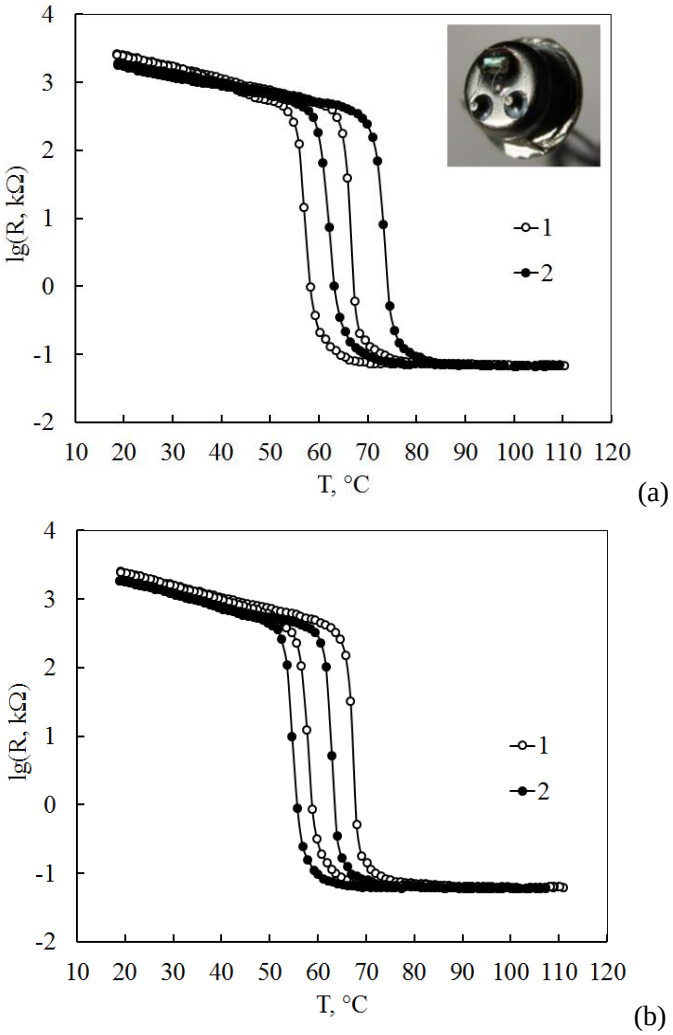

Figure 4. a) Dependence of the resistance of *TP-68* thermoresistor on the temperature (*1*) in the air flow and (*2*) in the flow of air saturated with ethanol vapor during heating (right-hand branch of the loop) and cooling (left-hand branch of the loop). Frequency of a measuring signal is 100 kHz. On an insert – the photo of the thermoresistor with the open case; b) Dependence of the resistance of TP-68 thermoresistor on the temperature (1) in the air flow and (2) in the flow of air saturated with water vapor during heating (right-hand branch of the loop) and cooling (left-hand branch of the loop). Frequency of a measuring signal is 100 kHz.

Measurements of transition parameters on alternating current for the thermoresistor on the basis of a vanadium dioxide film (*n*-type on a sign of Seebeck effect) with the open case in the atmosphere of vapors of ethanol (Figure 4 a) and water (Figure 4 b) yielded the following results. Addition of saturated ethanol vapors in an air flow leads to increase of resistance of vanadium dioxide in a semiconductor phase and, as a result, to shift of phase transition to high temperatures on average on four degrees. The cooling branch of a hysteresis loop is displaced towards more high temperatures slightly less so in general the loop in the atmosphere of ethanol vapors extends.

Such manifestation of chemisorptions field effect is characteristic for interaction of donor gas (reducer) with the *p*-type semiconductor. Vanadium dioxide in the reduction environment has to have the electronic conductivity determined by vanadium ions of lower oxidation level (V^{+3}). However, its ability to oxidation in air is known, and many authors note that on a surface of VO_2 there can be the highest vanadium oxide V_2O_5. Hole conductivity of vanadium dioxide in this case can be a consequence of anion excess of rather stoichiometry quantity, at least, in surface layers which define the adsorptive interaction.

In an air flow with saturated water vapors decrease in resistance of a sample and temperature of phase transition, also reversible is observed (Figure 4 b). Different influence of ethanol and water vapors is a little unexpected and demands further studying. We will notice also some distinction in electric characteristics of the thermoresistor with the closed and open case that can be defined by influence of the residual technological atmosphere in its case.

Research [2] had special aim to study an influence of chemisorptions of donor and acceptor gases on parameters of phase transition in the mixed vanadium oxide films formed by zol-gel method [12]. For films including metastable oxide VO_2(B) the phase transition with variation of conductivity and a hysteresis loop in the 50–70 °C temperature interval were observed. The total change of resistance induced by the phase transition in vanadium dioxide was not significant (by 2.5–3.0 times), which should be assigned to current flowing over other semiconductor phases.

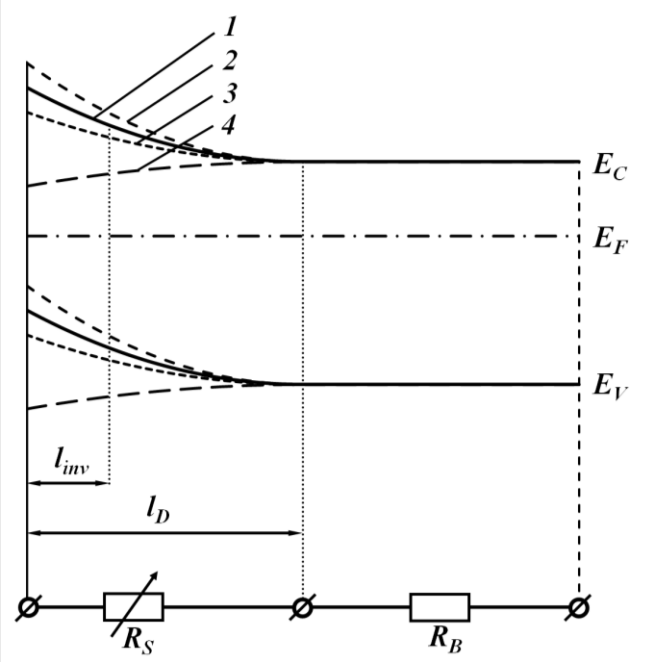

Figure 5. Qualitative zone model of a VO_2 surface layer in the conditions of gases chemisorptions: 1 – air, 2 – air with ozone, 3 – air with ethanol vapors, 4 – air with water vapors. E_C – lowest energy of conduction band, E_F – Fermi level, E_V – highest energy of valence band, l_D – Debye lengths, l_{inv} – length of an inversion layer, R_S –resistance of a surface layer (*n*- or *p*-type of conductivity), R_B – bulk resistance of vanadium dioxide (*n*-type of conductivity).

The width of the hysteresis loop for the phase transition in vanadium dioxide is about 15 degrees. Chemisorptions of ethanol vapor drives the phase transition into the high temperature region by more than 10 degrees, with the hysteresis loop becoming noticeably broader (by approximately 4 degrees). The total resistance of structure increased. Ozone of rather low concentration (at the level of 10 ppb) effects on phase transition less considerably and in an opposite direction – decreases the transition temperature and film resistance a little. The studied films of vanadium oxide were sufficiently stable in the conditions of thermo-cycling in the oxidation-reduction atmosphere without noticeable degradation of their electric characteristics.

About the mechanism of a chemisorptions influence on parameters of the semiconductor – metal phase transition in vanadium dioxide can be stated the following assumptions. On a film surface of *n*-type VO_2 as a result of atmospheric oxygen sorption, in principle, the inversion layer (with hole conductivity) can be formed. Its resistance in the reduction atmosphere has to increase, as is observed in experiment. Ozone only slightly strengthens effect of oxygen.

In Figure 5 the qualitative zone model of VO_2 surface layer explaining set of observed results is shown. The measured resistance of vanadium dioxide consists of resistance of a bulk layer (R_B) and a surface layer (R_S). The last can significantly increase or decrease at chemisorptions of gases – donors or acceptors of electrons (reducers or oxidizers, respectively).

During transition of conductivity of a surface layer from hole type to electron type (through area of intrinsic conductivity) in the reduction atmosphere a film resistance has to change not monotonously. Experiment under intermediate values of the relative air humidity confirms this assumption. Water molecules at a low temperature (about 20°C) appear "stronger" donor of electrons, than ethanol molecules, owing to their big dipole moment. Similar not monotony in change of optical properties during electrochemically induced phase transition in vanadium dioxide was found [13] earlier.

CONCLUSION

Thus, on a direct current and alternating current in range of frequencies of 12 Hz - 100 kHz are measured resistance of the tablet pressed from the VO_2 powder and serially released *TP-68* thermoresistor on the basis of VO_2 film. For the thermoresistor on a direct current and at a frequency of 100 kHz temperature dependence of resistance is measured in the range of temperatures including area of phase transition.

The analysis of the received results allows one to conclude that in this temperature area conductivity of a semiconductor phase of vanadium dioxide is carried out both on hopping, and on the zone mechanism. During the operation of the thermoresistor on alternating current an expansion of a temperature hysteresis loop is observed.

Chemisorptions (including change of quantity of atmospheric oxygen adsorbed on a film) affect, apparently, both concentration of zone charge carriers, and parameters of the defect centers involving in conductivity on the hopping mechanism.

On the example of ethanol and water vapors it is shown that by means of gases chemisorptions it is possible to operate reversibly parameters of the semiconductor – metal phase transition in vanadium dioxide films.

REFERENCES

[1] Tutov E. A., Al-Khafaji H. I., Manannikov A. V., Kvasova V. Yu. Prospects of chromogenic composite coatings for smart windows. - *Smart Nanocomposites* 7 (2016) 95-98.

[2] Tutov E. A., Zlomanov V. P. Effect of chemisorption of donor and acceptor gases on the semiconductor–metal phase transition in vanadium dioxide films. - *Physics of the Solid State* 55 (2013) 2351–2354.

[3] Tutov E. A., Kryukov P. I., Zlomanov V. P. Chemisorptions field effect in nanocrystalline films of vanadium oxide. - *Smart Nanocomposites* 4 (2013) 75-77.

[4] Kim H. T., Kim B. J., Lee Y. W., Chae B. G., Yun S. J. Switching of the Mott transition based on the hole-driven MIT theory. - *Physica B: Condensed Matter* 403 (2008) 1434-1436.

[5] Kim H. T., Chae B. G., Youn D. H., Maeng S. L., Kim G., Kang K. Y., Lim Y. S. Mechanism and observation of Mott transition in VO_2-based two- and three-terminal devices. - *New Journal of Physics* 6 (2004) 1-19.

[6] Andreev V. N., Klimov V. A. Electrical conductivity of the semiconducting phase in vanadium dioxide single crystals. - *Physics of the Solid State* 49 (2007) 2251-2255.

[7] Mott N. F., Davis E. A. *Electronic Processes in Non-Crystalline Materials*. - Oxford, 2012. – 605 p.

[8] Zhong X., LeClair P., Sarker S. K., Gupta A. Metal-insulator transition in epitaxial VO_2 thin films on TiO_2 (100). - *Phys. Rev. B* 86 (2012) 094114-1 – 094114-7.

[9] Ramirez J. G., Schmidt R., Sharoni A., Gomez M. E., Schuller I. K., Patino E. J. Ultra-thin filaments revealed by the dielectric response across the metal-insulator transition in VO_2. - *Appl. Phys. Lett.* 102 (2013) 063110-1 – 063110-4.

[10] Gentle A. R., Smith G. B., Maaroof A. I. Frequency and percolation dependence of the observed phase transition in nanostructured and doped VO_2 thin films. - *Journal of Nanophotonics* 3 (2009) P. 1-15.

[11] Gurvitch M., Luryi S., Polyakov A., Shabalov A. Nonhysteretic phenomena in the metal – semiconductor phase-transition loop of VO_2 films for bolometric sensor applications. - *IEEE Transactions on Nanotechnology* 9 (2010) 647-652.

[12] Berezina O., Kirienko D., Pergament A., Stefanovich G., Velichko A., Zlomanov V. Vanadium oxide thin films and fibers obtained by acetylacetonate sol-gel method. - *Thin Solid Films* 574 (2015) 15-19.

[13] Chenevas-paule A. Induction de la transition isolant/metal de VO_2 par substitution d'especes chimisorbees pour T << Tc. - *J. Physique Colloques* 37 (1976) C4-75 – C4-77.

Smart Nanocomposites
Volume 8, Number 1
ISSN: 1949-4823

THE COMPUTER SIMULATION OF MIXERS SIGNALS

Yu. A. Nikitin and V. A. Yurova*
The Bonch-Bruevich Saint Petersburg State University of Telecommunications,
Saint Petersburg, Russia

ABSTRACT

In the paper we obtained the basic spectral and temporal characteristics of the output signal of the frequency mixers on the basis of which the constructed schemes of the spectrum analyzers. We present results of a comparative analysis of the linearity of the signals multiplication by using a generic approach and the unified parameters of the active elements.

Keywords: bipolar transistor, frequency multipliers, spectrum analyzer, spectral characteristics, temporal characteristics

INTRODUCTION

Various materials are widely used in modern electronics, its combinations and the layered structures and the new are created. Currently, the typical dimensions of the electronic devices are several hundreds or thousands of nanometers. Therefore, the one of major task in the manufacture of electronic equipment is to measure the spectral characteristics with high accuracy. It means that such devices as spectrum analyzers make the strict demands on the linearity of the multiplication of the measurement signals at the circuits of frequency mixers, i.e., the level of nonlinearity of the active device. Generally, the different approaches, evaluation indicators and the mathematics are used in the investigations, devoted to the analysis parameters and operation modes of amplifiers and frequency converters. It's making difficulty to compare the parameters of the considering electrical circuits. So the aims of our research are obtaining spectral and temporal characteristics of the circuits of frequency mixers based on transistors, and a comparative analysis of the linearity of the multiplication, using a common approach and the unified active elements parameters.

* Corresponding Author: Valentina A. Yurova, Docent, the Bonch-Bruevich Saint Petersburg State University of Telecommunications, Saint Petersburg, Russia, E-mail: va-yurova@mail.ru

OBJECT OF RESEARCH

As the objects of research electric circuit mixers based on a transistor cascade (Figure 1) and cascade current mirror (Figure 2) were chosen. These electric circuits are widely used as an individual cascades, and are the basis for designing more complex circuits of frequency mixers, which are widely used in electronics and measuring technology of the manufacturing and the laboratory investigations of nanoelectronic devices and materials of the nanotechnology [1 – 4].

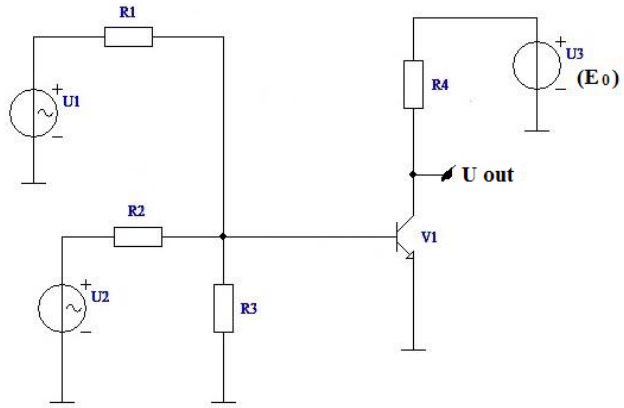

Figure 1. The diagram of the electric circuit of cascade based on the transistor cascade.

The signals from the generator and local oscillator are fed to input of the electric circuit of cascade based on the transistor cascade via a resistor R3. The output signal is generated in the collector circuit of a bipolar transistor.

In the electric circuit of cascade based on the current mirror the signals from the generator and local oscillator are fed to input similarly via a resistor R3. The output signal is generated in the collector circuit of a bipolar transistor V2. The V1 transistor operates in a diode-connected. Both electric curcuits are simple to design and have good thermal stabilization of the operation.

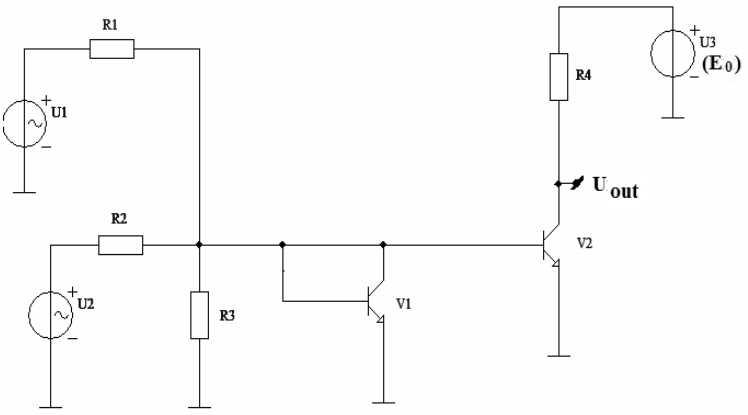

Figure 2. The diagram of the electric circuit of cascade based on the current mirror.

METHOD OF RESEARCH

To obtain the spectral and temporal characteristics of the output signal and to make the comparative analysis of the linearity's parameters of the cascades electric circuits the computer program for simulation of electrical circuits FASTMEAN 6.0 [5] was used. It makes possible to carry out spectral research of the different structures of the mixers over a wide dynamic range, applying a built-in database of the elements, or to use nonlinear models based on exponential or polynomial approximation with required accuracy.

There are strict requirements on the linearity of multiplication in the designing analog signals mixers of the measuring devices. Generally, the most schemes electrical circuits are based on semiconductor elements, comprising one or more *p*–*n* junctions. Current–voltage characteristic (CVC) of the *p*–*n* junction has a pronounced non-linear dependence form. In order to estimate the nonlinearity of the active devices based on *p*–*n* junction, the intermodulation distortion were used. This parameter is determined by the nonlinearity of the input and output characteristics of the active elements that are used in modern equipment. The choice of the best approximation of the CVC *p*–*n*–junctions the amplifying elements with a display of its nonlinearity based on experimental data is important to the qualitative analysis of the schemes. At this research, the nonlinear model of transistors based on experimental data was used.

To measure the intermodulation distortion is necessary feed at the input of the investigational electric schemes two signals with close value of frequencies – generator and local oscillator.

RESULTS AND DISCUSSION

In the research, we calculated the parameters of the cascade electric circuits, which allows for getting the specified amplitude of output signal and the transfer coefficient. Computer simulations of the frequency mixers schemes were made of common criteria, using the common computer simulation environment. In order to correctly describe the nonlinearity of current-voltage characteristics of bipolar transistors, the equivalent models based on the experimental data were used. The Figure 3 and the Figure 4 show the obtained spectral and temporal characteristics of the output signals of the mixers based on a transistor cascade and cascade current mirror.

Also we investigated the dependence of the level of combinational components of the value of the signal that set on the generator. At this stage we experienced with the necessity to create a computer algorithm in FASTMEAN 6.0 that reflect the changes in the spectral and temporal characteristics associated with changes in the magnitude of the input signal. So this dependence was investigated using the computer modulation of the electric schemes in Micro–Cap. The Micro-Cap program is a simulator of the electric circuits with an integrated schematic editor that provides an interactive sketch and simulated environment for electronics engineers. It is developed by Spectrum Software [6]. The Figure 5 and the Figure 6 show the dependences of the third – ninth level of combinational components of the value of the generator signal.

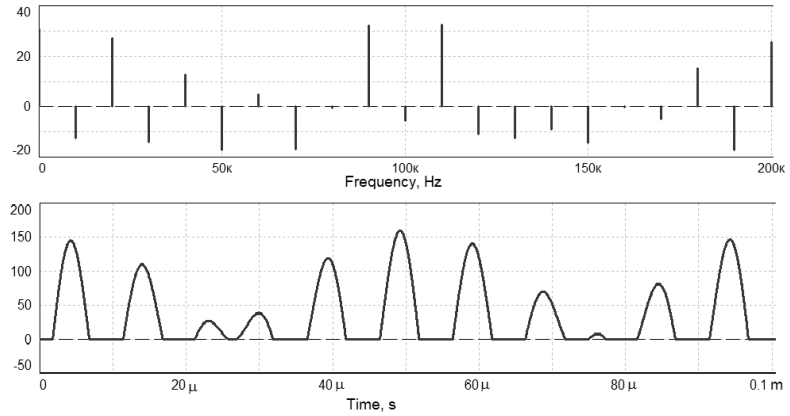

Figure 3. Spectrum and timing diagrams of the electric circuit of cascade based on the current mirror.

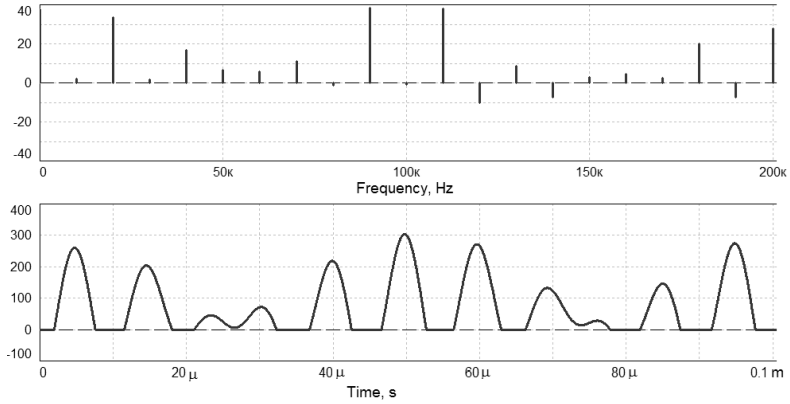

Figure 4. Spectrum and timing diagrams of the electric circuit of cascade based on the transistor cascade.

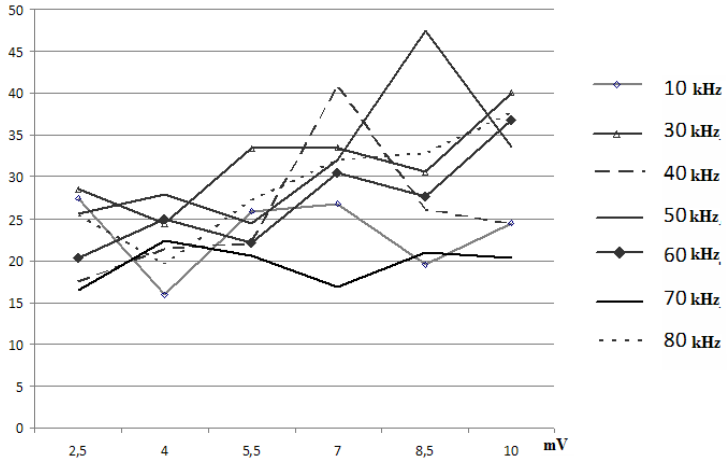

Figure 5. Dependence of the level of combinational components on the input signal level of the electric circuit of cascade based on the current mirror.

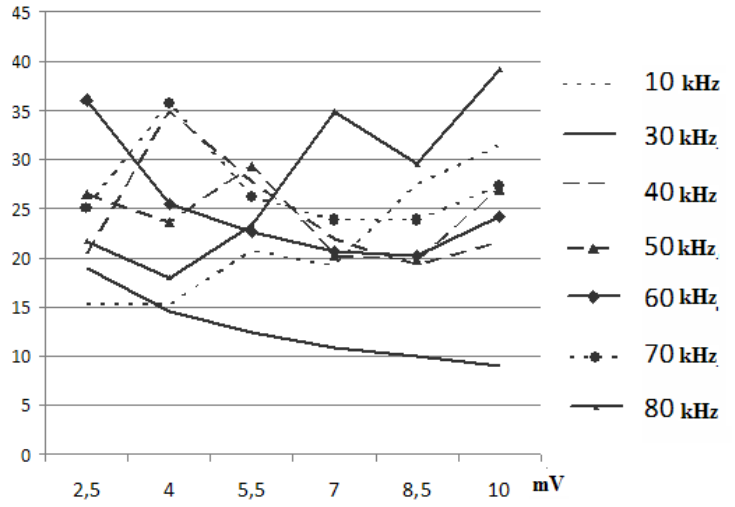

Figure 6. Dependence of the level of combinational components on the input signal level of the electric circuit of cascade based on the transistor cascade.

CONCLUSION

Thus the main spectral and temporal characteristics of the output signal for electric circuits of the frequency mixers based on the transistor cascade and the current mirror cascade were obtained. These electric circuits are widely used as the frequency mixers in different devices, such as spectrum analyzers, and as the basis to design more complex electrical circuits of frequency changers, such as balanced and circular mixers. It's seen from the analysis of results that the base cell mixer based on the current mirror provides a lower level of combinational components. It's important in develop a high-quality equipment for measuring different parameters of materials and nanoscale structures and manufacturing of modern electronic devices. Further it is interesting to investigate the influence of parameters of the input signal generator and the local oscillator (generator voltage or generator current) on the spectral and temporal characteristics of the considered schemes mixers, and investigate and analysis of the linearity of work the quasi-linear electric circuits of devices of different complexity.

REFERENCES

[1] Polyakov A. E., Strygin L. V. 2-Tone IP2 and IP3 Measurement Technique. *Trudy MIPT*, 2012, №2. – P. 54 – 63.

[2] Gilbert B. The Micromixer: a highly linear variant of the Gilbert mixer using a bisymmetric Class-AB input stage e. *IEEE Journal of Solid-State Circuits*, 1997. Vol. 32, N. 9. − P. 1412-1423.

[3] Fomin N. N., Buga, N., Golovin O. V. *Radio Receivers: Textbook for Universities*. - M: Techbook, 2007. – 520 p.

[4] Jones M. H. *A Practical Introduction to Electronic Circuits*. Third edition. Cambridge University Press, 1996. – 548 p.
[5] http://www.fastmean.ru.
[6] http://www.spectrum-soft.com.

SHORT COMMUNICATIONS

Smart Nanocomposites
Volume 8, Number 1
ISSN: 1949-4823

INVESTIGATIONS OF ION VELOCITY DISTRIBUTION FUNCTION FOR NOVEL PLASMA NANOTECHNOLOGIES

Alexander Mustafaev[1], Artiom Grabovskiy[1,*], Anastasiya Strakhova[1], and Vladimir Soukhomlinov[2]

[1]Department of General and Technical Physics, Saint Petersburg Mining University, Saint Petersburg, Russia

[2]Department of Optics, Saint Petersburg State University, Saint Petersburg, Russia

ABSTRACT

The paper proposed a new probe method for anisotropic ion velocity distribution function (IVDF) diagnostics. Potentialities of this method have been demonstrated under conditions, when on a mean free path an ion acquires velocity, comparable with average thermal velocity of atoms. Energy and angular dependencies of the first seven coefficients of IVDF expansion in Legendre series for Hg^+ in Hg, He^+ in He and Ar^+ in Ar have been measured, and the polar diagrams of the ion motion have been plotted. In order to verify the reliability and accuracy of the method the analytic solution of the kinetic Boltzmann equation for the ions in plasma of its own gas has been found. The conditions under which resonant charge exchange is a dominant process has been considered, whereas the electrical field magnitude is arbitrary. For the ambipolar field relation between the resonant charge exchange cross-section and the relative velocity has been taken into account. The results of theoretical and experimental data, with provision for the instrumental function of the probe method, correlate very accurately.

Keywords: gas discharge plasma, ion velocity distribution function, probe diagnostics of plasma

INTRODUCTION

IVDF research is of special interest for modern applications: plasma technologies, ion surface treatment, technology of selective etching and creation of relief by ion bombardment, new generation of nanoelectronics (single-electron transistors, spintronics, etc.). [1, 2].

In this context, experimental methods of IVDF measurements in different discharges, in particular, in DC self-sustained discharge plasmas are of special interest. The authors do not

* Corresponding Author Email: schwer@list.ru.

know papers, where the IVDF measurement data for such a discharge have been published. In reference to theoretical research, despite many existing papers it's difficult to select the ones where IVDF for the DC self-sustained discharge plasmas has been calculated.

The ion drift was theoretically considered in [3-6]. In [3] the drift velocity for ions of inert gases in plasma of its own gas in proximity of the strong field was analyzed, the distribution of atoms according to energies being given by delta-function. The results of drift velocity calculations for inert gas ions in its own gas were presented in [4], however, the author did not publish the analytical expression for IVDF.

Neglecting all processes, except charge exchange, in [5] a time interval of the ion movement in its own gas has been calculated, during which an ion has a velocity component along the electric field in the range of v_{iz} and $v_{iz}+dv_{iz}$. These data have been calculated for interpretation of the experimental results of [7]. However it is difficult to obtain IVDF for the total velocity using these results.

The treatise considers [6] IVDF problem solution in its own gas neglecting the creation of ions if they have Maxwellian distribution by velocities as a result of a charge exchange. Thus, for the uniform cross-section of a charge exchange a Maxwellian type of IVDF has been obtained with the temperature, determined by an electrical field in plasma.

In [8, 9] a new method of calculation of matrix elements of collision integral is represented which is intended for solving the non-steady Boltzmann equation by a method of moments for ions in conditions, when the main process is resonant charge exchange. However, in strong fields, when thermal energy of an atom and ion, acquired on the mean free path, is less than 0.1, this approach is difficult for calculation of a steady IVDF. In [10] an analytical solution of Boltzmann equation for ions in BGK-model [11] and a numerical solution for uniform cross-section of resonant charge exchange are compared. It should also be emphasized that the analytical solution gives incorrect asymptotics for the drift velocity of an ion in case of strong fields.

The paper [13] deals with analysis of IVDF in unbounded uniform plasma in the presence of steady (in time and space) electric fields and under condition that the main process that has an effect on the drift velocity of ions is resonant charge exchange. The problem is solved both numerically (by Monte-Carlo method) and analytically. When solving analytically a charge exchange cross-section is assumed to be independent on relative motion of colliding an ion and atom.

The paper [14] represents the problem of determining the IVDF in plasma in its own gas in the presence of strong E-field to have been analytically solved. Calculation results correspond well with the known experimental data for drift velocities in strong fields. It has been found, that IVDF differs significantly from Maxwellian and depends on two parameters. In addition, in [15] the authors state the IVDF for Hg^+ in Hg in vapors to have been measured for the first time. Experimental data correlate very accurately with calculation results.

In this work a new experimental probe method for full IVDF reconstruction in conditions of arbitrary electric field has been proposed. The main limiting factor for the method is a small thickness of Debye near-probe layer in comparison with the probe size.

In order to verify the reliability and accuracy of the developed method the analytical solution of Boltzmann kinetic equation for ions in plasma in its own gas has been found in case of resonant charge exchange being the dominant process. The E-field strength in plasma may be arbitrary and a charge exchange cross-section depends on relative velocities of an ion and atom.

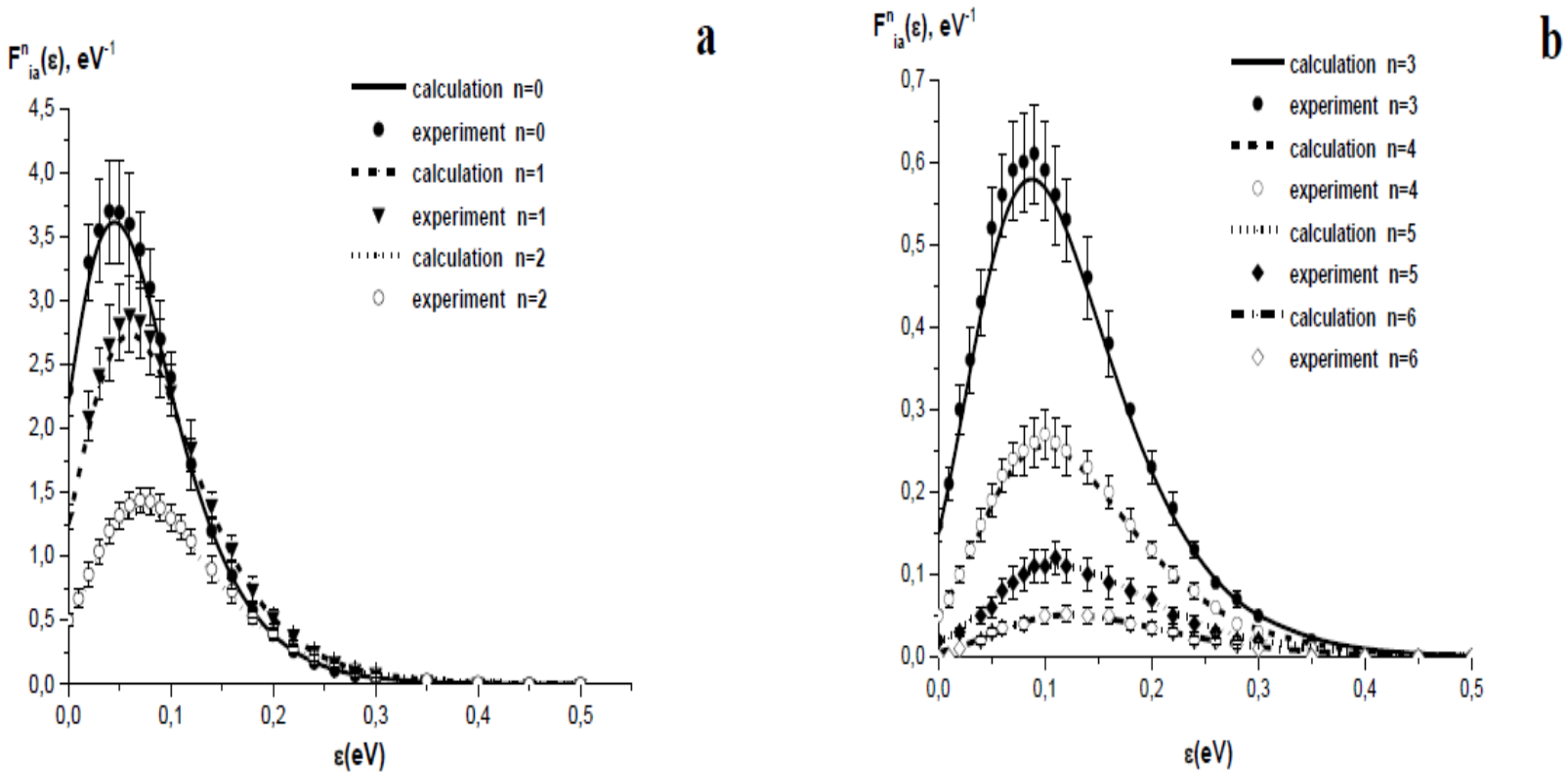

Figure 1a. The energy dependencies of the first three expansion coefficients (n = 1-3) of IVDF Ar^+ in Ar by the Legendre polynomials for value of differentiating signal $\Delta\varepsilon = 0.05$ V. Figure 1b. The same conditions, but n = 3-6.

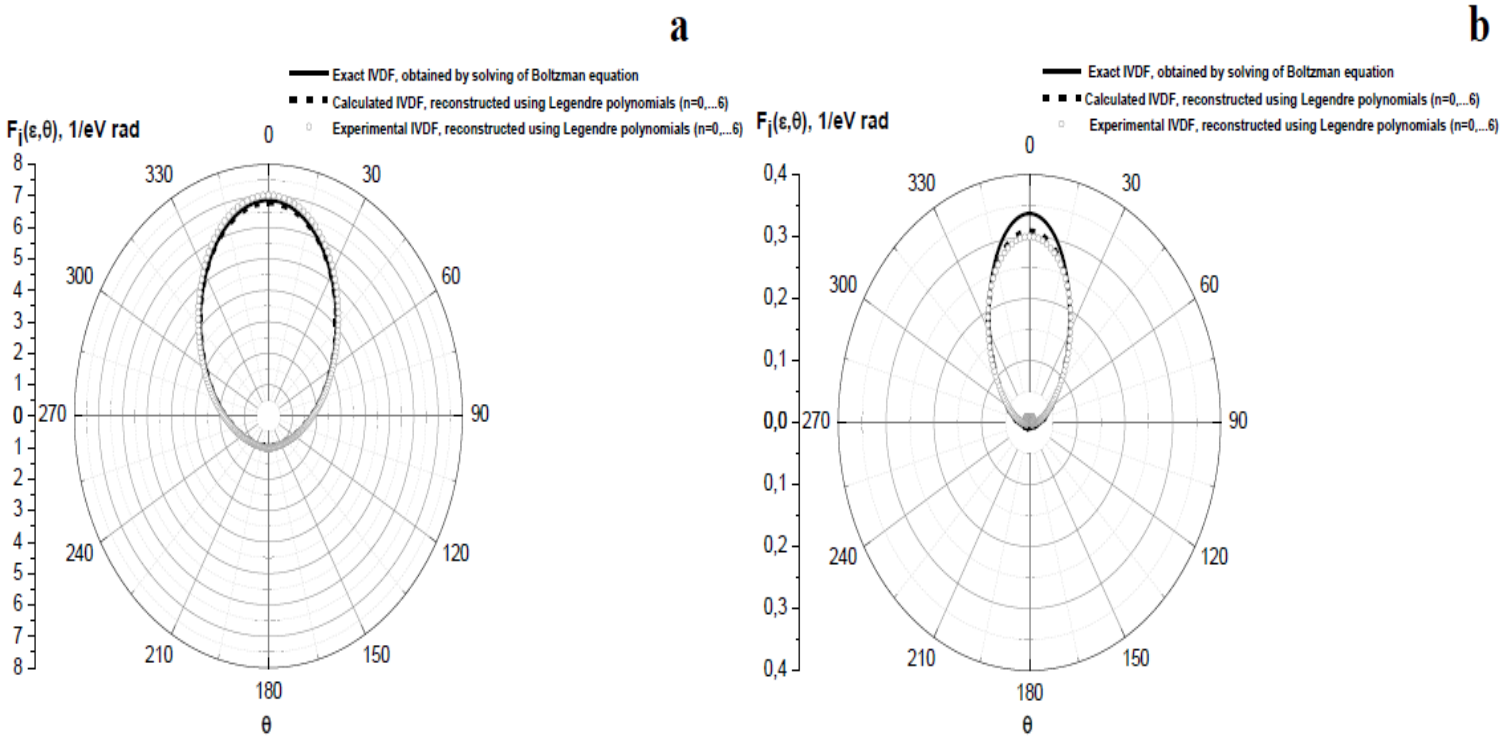

Figure 2a. Angular dependency of the IVDF for the same conditions as indicated in Figure 1a. Ions energy ε = 0.1 eV.
Figure 2b. The same, but for ions with energy ε = 0.3 eV.

Feasibilities of the developed method are demonstrated in this work. The energy and angular dependencies of seven Legendre coefficients have been measured and full IVDF for Hg^+ in Hg, He^+ in He and Ar^+ in Ar has been reconstructed for the first time (Figure 1a, b). A comparison of measured and calculated of Legendre coefficients and corresponding IVDF angular dependencies for Hg^+ in Hg, He^+ in He and Ar^+ in Ar has been made (Figures 1 and 2, respectively). The results of calculation and experimental data give good fit.

Figure 2a shows that when ion velocities are less than the average thermal velocity of atoms, IVDF is isotropic, despite the presence of a strong field. When ion velocities increase the distribution becomes more elongated in the direction of the electric field (Figure 2b), indicating its increasing anisotropy.

This work was supported by the Ministry of Education of the Russian Federation.

REFERENCES

[1] H. Abe, M. Yoneda and N. Fujiwara. Developments of Plasma Etching Technology for Fabricating Semiconductor Devices. *Jpn. J. Appl. Phys.* 2008. Vol. 47. P. 1435.

[2] Michael A. Lieberman. Plasma Processing for Nanoelectronics – History and Prospects. *Bull. of the APS*. 2010. Vol. 55. N 7. P. 105.

[3] Smirnov B. M. Mobility of ions in own gas. *JTP*. 1966. Vol. 36. № 10. P. 1864.

[4] Perel' V. I. Calculation of drift velocity of ions in own gas. *JTP*. 1957. Vol. 32. P. 526.

[5] Fok V. A. On motion of ions in plasma. *JTP*. 1948. Vol. 18. P. 1048.

[6] Golant V. E., Zhilinskii A. P., Sakharov S. A. *Plasma Physics Basics*. Moscow, Atomizdat. 1977. 150 p.

[7] Frisch S. E., Kagan Y. M. Spectral study of ion motion in plasma. *JTP*. 1947. Vol. 17. P. 577.

[8] A. Y. Ender, I. A. Ender. *JTP*. 2010. Vol. 80. № 2. P. 8.

[9] A. Y. Ender, I. A. Ender. *JTP*. 2010. Vol. 80. № 2. P. 18.

[10] D. Else, R. Kompaneets and S. V. Vladimirov. *Physics of Plasmas*. 2009. Vol. 16. P 062106.

[11] P. L. Bhatnagar, E. P. Gross and M. Krook. *Phys. Rev*. 1954. Vol. 94. P. 511.

[12] M. Lampe, T. B. Röcker, G. Joyce, S. K. Zhdanov, A. V. Ivlev, and G. E. Morfill. Ion distribution function in a plasma with uniform electric field. *Physics of Plasmas*. 2012. Vol. 19. P. 113703.

[13] Mustafaev A. S., Soukhomlinov V. S., Ainov M. A. Experimental and theoretical study of strongly anisotropic IDF by velocities in own gas plasma for strong fields. *Technical Physics* 2015, V. 60, No 12, P 1778.

[14] Lapshin V. F., Mustafaev A. S. Method of flat single-sided probe for diagnostics of anisotropic plasma. *JTP*. 1989. Vol. 59. P. 35.

[15] Mustafaev A. S. Dynamics of E-beams in plasmas. *JTP*. 2001. Vol. 71. P. 111.

Smart Nanocomposites
Volume 8, Number 1
ISSN: 1949-4823

PROBE PLASMA DIAGNOSTICS WITH NO VELOCITY SPACE SYMMETRY

Alexander Mustafaev[1], Artiom Grabovskiy[1,*], Anastasiya Strakhova[1], and Vladimir Soukhomlinov[2]
[1]Department of General and Technical Physics,
Saint Petersburg Mining University, Saint Petersburg, Russia
[2]Department of Optics, Saint Petersburg State University, Saint Petersburg, Russia

ABSTRACT

This paper is devoted to the development of the probe method used for analysis of non-equilibrium anisotropic plasmas. The probe method for determination of full electron and ion velocity distribution functions (EVDF) in axially symmetric plasmas was theoretically and experimentally approved. To recover the full EVDF to the Legendre polynomials of order N it is necessary to measure the second derivative of probe current I" U in probe's N different orientations. In there are the theoretical principles of the EVDF recovering method for plasmas with no velocity space symmetry. To determine the full EVFD with the same degree of accuracy it is necessary to measure I" U in flat probe's N^2 orientations. This paper gives further development of probe method. While restoring the full EVDF in plasma objects with bilateral symmetry it became possible to reduce the number of the probe's angular orientations by two. It opens up new possibilities to obtain new information about Langmuir paradox in plasma.

Keywords: electron and ion velocity distribution function, probe method, plasma

INTRODUCTION

One of the current fundamental problems of plasma physics is the so-called "Langmuir paradox," which has been long known and widely discussed in the literature [1-5].

In the paper [6] L. D. Tsendin attempted to explain the Langmuir paradox in plasma of low pressure. As a result it has been concluded, that in this case the main mechanism of EVDF formation is escape of the electrons to the walls, determined by their elastic scattering in the so-called "loss cone."

* Corresponding Author E-mail: schwer@list.ru

The first systematic experimental investigations of EVDF in conditions, when Langmuir paradox is exist, have been undertaken by Y. M. Kagan with collaborators [7]. The result was the assumption that EVDF Maxwellization occurs due to the unknown "wall" mechanism.

Paper [8] demonstrates the results of experiments, where spherical and cylindrical probes, oriented perpendicular to the discharge axis have been used. At this orientation, the cylindrical probe is unable to "feel" the loss cone, and Maxwellian EVDF have been registered in a wide range of energies. Most clearly the depletion of EVDF, associated with the escape of the electrons to the walls, was observed in experiment [8], where flat wall probe has been used. In [9] also noted the differences in the second derivatives, recorded at the two perpendicular orientations of the cylindrical probe - along and across the discharge axis.

The first focused investigations of electron loss cone have been conducted by the authors of [10] in argon high-frequency discharge. The EVDF has been measured by flat probe, located at a distance of 1 cm from the wall. It has been established, that increasing of electrons energy leads to the emergence of EVDF characteristic features, associated with the escape of electrons from plasma volume.

In order to register the loss cone and move forward in research of Langmuir paradox, it is vital to develop new reliable method of plasma diagnostics, providing the possibilities of EVDF investigations with angular resolution near the plasma boundaries, measurements of radial electric field profiles, near-wall potential jump, electron concentration, etc.

To solve this problem we propose new probe method for diagnostics of plasmas with arbitrary symmetry. This method has been experimentally tested and experimental results, testifying in favor of the conclusions [6, 10] have been obtained.

Theory

The known method of flat single-sided probe consists in the EVDF expansion in a series of Legendre polynomials and registration of the second derivative at different angles of the probe orientation with respect to the discharge axis [11]. It allow us to obtain the most complete information about the strongly nonequilibrium anisotropic plasmas. The basis of the method is given by following set of equations:

$$j_u''(\vec{r}; eu; \phi_0) = \frac{2\pi e^3}{m^2} \sum_{j=0}^{\infty} F_j(\vec{r}; eu) P_j(\cos\phi_0); \quad (1)$$

$$F_j(\vec{r}; eu) = f_j(\vec{r}; eu) - \int_{eu}^{\infty} f_j(\vec{r}; \varepsilon) \frac{\partial}{\partial(eu)} P_j\left(\sqrt{\frac{eu}{\varepsilon}}\right) d\varepsilon. \quad (2)$$

However, the scope of this method is limited by the requirement of plasma axial symmetry. Figure 1 demonstrates a case, where flat probe is located near the boundary of the plasma volume (radial area) and it is necessary to take into account the asymmetry, caused by presence of a radial electric field.

In this paper we propose new probe method for diagnostics of the plasma with arbitrary symmetry. In this case the equations of the flat probe method (1, 2) are transformed into the following equations:

$$j_u''(\vec{r};eu) = \frac{2\pi e^3}{m^2}\sum_{j=0}^{\infty}\{F_{jE}(\vec{r};eu)P_j(\cos\phi_{0E}) + F_{jG}(\vec{r};eu)P_j(\cos\phi_{0G})\}; \quad (3)$$

$$F_{jE}(\vec{r};eu) = f_{jE}(\vec{r};eu) - \int_{eu}^{\infty} f_{je}(\vec{r};eu)\frac{\partial}{\partial(eu)}P_j\left(\sqrt{\frac{eu}{\varepsilon}}\right)d\varepsilon\,; \quad (4)$$

$$F_{jG}(\vec{r};eu) = f_{jG}(\vec{r};eu) - \int_{eu}^{\infty} f_{jG}(\vec{r};eu)\frac{\partial}{\partial(eu)}P_j\left(\sqrt{\frac{eu}{\varepsilon}}\right)d\varepsilon\,, \quad (5)$$

where ϕ_{0E}; ϕ_{0G} - the angles between the normal to the flat probe surface and directions of the charged particles fluxes, caused by electric field and diffusion, respectively.

Similarly to the method of the flat probe, reconstruction of the components f_{jE} f_{jG} is connected with the solution of corresponding integral Volterra equations of second kind, binding Legendre components of the EVDF and of the second derivative.

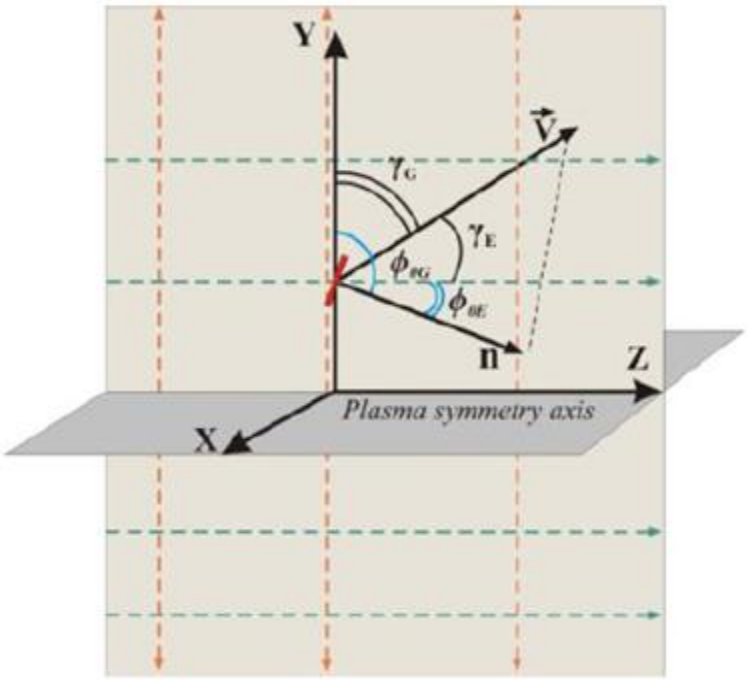

Figure 1. The geometry of the problem in the case of probe, located in radial area of the interelectrode gap.

EXPERIMENT

Probe measurements have been carried out in the range of helium pressure 0.1-1 torr and discharge current 0.1 A to 0.5 A at a distance of 1 cm from the plasma wall for two orientations of the probe with respect to the discharge axis (0 and 180°). Corresponding second derivatives have been registered, angular structure of the EVDF in the loss cone has been reconstructed and polar diagrams of the electron motion have been plotted (Figure 2).

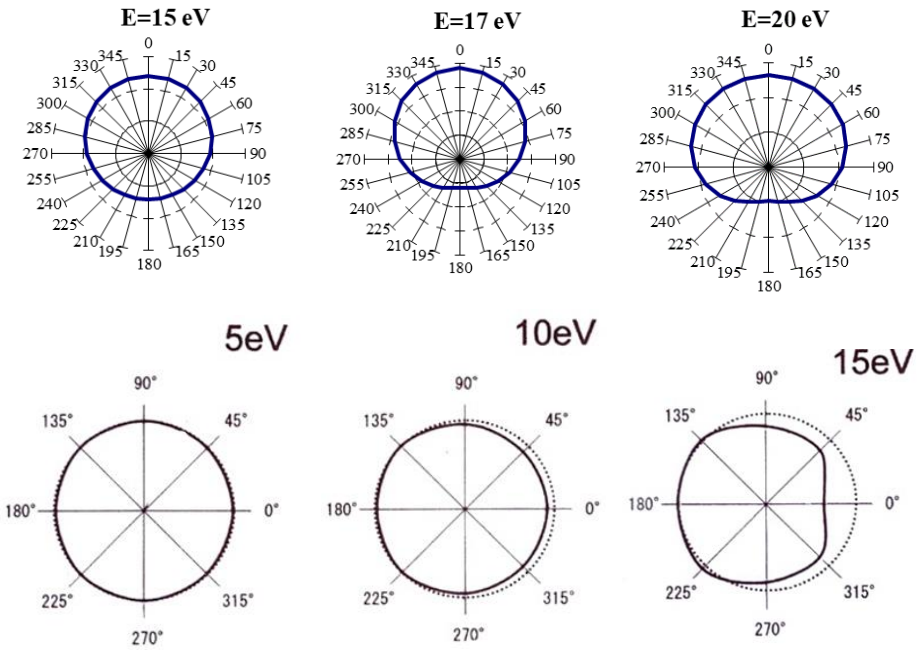

Figure 2. Above – angular structure of the EVDF, registered at a distance of 1 cm from the plasma wall in the positive column of helium glow discharge. P_{He} = 0,5 torr, I = 0,5 A. Angle 180° – collecting surface of the probe is turned to the wall. Below - angular structure of the EVDF, registered in plasma of high-frequency discharge in argon by authors [10]. Angle 0° – collecting surface of the probe is turned to the wall.

According to the paper [10], when energy of the electrons increase, on the diagrams of electron motion is clearly visible the depletion of EVDF, associated with the escape of electrons to the walls. If the wall potential exceeds the potential of the probe, the probe "feels" EVDF in the loss cone. Increasing of current and pressure does not affect EVDF shape. Rotation of the probe by 180° let us to measure EVDF in the main part of the plasma volume. In this case the polar diagrams demonstrate us isotropic EVDF, typical for positive column of glow discharge.

The obtained data correlate quite accurately with theoretical and experimental results of [6, 10]. This is evident about reliability of the developed method and could be a confirmation of the hypothesis, that Langmuir paradox in plasma is associated with physical characteristics of the EVDF formation as a combination of known mechanisms, not with a hypothetical mechanism of EVDF Maxwellization.

This work was supported by the Ministry of Education of the Russian Federation.

REFERENCES

[1] Langmuir I. *Phys. Rev*. 1925. Vol. 26. P. 585–613.

[2] Gabor D., Ash E. A., Dracott D. *Nature*. 1955. Vol. 176. N 11. P. 916–919.

[3] Granovskiy V. L. *Electrical Current in Gas. Sustained Current*. M.: Nauka, 1971. 272 P.

[4] Chen F. *Introduction to Plasma Physics*. Plenum Press. 1974. 421 p.
[5] Kadomtsev B. V. *Problems of Plasma Theory*. Ed. by. M. A. Leontovich. Vol. 4. M.: Atomizdat, 1964. 325 P.
[6] L. D. Tsendin. 2003, *Plasma Sources Sci. Technol*. 12 S51.
[7] Kagan Y. M. *Spectroscopy of Gas Discharge Plasmas*. L.: Nauka, 1970. P. 201-223.
[8] Rayment S. W., Twiddy N. D. *Proc. Soc. A.* 1968. Vol. 340. P. 87–98.
[9] Godyak V. A., Kuzovnikov A. A., Khadir M. A. Mess. of the MSU. *Phys and Astron*. 1971. № 3. P. 336-338.
[10] Ishijima T., Uenuma M., Tsendin L. D. and Sugai H. *Cont. Pap. of ESCAMPING 2002*. Grenoble, France. Vol 1, p. 221.
[11] Mustafaev A. S. *Probe Method for Investigation of Anisotropic EVDF. Electron Kinetics and Applications of Glow Discharges*. NATO Int. Sci. Session. Ed. By Kortshagen U., Tsendin L. N. Y. - London: Plenum Press, 1998. V. 367. P. 531.

Smart Nanocomposites
Volume 8, Number 1
ISSN: 1949-4823

DISCUSSION OF DATA INCONSISTENCIES ON TRANSPORT PHENOMENA IN CRYSTALS OF P-$SB_2TE_{3-X}SE_X$

Sergey A. Nemov[1,2,*], Ali A. Allakhah[1], and Arseny A. Rulimov[1]
[1]Peter the Great Saint Petersburg Polytechnic University, Saint Petersburg, Russia
[2]Zabaikal'skii State University, Chita, Russia

ABSTRACT

It is shown that accounting of interband scattering allows eliminating contradictions in the literature between interpretations of the electrical properties of $A_2^V B_3^{VI}$ materials with the hole conductivity and describing observed temperature dependences of the kinetic coefficients as well as the parameters of the band spectrum.

Keywords: $A_2^V B_3^{VI}$ materials, Interband scattering, Scattering parameter, Kinetic coefficients, Acoustic mechanism of hole scattering

INTRODUCTION

Investigations of layered semiconductor $A_2^V B_3^{VI}$ materials have been being carried out since the middle of last century. Constant interest in these materials is caused by their wide usage in thermoelectric energy converters (in the form of ternary and quaternary solid solutions based on bismuth and antimony chalcogenides).

DISCUSSION

The experimental data obtained in the middle of the 20th century were summarized and systematized in Gol'tsman monograph [1]. However, the features of the energy spectrum of $A_2^V B_3^{VI}$ materials and the mechanisms of charge-carrier scattering are still discussed. Also the differences in the interpretation of experimental data of transport phenomena at low (T = 4.2 K) and medium (77 - 300 K) temperatures are stored. Results of the quantum

* Corresponding Author: Prof. Sergey Aleksandrovich Nemov, Professor of the Department "Materials Science and Technology of Materials," Peter the Great Saint Petersburg Polytechnic University, Saint Petersburg, Russia, Tel.: +7 (921) 347-30-33, E-mail: nemov_s@mail.ru

oscillations research at liquid-helium temperatures have confirmed the Drabble-Wolfe one-band six-ellipsoidal model for crystals with low hole concentration [2, 3].

Most of experimental investigations of transport phenomena in $A_2^{V}B_3^{VI}$ compounds are related to the temperature range 77 - 300 K. Unlike the low-temperature data, the kinetic coefficients (the conductivity σ, the thermopower α, the transverse Nernst-Ettingshausen effect Q) do not have any differences from the nature of the temperature dependences predicted by the theory within one-band model (at the temperature range 77 – 450 K). Therefore, the one-band model is widely used for analysis of the electrical properties of materials, estimates of energy spectrum parameters and for the calculations of the thermoelectric efficiency.

From our point of view, the above-mentioned contradictions in interpretation of the experimental data can be eliminated by correction of the mechanisms of hole scattering. According to available literature data all three components of the Nernst-Ettingshausen tensor are negative numbers at temperatures $T \geq 77$ K in all investigated $A_2^V B_3^{VI}$ materials. In the one-band model such behavior of the Nernst-Ettingshausen coefficient clearly indicates the dominance of the acoustic mechanism of hole scattering. In the two-band model in the samples with the Fermi level located closely to the top of the secondary extremum of the valence band the channel of additional scattering of kinetic moment of charge carriers appears. This mechanism is called interband scattering. The concepts of interband scattering were originally introduced by N. V. Kolomoets [4] to explain anomalies in the concentration dependences of the thermopower in iron group alloys.

CONCLUSION

Produced estimates show that accounting of interband scattering allow describing observed temperature dependences of the kinetic coefficients and determining the parameters of the band spectrum more correctly.

REFERENCES

[1] B. M. Gol'tsman, V. A. Kudinov, I. A. Smirnov. *Semiconductor Thermoelectric Bi2Te3 Based Materials*. Nauka, Moscow (1972). 320 p.

[2] Von Middendorff, G. Landwehr. *Sol. State Com*., 11, 203, 1972.

[3] V. V. Sologub, R. V. Parfen'ev, A. D. Goletskaya. *JETP Letters*, 21, (12), 711 (1975).

[4] N. V. Kolomoets, *SSP*, 1966, t. 8, N 4, 997 p.

Smart Nanocomposites
Volume 8, Number 1
ISSN: 1949-4823

PHASE ANALYSIS OF INTERNAL OXIDATION ZONE OF ELECTRICAL STEEL

Sergey N. Saltykov*, Natalia V. Tarasova, Daria A. Mironova, Nikolay S. Saltykov, Tatyana A. Trunova and Nikolay A. Rogozhnikov
Lipetsk State Technical University, Russia

ABSTRACT

The possibility of analysis of electrical steel internal oxidation zone by FTIR-spectrometry with preliminary anodic etching of the surface is studied. During the etching the ferrite matrix is dissolving and fayalite and silicon oxide phases is appearing on the surface. Fayalite and silicon oxide has the most typical FTIR-reflections in the region of wave numbers 980-1100 cm^{-1}. The method for layer-by-layer analysis of internal oxidation zone of electrical steel is offered. It is found that the silicon oxide located at a depth of 0.5 μm while fayalite is located at a depth of at least 1 μm.

Keywords: internal oxidation zone, FTIR-spectrometry, fayalite, silicon oxide

INTRODUCTION

Operational characteristics of the electrical steel as a magnetic material are determined by quality of insulating coating, which formation largely depends on the structure and composition of the internal oxidation zone (IOZ) phase containing silicon oxide and fayalite [1, 2]. So, a method for the rapid laboratory testing for IOZ composition presents an important stage in the process producing high-quality electrical steel. Good prospect in this area is FTIR-spectroscopy in combination with layer-by-layer etching of the surface which can be accomplished by chemical or electrochemical method. However, the stability of fayalite and silicon oxide phases during the etching that is selective dissolution of ferrite matrix is very important. This paper is dedicated to possibility for using FTIR-spectrometry with preliminary anodic etching of IOZ surface.

* Corresponding Author E-mail: saltsn@mail.ru, +7(4742)-32-81-55.

OBJECTIVES OF THE RESEARCH

The electrochemical dissolution of the electrical steel surface is performed by potentiodynamic voltammetry and galvanostatic polarization methods in the sulfur-, hydrochloric- acid solutions. The composition of the surface layer is analyzed by FTIR-spectrometry.

RESULTS

It is found that the voltammetric curves of electrical steel contains of the inflection points indicated about changing of the surface state during polarization and probably about exit of fayalite and silicon oxide during the ferrite etched.

Given the layer-by-layer location of phases [3] it can be expected that electrochemical dissolution leads to uniform etching of iron matrix. It will be accompanied by gradual exit of silicon oxide and fayalite phase to the surface. Anodic etching was performed to a depth of 0.5, 1, and 2 μm under currents corresponding to the inflection points on the voltammograms.

FTIR results showed that the spectra of the initial surface, i.e., without etching, do not contain any characteristic reflections in the wave region 980-1100 cm^{-1} [4] corresponding to the fayalite and silicon oxide respectively [5]. Most likely, these phases are masked by ferrite matrix while anodic etching leads to reflections in these wave-numbers. It was established that the silicon oxide phase is detected at a depth of 0.5 μm while fayalite phase - to a depth of at least 1 μm.

Thus, the combination of FTIR-spectrometry techniques with preliminary anodic etching allowed not only to identify the fayalite and silicon oxide phases in the composition of the internal oxidation zone but also to quantify determine the location depth of their in the structure.

CONCLUSION

1. Voltammograms of electrical steel contain inflection points corresponded to the appearance of fayalite and silica during anodic etching of the surface.
2. Anodic etching of the surface leads to the dissolution of the ferritic matrix which makes possible the visualization of fayalite and silica phases by FTIR-spectrometry.
3. Compex method developed in present paper and included the anodic etching and FTIR of the surface allows identify layer-by-layer the silica and fayalite phases on the depth of the internal oxidation zone of electrical steel.

REFERENCES

[1] Dragoshanskii Y. N., Pudov V. I., Gubernatorov V. V. *The Physics of Metals and Metallography*. 2001. V. 111. №5. P. 464-470.

[2] Puzhevich R. B., Tsyrlin M. B., Korzunin G. S. *The Physics of Metals and Metallography*. 2006. V. 102. №4. P. 366-375.

[3] S. Jung, M. S. Kwon, S. B. Kim, K. S. Shin. *Surface and Interface Analysis*. 2013. V. 45. P. 1119-1128.
[4] Poultney D. Snell D. E *Jouɔnal of Magnetism and Magnetic Materials* 2008. V. 320. P. 645-648.
[5] An X., Cawley J., Rainforth W. M., Chen L. *Spectrochim. Acta B*. 2003, V. 58, P. 689-693.

The researching was supported by RFBR (project 16-48-480162-p_a.)